Fall 2016

Data Reduction of a Shake-Table Experimental Study of Architectural Precast Concrete Cladding

Kanotha Charles Kamau-Devers
San Jose State University

DATA REDUCTION OF A SHAKE-TABLE EXPERIMENTAL STUDY OF ARCHITECTURAL PRECAST CONCRETE CLADDING

A Thesis

Presented to

The Faculty of the Department of Civil and Environmental Engineering

San José State University

In Partial Fulfillment

of the Requirements for the Degree

Master of Science

by

Kanotha Kamau-Devers

December 2016

The Designated Thesis Committee Approves the Thesis Titled

DATA REDUCTION OF A SHAKE-TABLE EXPERIMENTAL STUDY OF ARCHITECTURAL PRECAST CONCRETE CLADDING

by

Kanotha Kamau-Devers

APPROVED FOR THE DEPARTMENT OF CIVIL AND ENVIRONMENTAL ENGINEERING

SAN JOSÉ STATE UNIVERSITY

December 2016

Kurt McMullin, Ph.D.	Department of Civil and Environmental Engineering
Ajay Singhal, Ph.D.	Department of Civil and Environmental Engineering
Thalia Anagnos, Ph.D.	Office of Graduate and Undergraduate Programs

ABSTRACT

DATA REDUCTION OF A SHAKE-TABLE EXPERIMENTAL STUDY OF ARCHITECTURAL PRECAST CONCRETE CLADDING

by Kanotha Kamau-Devers

Two full-scale architectural precast concrete (APC) panels were tested in 2011 on a full-scale five-story steel frame building at the E-Defense shake table facility in Miki, Japan. The panels were designed according to common U.S. practice. The main issues evaluated were: 1) the effect of acceleration on the APC panels, and 2) the effectiveness of the current slotted-bolt sliding connection to allow for inter-story earthquake motion. The testing represented one type of standard US APC façade design where the APC panel is designed to accommodate inter-story drift through rocking. Instrumentation measured the acceleration of the panels and floors as well as the movement of the slotted connections. The difference between the inter-story drift at the center and corner of the building was large enough to suggest that it may be inaccurate to consider the drift at the floor center to be the same as the drift at the actual panel location, when trying to predict the behavior of an APC panel. Neither panel experienced damage at maximum recorded inter-story deflections of 13.1 and 22.7 mm (maximum out-of-plane and in-plane deflections). Displacement and acceleration data from instruments placed on the panels themselves suggest a possible correlation between vertical acceleration recorded on the APC panel and the occurrence of uplift at the base slotted connection (possible rocking). Acceleration amplification ratios were developed as well.

ACKNOWLEDGEMENTS

The author gratefully acknowledges Dr. Kurt McMullin of the Civil and Environmental Engineering Department at San Jose State University (SJSU), the NEEShub, the SJSU Charles W. Davidson College of Engineering, and the SJSU King Library for support of this research.

The author would also like to thank Dr. Keri Ryan and doctoral student Nhan Dao of the Civil and Environmental Engineering Department at the University of Nevada, Reno for their assistance in research in the preparation of this thesis.

This material is based upon work supported by the National Science Foundation under Grant Nos. CMMI-0619157, CMMI-1113275, CMMI-0936505, and CMMI-0927178. Any opinions, findings, and conclusions or recommendations expressed in this material are those of the authors and do not necessarily reflect the views of the National Science Foundation, other sponsors, or assisting industry groups.

TABLE OF CONTENTS

LIST OF TABLES

LIST OF FIGURES

LIST OF EQUATIONS

LIST OF ABBREVIATIONS

ASCE	American Society of Civil Engineers
CQC	Complete Quadratic Combination
ICC	International Code Council
IFC	International Fire Code
IMRF	Intermediate Moment Resisting Frame
OMRF	Ordinary Moment Resisting Frame
PGA	Peak Ground Acceleration
SEI	Structural Engineering Institute
SMRF	Special Moment Resisting Frame
SRSS	Square Root of the Sum of the Squares
6vb2	6-story braced frame structure with inverted V chevron bracing and flexible beams. Used for Building 1 of this paper.
(10BC)	Partial Composite Behavior (10). Weight distribution only at the steel beam (B). Restricted slip at the central beam-column joint boundary conditions (C). Used for Building 2 of this thesis.
(10SC)	Partial Composite Behavior (10). Weight distribution only at the slab (S). Restricted slip at the central beam-column joint boundary conditions (C). Used for Building 2 of this thesis.
(10TC)	Partial Composite Behavior (10). Weight distribution between steel and concrete components (T). Restricted slip at the central beam-column joint boundary conditions (C). Used for Building 2 of this thesis.
(14TC)	Full Composite Behavior (14). Weight distribution between steel and concrete components (T). Restricted slip at the central beam-column joint boundary conditions (C). Used for Building 2 of this thesis.

Greek Symbols

ξ	Damping Ratio
Ψ	Steel-Composite Interaction Factor (Building 2)
δ	Drift ratio (units of radians)

1 Introduction

1.1 Seismic Behavior of Architectural Precast Concrete (APC) Cladding

A full-scale shake table test of a 5-story steel moment frame building was conducted at the Hyogo Earthquake Engineering Research Center (E-Defense) in Miki, Japan in August 2011. The building was tested under fixed-based and various isolative conditions as a part of the Network for Earthquake Engineering Simulation TIPS Project - Tools to Facilitate Widespread Use of Isolation and Protective Systems. The TIPS Project consisted of a total of 14 experiments observing the behaviors and outcomes of the various configurations. This thesis focuses on the performance of one building non-structural subassembly, the architectural precast concrete (APC) for the fixed-based configuration. More specifically, the study evaluates the performance of the APC panels under the earthquake loadings of five different input ground motions with the goal of relating the cladding behavior to inter-story drift and acceleration. The APC specimens were located at the 4^{th} story (between the fourth and fifth floors). Damage levels were observed as the cladding experienced acceleration and displacements with the shaking of the building.

Seismic drift and acceleration relationships are important for modeling structural behavior. Detecting these relationships may lead to easier, faster, more efficient methods of determining drift demand for specific loadings. Understanding drift or acceleration characteristics such as the locations of response peaks and the interactions between structural and architectural elemental behavior, for example, can be quite valuable. Specifically the development of more realistic relationships between these drift demands

and seismic code requirements will lead to better modeling of structural performance issues pertaining to both analyses and design.

There are three main types of recorded data of building drift and acceleration values: actual real-time data measured from recording devices placed on the buildings themselves, shake table recordings, and virtual recordings from computer software analysis. This thesis focuses on shake table recordings and computer software analysis. The peak inter-story drift of the shake table results at E-Defense are compared to the drift demands of three different structures defined in engineering literature. The three types of structures chosen for evaluation are: (1) a buckling-restrained braced steel frame system, (2) a steel-concrete composite frame system, and (3) a concrete special moment resisting frame system. Essentially, one steel system, one concrete system, and a combination of both systems are reviewed and compared to the experimental data obtained from the fixed-base shake table results at E-Defense.

1.2 Research Goals and Objectives

The goal of this study is to quantify the dynamic behavior of two APC cladding panels tested on the shake table at E-Defense in 2011. The objectives of the study are:

1. Determine the floor acceleration time history records at the connection points of the APC panels to the structure floor.
2. Compare the acceleration time history of the individual panels to the support points on the structure floor.
3. Determine the magnitude of the peak acceleration amplification factor for each panel.

4. Determine the relationship of the inter-story drift ratio and the rocking behavior of the panels.
5. Compare the peak inter-story drift ratios achieved during the shake table testing with structure inter-story drift demands defined in engineering literature.
6. Develop an algorithm for determining drift at the corner of the building from data recorded on the global movement of the building.
7. Develop relationships between drift and acceleration measured at the center of the building to the movement of the APC panel (drift and amplification).
8. Develop relationships between drift and acceleration measured at the connection points of the panels to the movement of the APC panels (panel deflection and amplification).
9. Determine inertial forces generated during an earthquake and compare those values to the design forces assigned by current building codes.

The hypothesis of this thesis is that modern designs of APC panels using rocking behavior will perform well when subjected to a 3D dynamic loading.

1.3 Background

1.3.1 Architectural precast concrete (APC) systems.

The performance of architectural precast concrete during seismic excitation is an area of concern for engineers and architects. Limited research has been done in the area of dynamic testing of full-scale structures. Research such as that conducted at the University of California, San Diego (Hutchinson, 2010) provides quantitative data related to façade systems, but the wide variety of façade designs and characteristics require extensive experimental studies to capture a complete picture of the dynamic behavior of these systems.

Architectural precast concrete (APC) is commonly used in residential, commercial, and industrial construction. The function and demand of APC cladding have evolved since it was first introduced. APC is also relied upon for the beneficial thermal insulating characteristics of the concrete and may be designed as shear walls as well (Walker, 2006). The popularity of APC panels has grown for many reasons including construction benefits and wide ranges of finishes. The types of available finishes of APC cladding give the owner and architect almost limitless options. Cladding may be acid-etched for a more aged appearance or the aggregate may be chosen specifically to attain the style and feel of natural stone or masonry. Different shapes, sizes, and colors are also achievable.

Cladding can be manufactured in bulk. Constructability and ease of installation is of great importance as an owner may gain many advantages in both schedule and budget. In general, bigger cladding panels can be installed more efficiently, especially if they

match the story heights (Maddalena, 2003). Also the lack of need for scaffolding saves time and money, and the cladding itself can be speedily installed by use of a crane if delivered properly to the site. In fact, one of the greatest design constraints with respect to panel dimensions is vehicular transportation to the construction site itself (Maddalena, 2003). These cladding systems have become so popular that an APC consultant may be hired before the architect in the initial design phases, allowing for more efficient design strategy and construction planning (Maddalena, 2003).

1.3.2 Rocking mechanism design for seismic motion.

The type of detailing required for design correlates to the expected level of seismic activity. Regions of lower seismic levels may require less detail by code and vice versa for areas of higher seismic levels. Both architectural and structural components are designed to withstand their loading demands. APC panel connections are required to support the vertical weight of the panel while also performing satisfactorily during an earthquake.

One way that engineers design APC cladding panels is by means of a rocking mechanism. This type of connection allows the panels to "rock" with the motion of the building in a manner where the panels do not inhibit inter-story drift of the floors. The connections are designed to allow movement of the floor slabs without restraint by the APC panels, in both the vertical and horizontal directions. This movement is usually allowed by fabricating steel connections with slots for support bolts. Sliding of the bolt in the slot thus can allow relative movement of the panel and the building slab. Vertical slotted connections are installed at both upper and lower corners of the panels to allow

for rocking to occur when the supporting steel frame displaces laterally. The rocking style connection systems allow for the base of the panel to lift off its supports. This vertical translation is also referred to as uplift of the panels.

Uplift from rocking has the potential to cause damage to the panel. As the panel returns to its initial positioning, the impact of landing and the sudden deceleration may damage the panels. This impact is one of the main anticipated behaviors and a primary concern of the APC rocking mechanism design.

1.3.3 Network for Earthquake Engineering Simulation NEEShub project database.

The Network for Earthquake Engineering Simulation (NEES) was a multi-university center funded by the National Science Foundation. The NEEShub is an online repository that contains published data and reports from NEES funded experiments. NEEShub hosts a variety of tools for research professionals to collaborate and promote the advancement of seismic engineering. The experimental data along with various resources surrounding this project, such as video documentation and supporting publications have been compiled on the NEEShub. The study is available to the public as Project 571. Project 571 is more specifically known as the TIPS Project - Tools to Facilitate Widespread Use of Isolation and Protective Systems, a NEES/E-Defense Collaboration – and consists of 13 experiments. Some data used in this research was obtained directly from researchers involved with Project 571. All other data used and analyzed in this thesis regarding the E-Defense study is available from the NEEShub.

1.3.4 Scope of work.

The primary scope of work included:

- Evaluation of data collected during five ground motion experiments conducted at E-Defense in 2011 with a total of two APC panels installed
    - Drift data considered for multiple ground motions run at E-Defense
    - Acceleration data considered for only one ground motion run at E-Defense
- Development of research methodology and implementation

2 Research Methodology

This thesis examines, derives, and evaluates the behavior the APC cladding tested at E-Defense. Specifically this study involves data reduction of Experiment 5: *Full Scale 5-story Building in Fixed-Base Condition at E-Defense*. Data as well as supporting documentation such as live video feed from the actual testing, photos of the construction and testing, and publications pertaining to this study were also obtained through NEEShub (Ryan et al., 2013).

The data and theory collected by means of a literature review have been quantified and expanded upon, appropriate to the topics presented in this thesis. The literature review consisted of finding peer reviewed published studies and books surrounding the following topics:

- Structural dynamics – with a focus on acceleration amplification
- Drift demand
- Inter-story drift demands
- Experimental testing of APC cladding – particularly dynamic testing
- Shake table at E-Defense
- NEES – TIPS Project – emphasis on the E-Defense experiments – ground motions used for experimental study.
- Existing publications of experiment and results

A primary focus of this thesis is determining correlations between the seismic loading response of the floor and the APC cladding behavior. Determining the positioning, locations, and nomenclature of the instrumentation used to record the real-time drifts and accelerations was necessary to conduct appropriate data reduction. Displacements and accelerations needed to be determined at locations where no experimental instrumentation was installed. Hence, extrapolation and interpolation algorithms were developed to expand the available data to the locations of interest as necessary and within reason. Verification of the derived data was accomplished by comparison to similar quantified measurements reported in other publications of the TIPS Project, which were developed independently of the work in this thesis. This thesis also proposes methods of determining behaviors, such as how to interpret the rocking design mechanism behavior of the APC panels from the APC panel response data.

Acceleration amplification relationships are of interest for gauging the acceleration responses in relation to the input acceleration. The input earthquake loading functions were defined (such as peak displacement, velocity, durations, and acceleration parameters) in order to accurately and effectively present acceleration amplification data.

3 Literature Review

3.1 Structural Dynamics

Structural dynamics is the study of structures under dynamic loadings, or loadings that vary with time. These dynamic loadings may also be referred to as input loadings. The source of dynamic loading discussed in this thesis is seismic loading. The response, or output function, of the system is therefore time varying as well.

Equation 3.1 is the second order differential equation of motion that can be applied to a structural system. The three main responses of interest for a structure in motion are displacement (x), velocity (x'), and acceleration (x''). Simple structures are structures that can be idealized as lumped masses with equivalent lateral story stiffness' (Chopra, 2012). In Equation 3.1, m symbolizes the system mass, c is the system's viscous damping coefficient, and k is the lateral stiffness of the system. Stiffness relationships can be used to convert the displacement response into design forces (relatively simple for systems that may be idealized as linear elastic).

$$[m]x'' + [c]x' + [k]x = \mathrm{p(t)} \tag{3.1}$$

The IBC allows the use of code response spectra, which defines a design maximum pseudo acceleration experienced by a structure based upon the structure's period. This pseudo acceleration allows for the development of a design base shear which can be used to design the entire lateral system, when in fact a static analysis is deemed appropriate. The IBC states that dynamic analysis may be required if the structure is taller than a certain number of stories and contains mass, stiffness, or

geometric irregularities (Lindeburg & McMullin, 2011). For a multiple degree of freedom (MDOF) structure that requires dynamic analysis, mathematical algorithms are used to sum individual modal contributions. Dynamic modal analysis of a linear system may be done by hand; however software is more practical for more complex structures (Lindeburg & McMullin, 2011). The three common types of dynamic analysis are: (1) response spectra analysis, (2) time history analysis, and (3) shake table analysis. Dynamic response spectra analysis outputs peak responses whereas time history analysis outputs response as a function of time. A shake table accelerates a scaled physical structure model at a given seismic input loading, and the responses can be recorded via instrumentation on the specimen in real time. Shake tables range in size and capability. Shake table responses are output as a function of time similar to time history analysis, except that the shake table model is not idealized by computer software.

3.1.1 Acceleration amplification background.

When a dynamic load is defined and applied to a structure for analysis, the peak response as well as the time history response may be of interest. The solutions to dynamics problems modeled by Equation 3.1 may include amplifications that are used to predict the dynamic response using the static response, for simplicity of analysis. Chopra (2012) defines these static to dynamic amplifications as response factors. Response factors are developed for deformation, velocity, and acceleration.

Harmonic, periodic, step, and pulse excitations are examples of dynamic loading. When a dynamic loading is applied to a simple structure, an equivalent static force can be developed at each instant in time that would deliver the same response as the dynamic

force, allowing one to use static analysis (Chopra, 2012). Therefore the peak amplitude of an idealized dynamic loading function can be used to determine the peak static displacement response of a simple one-story single degree of freedom (SDOF) system that is linearly elastic, as force and displacement are linearly proportional to one another and related by an equivalent stiffness. Likewise, for the same system and loading, the peak dynamic base shear response can be determined from the peak dynamic displacement response using linear static stiffness relationships. For most simple dynamic loading types, the dynamic displacement responses as a function of both time and peak static displacement have already been developed. The dynamic velocity and acceleration responses may then be determined by differentiation of these functions. Chopra (2012) also discusses amplification factors which develop the elastic design spectra based on the input ground motion. This concept of predicting a response based upon another known quantity is utilized in this thesis.

Once the maximum acceleration of the building is determined by a dynamic analysis, acceleration amplification as the ratio of response acceleration to input acceleration may be developed. Output responses of the structure may even be amplified among one another, for example structure floor to architectural component and vice versa. These amplification factors can be important parameters for design. An engineer can forecast accelerations of desired components and floors based upon these documented amplification relationships. This may be especially useful in academia where understanding structural response behavior is often a key focus and desire of study, in order to advance design practices. This thesis expands Chopra's definitions of

response factors and amplification factors to non-structural elements, specifically the APC panels. Taking into account the flexibility of the APC panels, the researchers developed amplification for these elements. These amplifications can be used for predicting the panel accelerations (desirable for design performance purposes and manufactures in the APC industry). Floor acceleration amplification was developed in order to analyze the floor behavior based upon geometric location.

3.1.2 Static procedure and seismic forces on non-structural components.

The *ASCE 7-10* (ASCE, 2010) seismic provision of the IBC allows a static analysis of certain structures. This static procedure idealizes the dynamic load on the structure as a static linear distribution of the base shear along the height of the structure. The base shear is the overall lateral force that the foundation of a structure must resist during the earthquake. The building's floors are idealized as individual lumped masses and the supporting columns are idealized as massless and with a single equivalent stiffness. Each floor contributes a fraction of the total base shear as a function of the individual story mass and height relative to the ground. A seismic coefficient is developed for each floor as input for the design of the diaphragm. The seismic coefficient is an idealization of acceleration. The diaphragm must transfer the loads across the floor to an *ASCE 7-10* (ASCE, 2010) recognized lateral system. Static code forces are therefore essentially derived from Newton's Second Law of fundamental mechanical theory, the product of mass and acceleration (Lindeburg & McMullin, 2011). Both structural and architectural components have mass, and contribute to the base shear

lateral force developed during an earthquake excitation. Supporting connections of non-structural components have to be designed as well to withstand their own accelerations.

Seismic codes develop a static design force for each non-structural component based upon fundamental mechanics theory whereby the mass of each individual component is considered. As shown by Equation 3.2, the acceleration of the component is a function of its own weight (W_P), its relative height above the ground (z), the height of the structure roof above the ground (h_r), the structure's spectral response acceleration (S_{DS}) and three factors: (1) importance (I_P), (2) component response modification (R_P), and (3) component amplification (a_P):

$$F_P = \left(\frac{0.4 a_P S_{DS} W_P}{\frac{R_P}{I_P}}\right)\left(1 + \frac{2z}{h_r}\right) \quad \textit{ASCE 7-10} \text{ (ASCE, 2010)} \tag{3.2}$$

The component amplification factor varies greatly depending upon whether the component is rigidly connected or flexibly connected. If flexibly connected, the component is designed to experience 2.5 times the acceleration. The "rocking" mechanism design of the APC cladding means that the amplification factor should be 2.5 (Lindeburg & McMullin, 2011).

3.2 Drift Demand

3.2.1 General seismic drift demand overview.

Several important terms must first be defined to understand the characteristics of drift demand discussed in this thesis. Roof deflection, also known as global drift, is the total horizontal displacement of the roof relative to its original position. Roof deflection is the displacement of the top story. Inter-story drift is another relative displacement,

specifically the horizontal displacement of one story with respect to the story below (Lindeburg & McMullin, 2011). The global drift ratio, measured in radians, is the global deflection divided by the height of the roof (Lindeburg & McMullin, 2011). Inter-story drift ratio is the inter-story drift divided by the story height of that specific story and is measured in radians.

Drift is an outcome of lateral horizontal load from the environment. Demands may be due to seismic, wind, ice and/or blast loading. Design codes such as the *Seismic Design Provisions of ASCE 7-10* (ASCE, 2010) and the *International Fire Code 5607* (ICC, 2007), have developed criteria to address each of these loadings. With seismic loading, the ground acceleration of the earth displaces the structure laterally. The peak ground acceleration (PGA) is usually of particular interest and expressed in units of gravitational acceleration, g. In modeling and analysis, the ground motion is converted to a forcing function and applied to a structure. A response spectrum plots the maximum response of several building periods (a defining characteristic) to one earthquake loading. Earthquake loadings are usually recorded in small time steps, so approximation by linear interpolation numerical analyses can be quite accurate for determining response (Chopra, 2007). Drift demand determined from the response of a structure is a factor of many variables such as damping, variable lateral stiffness, building period, and ground motion, which are all uniquely complex on their own (Chopra, 2007).

3.2.2 The significance of drift demand on structures.

Drift is an important design parameter because excessive drift can lead to damage and possible collapse. Drift must be limited to prevent such catastrophes from occurring.

One specific problem is adjacent building pounding. When lateral displacements at any point along a structure overlap within the vicinity of another structure, pounding is a possibility. Because pounding can lead to structural damage, design codes require a building separation that considers the maximum predicted deflections of adjacent buildings (Lindeburg & McMullin, 2011).

It is necessary to control drift to limit deformation resulting damages (Hokmabadi, 2012). For example, drift can place heavy demands on the structure in which the members may have not been designed to withstand or more complex stress patterns, such as excessive bending moments combined with axial load. Secondary shear developed by P-delta effects may overcome the shear strength of an individual story resulting in failure (Medina, 2005). Large drifts may create an overturning effect on the entire structure. Although global collapse is rarely a result of excessive drift alone, combined with other effects, drift is still a major design parameter (Krawinkler, 2003). Some plastic hinge analysis, such as the moment distribution within steel connections, has also been directly related to the amount of local deformation, which is yet another reason why inter-story drift is such a critical measurement.

3.3 Inter-story Drift Demand from Engineering Literature

Sections 3.3.1 to 3.3.3 present the drift demand of three unique building studies. Each study notes if the data for drift was obtained from one of the three main types of drift recordings: actual real-time data measured from drift recording devices placed on the buildings themselves, shake table recordings, and virtual recordings from computer software analysis. For each building reviewed, supporting findings included: tabulated

quantitative data that can be used to expand the database of this topic, floor plan and frame elevation graphics, and research methods.

Drift is a product of many controlling factors. It was necessary to note certain criteria to understand the conditions and uniqueness of each experiment. A specific structure type and loading was selected to narrow the research and draw more concentrated conclusions. The desired buildings were regular, had distinct lateral systems, were of either steel or concrete, had five or more stories, and were subjected to non-linear dynamic analysis of earthquake loading. Only certain models from any given reviewed study were analyzed.

Table 3.1 summarizes of the three building models, including types of loading and analysis technique. Table 3.2 summarizes the building model properties including number of stories, height, and period. Seismic peak drift demand using non-linear dynamic analysis was the focus of the comparison of the three buildings. Several types of ground motion analyses were considered. The peak drift ratios of these three buildings were used to gauge the relative sizes of the ground motions of the shake table study at E-Defense.

Table 3.1. *Building Models for Inter-Story Drift Research*

Building No.	Building Model	Type of Loading	Analytical Technique	Year of Study	Author Reference
1	Buckling-Restrained Braced Steel Frame	Seismic; Ground Motion with 5% damping; 50%, 10%, and 2%, 50-year probability of exceedance	SNAP-2DX, Non-linear Dynamic Analysis, Inelastic	2003	Sabelli et al.
2	Steel/Concrete Moment Frame; Composite Frame, Partial/Full Composite Action; (10SC), (10TC), (10BC), (14TC)	Seismic; Ground Motion with 5% damping; 1994 Northridge Earthquake	Matlab, FEDEASLab toolbox, Non-linear Dynamic Analysis, Inelastic	2008	Zona et al.
3	Concrete Special Moment Resisting Frame	Seismic; Ground Motion with 5% damping; 1995 Kobe, 1994 Northridge, 1940 El Centro	SAP2000 V.14, Non-linear Dynamic Analysis	2010	Hokmabadi et al.

Table 3.2. *Building Data from Literature Review: Building No., No. of Stories, Roof Height, and Remarks*

Building No.	No. of Stories	Roof Height	Remarks
1	6	83 ft	Natural Period of 0.55 seconds
2a	5	15 m	Natural Period of 0.2988 seconds
2b	5	15 m	Natural Period of 0.2988 seconds
2c	5	15 m	Natural Period of 0.2988 seconds
2d	5	15 m	Natural Period of 0.2961 seconds
3	15	45 m	Natural Frequency of 0.56 Hz

Note. Data from Sabelli et al. (2003), Zona et al. (2008), & Hokmabadi et al. (2012).

3.3.1 Building 1: a multi-story buckling-restrained concentric braced steel frame System.

Sabelli, Mahin, & Chang (2003) published the analysis of a steel braced frame building with buckling-restrained braces. Ordinary concentric braced steel frames have become increasingly popular because of their lower price to construct for the provided lateral stiffness; however, certain performance flaws under seismic loading have been identified (Sabelli et al., 2003). There have been studies (e.g., Kamura, Katayama, Shimokawa, & Okamoto, 2000; Ohi, Shimawaki, Lee, & Otsuka, 2001) conducted to test new steel braced frame systems that will withstand these performance flaws such as buckling, in hopes of improving future code and design procedure (as cited in Sabelli et al., 2003, p. 655).

A limitation of braced steel frame systems can be the global buckling of the braces under lateral loading that leads to brittle failure of the braces themselves (Sabelli et al., 2003). Braced members are controlled by compression. Tremblay (2002) found

that the energy from the lateral loading is dissipated by the braces as they encounter both tensile and compressive cyclic strain. The steel is particularly good for tensile yielding. The inelastic buckling due to compression results in sudden failure, the worst possible case and one which undermines the design dependency on the ductility properties of the steel members in tension. To prevent buckling, the method of encasing the braces with a compressive material such as concrete for composite action was considered and applied to the building model. This type of brace is called a buckling-restrained brace. With adequate encasing to alleviate compressive stresses, the steel braces are capable of withstanding larger loads far beyond yielding without buckling (Sabelli et al., 2003). Kiggins & Uang (2006) found that even though the system is able to access the post-yield strength of the steel, as the braces are prevented from buckling, the post-yield stiffness of the braces is low, which causes greater inelastic deformations. Though greater inelastic deformation is better than sudden failure due to buckling, large inelastic deformations can cause damage. This doesn't discredit the use of buckling-restrained braces, but instead presents a second stage of research associated with this particular solution.

In this research, Sabelli's model is referred to as Building 1. The model was conventional without any irregularities and consisted of an 83 foot tall building. The first story was defined at 18 feet while the remaining five stories were equally spaced at 13 feet, with 30 foot bays (Sabelli et al., 2003). Non-adjacent bays along the perimeter were braced with concentric inverted V chevron braces and the frame had flexible beams (Sabelli et al., 2003). The building period was 0.55 seconds. Sabelli et al. (2003) classified the frame as 6vb2 in his study. The floor plan and frame elevations of Building

1 are shown in Figures 3.1 and 3.2, respectively. The nominal plan dimensions were 154' by 154' with 30' bays (see Fig. 3.1). Sabelli et al. (2003) explained that a total of "twelve bays of bracing are provided; six in each direction" (p. 659). Figure 3.2 is an elevation of a single bay of bracing and the nominal dimensions are 30' by 83.'

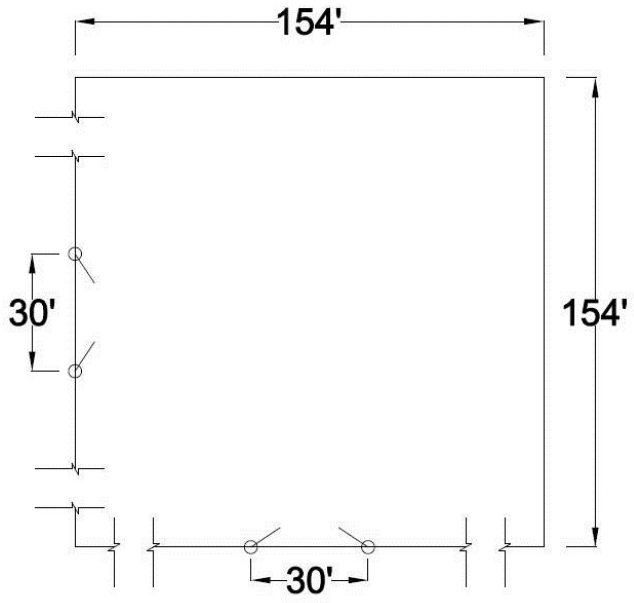

Figure 3.1. Plan View of Building 1 – Buckling-Restrained Braced Steel Frame

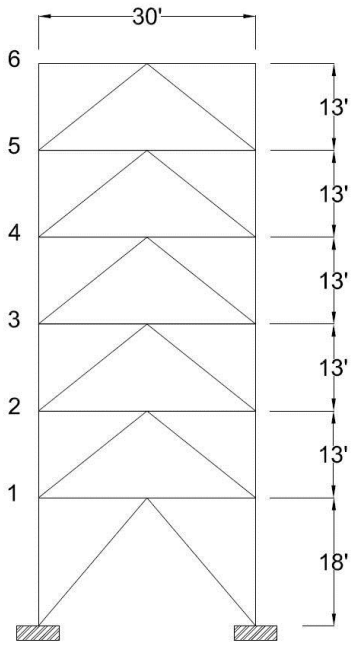

Figure 3.2. Frame Elevation of Building 1 – Six-Story Buckling-Restrained Braced Steel Frame with Inverted V Chevron Braces (only one bay is shown)

Non-linear inelastic dynamic analysis using SNAP-2DX was performed on the building. The input loadings were earthquake ground motions of 50, 10, and 2% probability of exceedance within a 50 year range in the Los Angeles, California region (Sabelli et al., 2003). A damping ratio of ξ=5% was chosen, which is common in code for steel systems (Sabelli et al., 2003). Sabelli et al. (2003) presented a plot of the peak inter-story drift. Peak inter-story drift ratios are reported in Table 3.3.

Table 3.3. *Peak Inter-Story Drift from Literature Review – Building 1*

Building No.	Earthquake Motion	Peak Inter-Story Drift Ratio (%)
1	50% 50-year probability exceedance	1.00
1	10% 50-year probability exceedance	1.38
1	2% 50-year probability exceedance	4.38

Note. Data from Sabelli et al. (2003).

3.3.2 Building 2: a steel-concrete composite frame structure.

The second study reviewed reports on the nonlinear response of steel-concrete composite (SCC) frame structures (Zona, Barbato, & Conte, 2008). The SCC frames take advantage of the composite action of the concrete slab and steel beams using the traditional design. The composite behavior of traditional composite beams is based upon the connection between the concrete slab surface and the steel beam surface. An effective portion of the slab acts as a beam and participates in sharing the flexural loading of the steel beam. Theoretically when there are enough shear connectors between the concrete and steel, preventing slip, full composite action will develop as they both bend together (McMullin, 2013). On the contrary, with no shear connectors, the concrete slab and steel beam will act separately on their own. Partial composite behavior occurs when there are only enough connectors to allow some slip (McMullin, 2013). The desired action is chosen by the engineer. Full, partial, or non-composite behavior may be adopted for design.

Zona et al. (2008) studied how to properly model SCC frames using finite-element response analysis. It was determined that modeling the composite behavior through deformable shear connectors and boundary slip conditions between the slab, beam, and column was crucial for deriving accurate results. The location of the mass distribution between the concrete and steel was also considered and found to be negligible (Zona et al., 2008). Based on these conclusions, the model considered drift demands for both full and partial composite conditions as they were both found to be accurately depicted for SCC frame analysis. More specifically, the models compared from this study were those with (1) full and intermediate shear connection describing the interaction between beams and slab slip and (2) slip prevented at the boundary condition at central beam column joints, except for the roof. Zona et al. (2008) also noted that some boundary conditions should not be applied at locations where slip is unpreventable such as at external columns, as application at these locations have significant effect and would lead to non-conservative results.

An SCC frame was analyzed from Zona et al. (2008). For the purposes of this thesis, the four structures are Building 2a (10SC), Building 2b (10TC), Building 2c (10BC), and Building 2d (14TC). The nomenclatures 10SC, 10TC, 10BC, and 14TC each refer to modeling attributes (composite behavior, weight distribution, and slip boundary conditions) from Zona's study and are adopted in this thesis as well for clarification. Three kinds of steel-to-concrete composite interaction factors, or Psi (Ψ), were examined representing the strength of the bond between the steel and concrete (numbers in parentheses refer to the actual input value used in the computer analysis).

The values were Ψ= 0.6 (06), 1.0 (10), and 1.4 (14), ranging from lowest to highest interaction, respectively. As previously stated, Ψ= 0.6 (06) and 1.0 (10) represent partial interaction and Ψ=1.4 (14) represents full interaction. Only frames 10 (partial interaction) and 14 (full interaction) were inspected as the purpose was to compare the higher degrees of composite action. The models consisted of five-story two bay SCC frames with traditional composite beams (concrete slab and steel W beams) and W steel columns. Bay widths were 5 m and story heights were 3 m for a combined height of 15 m. Slip at the central beam-column joint boundary conditions was also restricted appropriately for accurate representation and classified as (C) type. The placement of the weight distribution was negligible, so mass distributed at the slab (S), between steel and concrete components (T), and only at the steel beam (B) was analyzed. The model was conventional without any irregularities. The floor plan and frame elevations of Building 2 are shown in Figures 3.3 and 3.4, respectively.

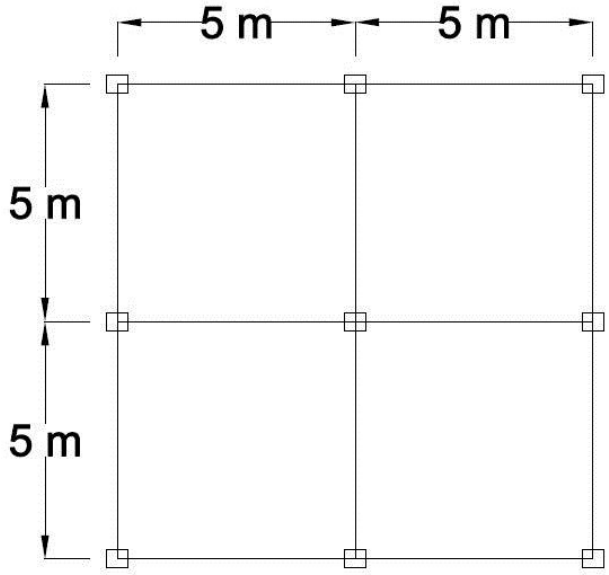

Figure 3.3. Plan View of Building 2 – Steel-Concrete Composite Frame (nominal plan dimensions were 10 m by 10 m, with two 5 m bays in each direction)

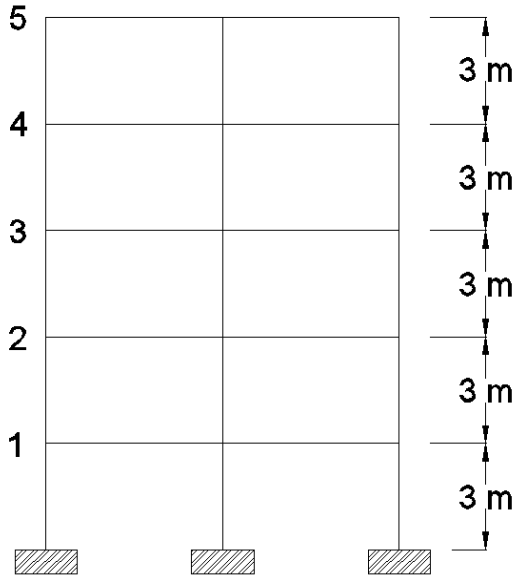

Figure 3.4. Frame Elevation of Building 2 – Five-Story Steel-Concrete Composite Frame (the height of the structure was 15 m and each bay measured 5 m in width)

Non-linear inelastic dynamic analysis of the SCC frames for finite-element structural response was developed using FEDEASLab, a toolbox of Matlab, and the Newton-Raphson iteration theory (Zona et al., 2008). Both monotonic and cyclic loadings were considered; however, the results were not specific to either one, as the differences between the two were deemed negligible (Zona et al., 2008). The two earthquakes considered were the 1979 Imperial Valley 'El Centro' Earthquake (40 year hazard correspondence with PGA=0.775g) and the 1994 Northridge Earthquake (180 year hazard correspondence with PGA=1.585g); however, only results from the latter were reviewed at a damping ratio of ξ=5%. Zona et al. (2008) directly reported peak inter-story drift ratios as summarized in Table 3.4.

Table 3.4. *Peak Inter-Story Drift from Literature Review – Building 2*

Building No.	Earthquake Motion	Peak Inter-Story Drift Ratio (%)
2a	1994 Northridge	1.70
2b	1994 Northridge	1.72
2c	1994 Northridge	1.72
2d	1994 Northridge	1.71

Note. Data from Zona et al. (2008).

3.3.3 Building 3: a multi-story concrete moment resisting frame system.

Moment resisting frames dissipate earthquake forces through both moment and axial strain (Lindeburg & McMullin, 2011). The members of this frame system are designed to carry both vertical and horizontal loadings. Joints are idealized as rigid, meaning that moment from both lateral and vertical loading are transferred from beam members to columns and ultimately to the foundation. For systems such as a braced frame systems, where joints are idealized as pinned, members experience axial strain only from lateral loading, as none of the load is transferred through moment in theory (Lindeburg & McMullin, 2011).

Concrete moment frames can be characterized as special (SMRF), intermediate (IMRF), or ordinary (OMRF) moment-resisting frames. Both special and intermediate moment resisting frames are detailed to guarantee code specified ductile behavior, or ability to deform elastically and plastically before collapse (Lindeburg & McMullin, 2011). Intermediate moment-resisting frames are not as heavily detailed as special moment resisting frames and may not be permitted in some areas (Lindeburg &

McMullin, 2011). Ordinary moment resisting frames are not detailed to meet the special code ductile requirements and are not permitted in areas of high seismic activity (Lindeburg & McMullin, 2011).

Building 3 was a concrete SMRF. The model consisted of a 15-story frame structure with three equally spaced bays and a natural frequency of 0.56 Hz (Hokmabadi, Fatahi, & Samali, 2012). Story heights were 3 m for a combined height of 45 m, and bay widths were 4 m. Hokmabadi et al. (2012) described the building as, "a conventional type of mid-rise buildings in a relatively high risk earthquake prone zone" (p. 175). The model was conventional without any irregularities. The floor plan and frame elevations of Building 3 are shown in Figures 3.5 and 3.6, respectively.

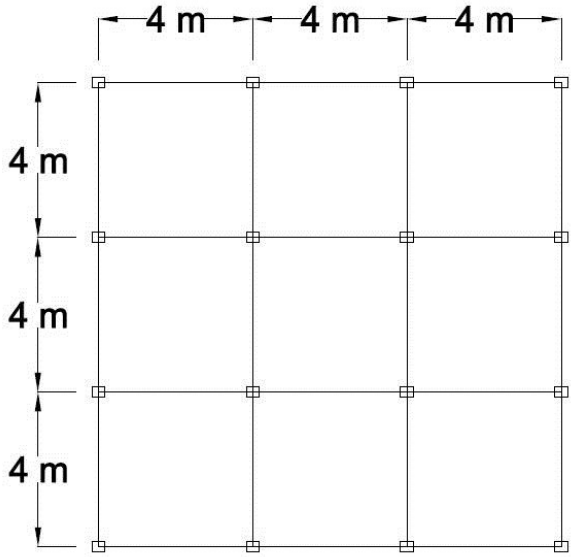

Figure 3.5. Plan View of Building 3 – Concrete SMRF (nominal plan dimensions were 12 m by 12 m, with three 4 m bays in each direction)

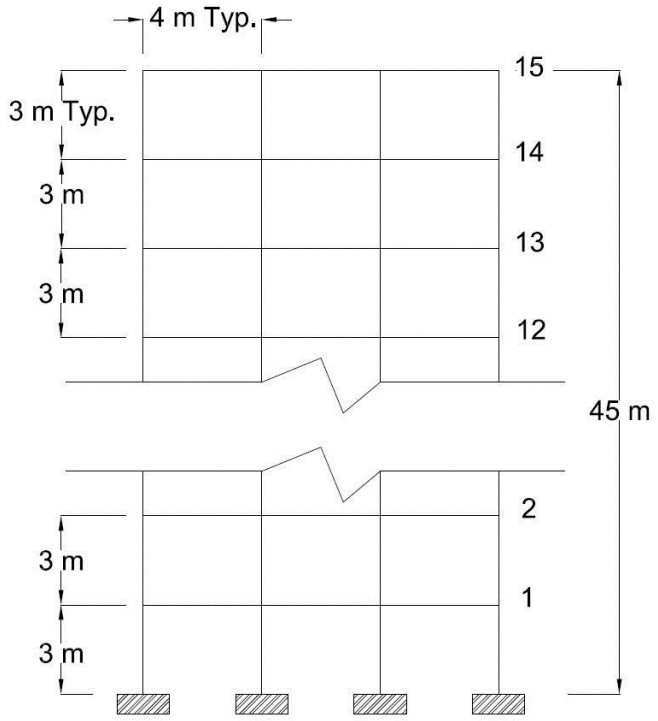

Figure 3.6. Frame Elevation of Building 3 – Fifteen-Story Concrete SMRF (the height of the structure was 45 m and each bay measured 4 m in width)

Hokmabadi et al. (2012) studied on how to properly analyze the response of a concrete SMRF using incremental non-linear inelastic dynamic analysis. Three design earthquakes were used for analysis: the 1995 Kobe, the 1994 Northridge and the 1940 El Centro earthquakes. Non-linear dynamic analysis was implemented using SAP2000 V.14 finite element software and peak story drifts were determined considering all time-steps (Hokmabadi et al., 2012). A damping ratio of 5% was used for each earthquake. Non-linear cyclic loadings were considered by varying the stiffness and gravitational loadings were also applied to the frame structure (Hokmabadi et al., 2012). Hokmabadi et al. (2012) presented a peak inter-story drift plot in his study and peak inter-story drift ratios found in Table 3.5.

Table 3.5. *Peak Inter-Story Drift from Literature Review – Building 3*

Building No.	Earthquake Motion	Peak Inter-Story Drift Ratio (%)
3	1995 Kobe	1.27
3	1994 Northridge	0.970
3	1940 El Centro	0.360

Note. Data from Hokmabadi et al. (2012).

3.4 Experimental Testing of APC Cladding

APC cladding has been tested experimentally for performance under various loading conditions, including seismic and blast. Several studies have examined the experimental testing of layered "sacrificial" cladding systems for blast loading (e.g., Linkute, Juocevicius, & Vaidogas, 2013; Van Paepegem et al., 2014). APC cladding systems are commonly used in construction and observing cladding performance under loadings such as seismic, blast, and wind is desirable and necessary for effective building design. In areas of high seismic activity an owner may need more detailed and expensive panels, and damage costs to the panels can be high warranting the need of insurance.

Dynamic testing places high emphasis on the behavior of the APC plates themselves as well as their connections, under lateral loading. APC cladding may need to have rigid connections if they are expected to resist lateral loads as shear walls. Otherwise, flexible panel connections may be designed to achieve zero absorption of the lateral energy. A "rocking mechanism" design using slot action, discussed in Section 1.3.2 can achieve desired flexibility. Experiments have examined the behavior of the

panels related to inter-story drift, as the cladding must perform adequately to account for it (e.g., Searer & Freeman, 2004; Carpenter, 2004). Fragility analysis of APC cladding has also been a focus of recent experimentation (e.g., Lee, Ham, & Kim, 2013; Olmati, Petrini, & Gkoumas, 2014).

3.5 The E-Defense TIPS Project Experiments – Emphasis on Experiment 5

NEES Project 571, also known as the TIPS Project - Tools to Facilitate Widespread Use of Isolation and Protective Systems, was a multi-faceted research study covering several aspects of structural response to seismic loading. The TIPS Project was led by Dr. Keri Ryan of the University of Nevada-Reno. Testing took place at three different facilities from October 2007 to September 2012: (1) State University of New York at Buffalo, NY, United States (2) University of California, Berkeley, CA, United States, and (3) Hyogo Earthquake Engineering Research Center (E-Defense), Miki, Japan. Testing for the TIPS Project occurred over a period of six years at three different facilities.

The shake table at E-Defense is one of the largest in the world located in Miki, Japan. Its dimensions measure 65 feet by 49 feet and it can support vertical loads of up to 2.5 million pounds (Hayama, n.d.). All of the shaking for the fixed-base building spanned approximately seven hours on August 31, 2011 (Dao & Ryan, 2012). Some input loading functions only considered X and Y planar motion while other loadings took into consideration all three dimensions. Target shake table accelerations were compared to actual accelerations of the shake table. This research only needed to consider the

actual accelerations experienced by shake table. Figure 3.7 shows the structure specimen on the shake table.

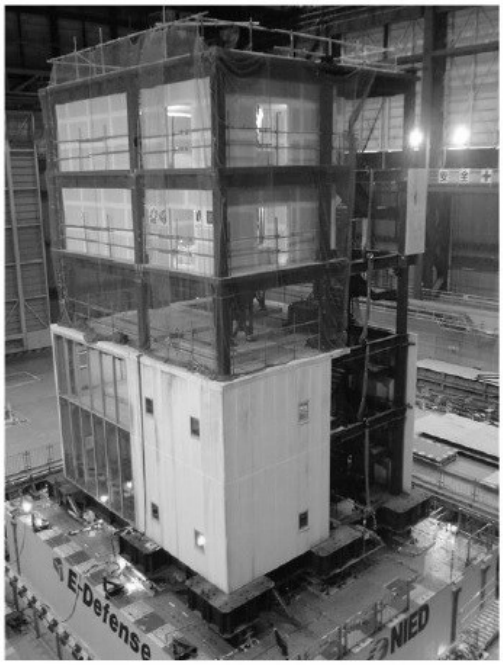

Figure 3.7. Structure Positioned on Shake Table at E-Defense (Ryan, n.d.)

Project 571 consisted of 14 experiments, 12 of which were experiments conducted when the test structure was supported with various isolation devices. For the 12 isolated experiments, inter-story drifts and floor accelerations were relatively small as the majority of distortion of the structure was contained in the isolation supports at the base. However two experiments were completed with a fixed-base configuration. The fixed-base configuration was obtained by bolting the base of the steel columns directly to the shake table platform. Thus all distortion of the structure during the experiment was a result of inter-story deflection with corresponding floor accelerations being comparable to the values seen in recorded earthquakes.

The intensities of the input ground motions of the fixed-base experiments were limited due to concerns of potential damage to the table and instrumentation in the event of partial structural collapse of the specimen. A "catch system" would have been necessary for protection of the shake table for the fixed-base building, as high accelerations and inter-story drifts were expected without the aid of the base isolating system. However, the funds were not available for this "catch system" and the experiment could only support inputs that would result in 4^{th} and 5^{th} floor inter-story drift ratios of approximately 1% and peak accelerations of approximately 1 g, exhibiting linear elastic behavior only (Ryan, n.d.). The building had a design drift of 0.5% (Ryan, n.d.).

The experiments of Project 571 are as listed in Table 3.6. These experiments tested and compared a variety of characteristics for fixed-base and base isolated configurations of the steel moment frame system, including post yield and limit state behavior. The experiments also included a wide variety of non-structural components and contents. This research focuses on the cladding testing of Experiment 5, which was funded as a part of the NEESR Grand Challenge Project: Simulation of the Seismic Performance of Non-structural Systems. Particularly, the cladding tests represented one type of standard US cladding façade design. The cladding tested was designed to accommodate inter-story drift through rocking of individual panels; hence panels were expected to lift off the lower level and rack horizontally to allow relative inter-story displacement.

Table 3.6. *Experiments of the TIPS Project 571*

Experiment*	Location	Date
Experiment 1: Stability of Elastomeric Bearings	State University of New York at Buffalo, NY, United States	2009
Experiment 2: Bi-Directional Characterization of Triple Friction Pendulum Isolators	University of California, Berkeley, CA, United States	2008
Experiment 3: Full Scale 5-story Building with Triple Pendulum Bearings at E-Defense	E-Defense, Miki, Japan	2011
Experiment 4: Full Scale 5-story Building with LRB/CLB Isolation System at E-Defense	E-Defense, Miki, Japan	2011
Experiment 5: Full Scale 5-story Building in Fixed-Base Condition at E-Defense	E-Defense, Miki, Japan	2011
Experiment 7: Berkeley - Intermediate Moment Frame Post Yield Behavior	University of California, Berkeley, CA, United States	2012
Experiment 8: Limit State Behavior of Base Isolated Structures: Fixed-Base Moment Frame	State University of New York at Buffalo, NY, United States	2010
Experiment 9: Limit State Behavior of Base Isolated Structures: Base Isolated Moment Frame without Impact	State University of New York at Buffalo, NY, United States	2010
Experiment 10: Limit State Behavior of Base Isolated Structures: Base Isolated Moment Frame with Impact on Concrete Moat Wall	State University of New York at Buffalo, NY, United States	2010
Experiment 11: Limit State Behavior of Base Isolated Structures: Base Isolated Moment Frame with Impact on Steel Moat Wall	State University of New York at Buffalo, NY, United States	2010
Experiment 12: Limit State Behavior of Base Isolated Structures: Base Isolated Moment Frame with Moat Wall Impact and Bumpers	State University of New York at Buffalo, NY, United States	2010
Experiment 13: Berkeley - Special Moment Resisting Frame Post Yield Behavior	University of California, Berkeley, CA, United States	2012
Experiment 14: Berkeley - Seismic Evaluation of Aged Lead Rubber Bearings	University of California, Berkeley, CA, United States	2012

*NEEShub does not document an Experiment 6

Results of the TIPS Project 571 are presented in numerous publications (Dao & Ryan, 2012; Dao & Ryan, 2013; Ryan, Dao, Sato, Sasaki, & Okazaki, 2012a; Ryan, Dao, Sato, Sasaki, & Okazaki, 2012b; Soroushian et al., 2012). All reports are available in the NEEShub repository. Each project of the NEES Project Warehouse has the project description/overview, experiments, team members, file browser, and reviews. Within the experiment subdivision, documentation and papers published in relation to the experiment are listed.

3.6 Building Overview

The building specimen of Experiment 5 consisted of a five-story steel moment frame structure, weighing nearly 1.2 million pounds (Ryan, n.d,). The building was lifted via crane from the shake table in order to remove the isolation dampers (Ryan, n.d.). The buildings plan dimensions were 10 m by 12 m with two bays in each direction. The transverse side had two bays each measuring 5 m. The longitudinal side had two bays, one measuring 7 m and the other 5 m. The 4^{th} and 5^{th} floor plan layouts were similar in dimension as shown in Figure 3.8. Accelerometers at the SE and NW corners are labeled for each floor. Note that the APC panels were installed between the 4^{th} floor and the 5^{th} floor and located around column X1-Y3 at the stairwell. Figure 3.8 also shows the X and Y coordinate directions as well as the North and South orientations for reference. The X direction contains gridlines, X1, X2, and X3. Similarly the Y direction is split into three gridlines, Y1, Y2, and Y3.

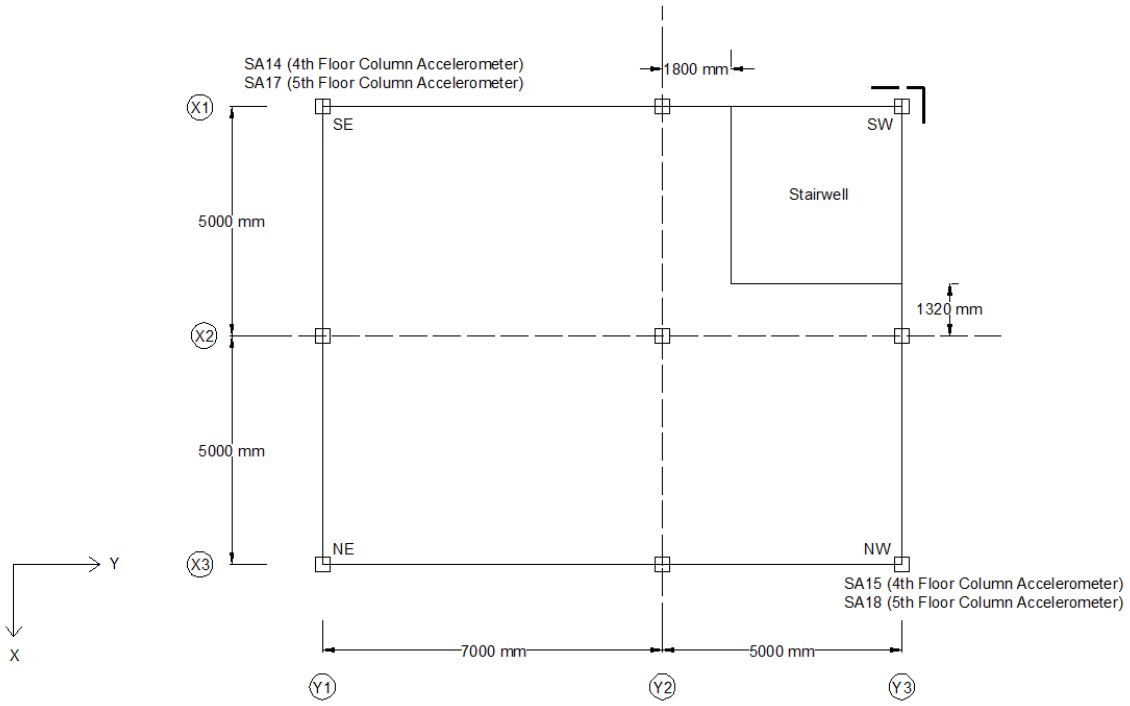

Figure 3.8. Typical Plan View of 4th and 5th Floors (dimensions and location of panels at the SW Corner are shown)

Elevation views of the structure and location of the panels on the 4th story are shown in Figure 3.9. The height of the building is 15.835 m. Floor 1 is the base of the table and floor 6 is the roof. Therefore, the fourth story refers to the story between the 4th and 5th floors. Stories 2 through 4 have equal heights of 3 m. Story 1 has a height of 3.85 m and story 5 has a height of 2.985 m. The building period is approximately 0.68 seconds (Ryan, n.d.). Material properties of the steel (beams and columns) and reinforced concrete (slabs) are shown in Tables 3.7 to 3.9.

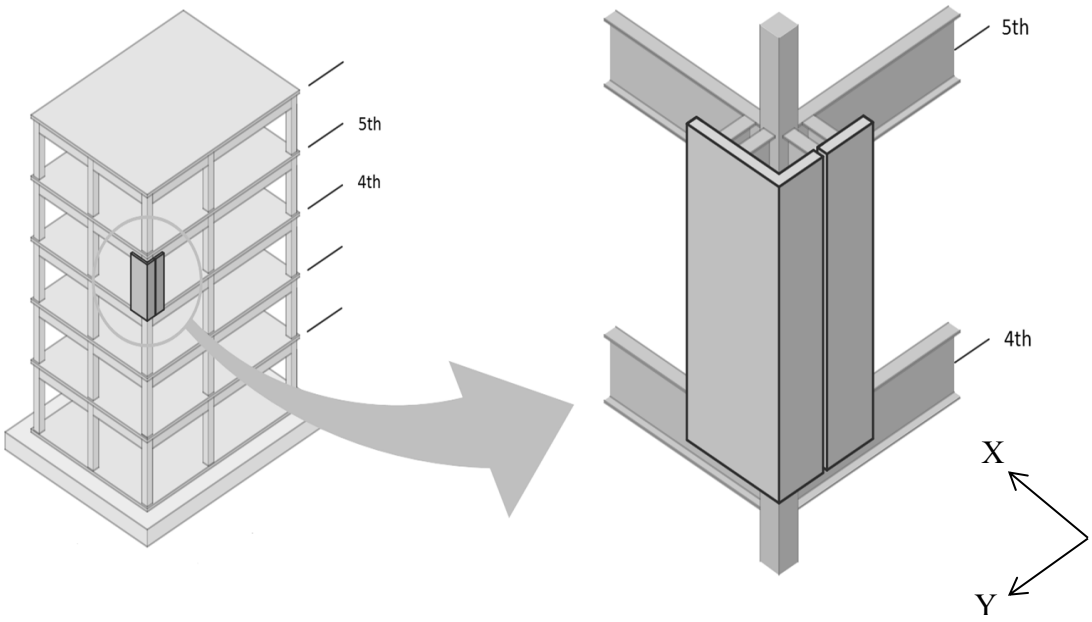

Figure 3.9. Sketch of Building Showing Locations of PD-1 and PD-2 and Coordinate Axes

Table 3.7. *Specified Yield and Ultimate Strength of Steel*

Member	**σ_{y} (MPa)**	**σ_{u} (MPa)**
Columns	295	325
Beams	400	490

Note. Data from Ryan (n.d.).

Table 3.8. *Yield and Ultimate Strength of Steel from Coupon Tests*

Member	**σ_{y} (MPa)**	**σ_{u} (MPa)**
Columns	346 - 398	430 - 470
Beams	331 - 422	510 - 557

Note. Data from Ryan (n.d.).

Table 3.9. *Reinforced Concrete Properties of Slab and Rebar*

Reinforced concrete properties	**σ (MPa)**
Compressive strength of the normal weight concrete used in the slabs	21
Compressive strength of standard samples	24
Nominal yield stress for the rebar	295

Note. Data from Ryan (n.d.).

3.7 Ground Motions used for Experimental Study

The analysis documented in this thesis specifically used data presented in Experiment 5. Experiment 5 used the ground motions of three different earthquakes: Imperial Valley Westmorland 1979 (WSM), Northridge Rinaldi 1994 (RRS), and Iwanuma (IWA). Each earthquake loading input function for the shake table was scaled in the X, Y, and Z directions to match a target response spectrum. Table 3.10 lists the scales used to achieve the target response spectrum and Table 3.11 lists the achieved peak table accelerations of the five ground motions conducted in the fixed-base configuration.

Table 3.10. *Scale Factors for Fixed-Base Experiment Input Ground Motions*

Test No.	Earthquake Record	Table Scale Factors			Comments
		Global X	Global Y	Global Z	
1	Westmorland (80WSM)	0.80	0.80	0.80	Applied to all three directions
2	Rinaldi (35RRSXY)	0.35	0.35	0	Applied only to X and Y directions
3	Rinaldi (35RRS)	0.35	0.35	0.35	Applied to all three directions
4	Rinaldi (88RRS)	0.35	0.35	0.88	Applied to all three directions
5	Iwanuma (70IWA)	0.70	0.70	0	Applied only to X and Y directions

Note. Data from Dao & Ryan (2012).

Table 3.11. *Fixed-Base Configuration Experiments – Peak Accelerations*

Test No.	Earthquake Record	Table Scale Factors			Comments
		Global X (g)	Global Y (g)	Global Z (g)	
1	Westmorland (80WSM)	0.219	0.175	0.136	Applied to all three directions
2	Rinaldi (35RRSXY)	0.201	0.398	0.011	Applied only to X and Y directions
3	Rinaldi (35RRS)	0.201	0.406	0.350	Applied to all three directions
4	Rinaldi (88RRS)	0.228	0.409	1.062	Applied to all three directions
5	Iwanuma (70IWA)	0.270	0.373	0.013	Applied only to X and Y directions

Note. Data from Dao & Ryan (2012).

3.7.1 Westmorland (WSM).

The 1979 Imperial Valley Earthquake had a magnitude of 6.53. The Westmorland Fire Station recorded a PGA of 0.249 g with a duration of 40 seconds (Dao & Ryan, 2012). The peak acceleration was recorded at the Westmorland Fire Station, and this input record is specifically referred to as 80WSM. Even though the input loading is referred to as "Westmorland," this is not to be confused with the Westmorland earthquake of 1981.

3.7.2 Northridge (RRS).

The 1994 Northridge Earthquake had a magnitude of 6.7 and occurred in San Fernando Valley region of Los Angeles, California. The Rinaldi Receiving Station logged the highest ground velocity ever recorded at 183 cm/sec (USGS, 2016). The

earthquake had a duration of 19.91 seconds and a PGA of 0.834 g (Dao & Ryan, 2012). The fixed-based experiment at E-Defense used three sets of scale factors: 35RRSXY, 35RRS, and 88RRS.

3.7.3 Iwanuma (IWA).

Iwanuma is a small city located in the region of Tohoku, Japan. The city experienced severe casualties from the tsunami that was triggered by the 2011 Tohoku earthquake, magnitude 9.0 (USGS, 2016). The earthquake had a maximum PGA of 2.7 g, which was recorded at Miyagi Prefecture Receiving Station, and lasted 6 minutes (Hayes, 2011). The shake table input motion had a duration of approximately 3.5 minutes. This input function is specifically referred to as 70IWA.

4 Experimental Design

Two full-height column cover APC panels were tested, a return cover 3D shape, and a flat panel (see Appendix A for panel detailing). The primary issues evaluated during the experimental testing were: 1) the effect of acceleration on the mass of the cladding panel, and 2) the effectiveness of the current slotted-bolt sliding connection to allow for inter-story earthquake motion.

4.1 Loading Protocol

While the shake table testing considered several input records of varying intensity, only three different input records were reviewed for this project: Iwanuma (IWA), Westmorland (WSM), and Northridge (RRS). For the acceleration evaluation, only the Iwanuma motion was evaluated. This experiment was chosen for the current study due to the relatively high table input accelerations of the record. While other experiments also contained high table accelerations, the research team felt the Iwanuma motion was representative of all the experiments. Drift data were evaluated for all three motions (Westmorland, Northridge and Iwanuma). The Northridge record was applied at three different scaling factors; hence, the drift was evaluated for a total of five experimental records.

4.2 Construction and Experimental Test Setup

Figures 4.1 to 4.5 are photos taken during construction and testing. Figure 4.1 displays the entire structure positioned on the shake table. Figures 4.2 and 4.3 show the bearing and slotted connections, respectively. Figure 4.4 shows the panels as they are situated on the corner of the 4th story.

Figure 4.1. Panels Mounted on Support Structure (Photo credit: Kurt McMullin, 2011)

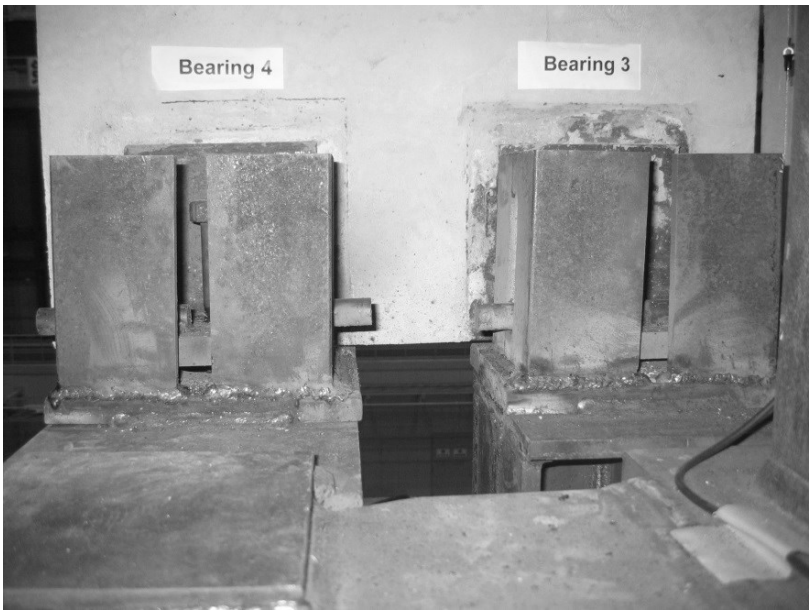

Figure 4.2. Bearing Connections at Base of 4th Floor (Photo credit: Maggie Ortiz, 2011)

Figure 4.3. Slotted Connections at Top of Panels at 5th Floor (Photo credit: Maggie Ortiz, 2011)

Figure 4.4. Accelerometer Instrumentation on Inside Face of Panel (Photo credit: Maggie Ortiz, 2011)

Displacement transducers, accelerometers, stringpots, and video cameras were the main measuring instrumentation. Instrumentation of both the building superstructure and the APC panels was used to capture the full range of data to evaluate the panel performance. A triaxial accelerometer was installed near the center of mass of each panel. Vertical displacement transducers (stringpots) were installed near two connections on each panel to record uplift of the panel and/or movement along the vertical slots of the connections. The accelerometer and stringpot nomenclature for the panels are summarized in Table 4.1. In addition, two video cameras were dedicated to the APC panels and were installed on the superstructure floors to collect qualitative data related to the movement of the panels. Figure 4.4 also shows the accelerometers and stringpots attached to the back face of the panels. The setup of the laser transducers used to measure the inter-story displacements are shown in Figure 4.5.

Table 4.1. *Nomenclature of the Panel-Specific Instruments that Recorded Quantitative Data*

Panel	Location of instrument	Instrument Type	Channel Number	Name
Return panel	Center of panel	Accelerometer	351	EA01X4_PANEL
Return panel	Center of panel	Accelerometer	352	EA01Y4_PANEL
Return panel	Center of panel	Accelerometer	353	EA01Z4_PANEL
Flat panel	Center of panel	Accelerometer	354	EA02X4_PANEL
Flat panel	Center of panel	Accelerometer	355	EA02Y4_PANEL
Flat panel	Center of panel	Accelerometer	356	EA02Z4_PANEL
Return panel	Top of panel	Stringpot	357	ED01Z_UPLIFT
Return panel	Bottom of panel	Stringpot	358	ED02Z_UPLIFT
Flat panel	Top of panel	Stringpot	359	ED03Z_UPLIFT
Flat panel	Bottom of panel	Stringpot	360	ED04Z_UPLIFT

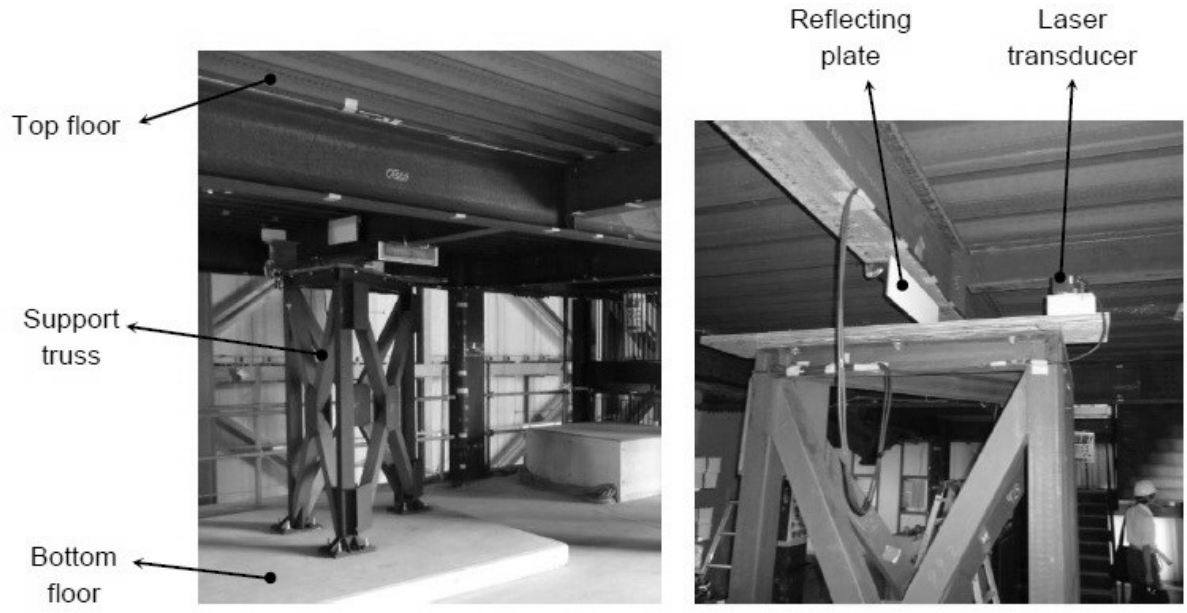

Figure 4.5. Laser Transducer and Reflecting Plate Instrumentation Mounted on Support Truss used for Measuring Inter-Story Drift (Ryan, n.d.)

In addition to the panel-dedicated instrumentation, data were collected to capture the global movement and behavior of the steel structure. Inter-story deflection was recorded by measuring the horizontal displacement between items cantilevered from the floor above and the floor below by means of a laser and reflective plate. Thus, inter-story deflections were directly measured during the experiment rather than obtained from double integration of the recorded accelerations.

The global behavior of the structure has been evaluated and reported (Dao & Ryan, 2012). Dao reported data based upon the geometric center of the floor rather than the center of mass. The geometric center is more easily determined and is at a constant location for all floors. Since the difference between the center of mass and the geometric

center of the floor is minimal, results from this research are also based on the geometric center of the floor.

Figure 4.6 shows the location layout for the displacement transducers for the 5th floor, typical for floors 2 through 5 (Dao & Ryan, 2012). The transducers measured both the X and Y inter-story displacements at the NW and SE corners of every story.

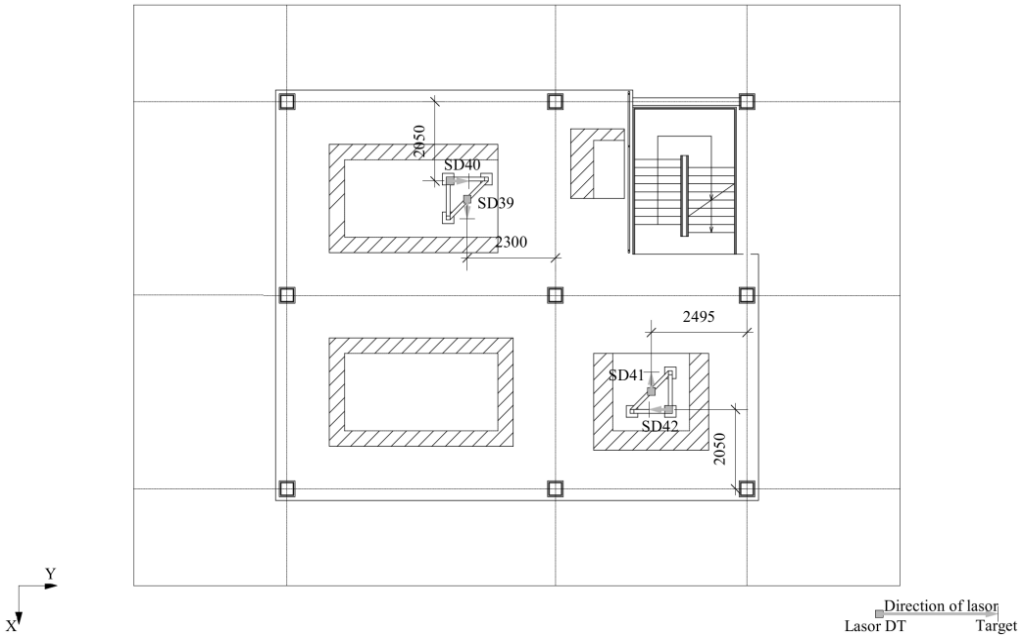

Figure 4.6. Plan View of Typical Location of Displacement Transducers used for Measuring Inter-Story Drift – 5th Floor is shown (Ryan, n.d.)

Figure 4.7 shows the layout and positioning of the accelerometers. There were six unidirectional accelerometers attached to each of floors 2 through 5, three underneath the floor and three above the floor. The accelerometers attached to the floor above and below only measured accelerations in the vertical direction. In addition, there was a triaxial accelerometer attached to the SE, NE, and NW corner columns of floors 2

through 5. The accelerometers measured acceleration in all three directions X, Y, and Z. There were no accelerometers placed at the floor connections of the panels, as there was a stairwell located in the SW corner of the building.

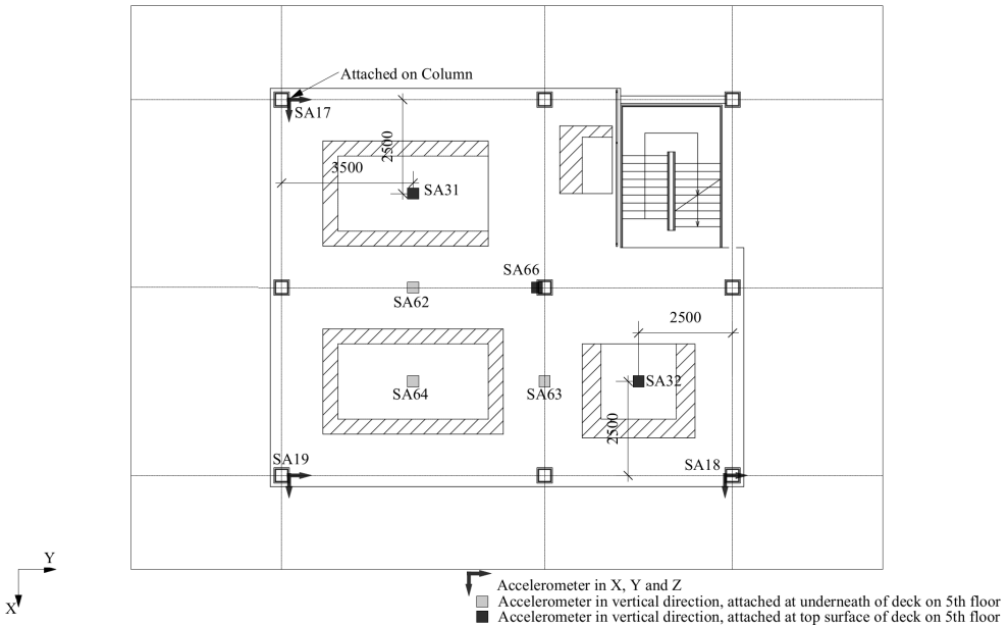

Figure 4.7. Typical Location of Accelerometers Attached to Floors and Columns of the Building Structure – 5th Floor is shown (Ryan, n.d.)

5 Setup for Data Reduction

Dynamic experiments develop a plethora of quantitative data. The 3D dynamic movement of the structural frame and APC panels results in multiple time steps that may cause critical loadings. These include the time step when each of the floors reach their peak displacement and when the panel-dedicated instruments reach their peak values. The time steps are very closely spaced, with intervals less than 0.1 seconds. Identifying the occurrence of these peak time steps was of interest for interpreting the behavioral aspects of the APC façade panels.

Processing the data for the global test specimen was previously conducted by the Nevada-Reno research team and made available through the NEEShub (and was discussed in the literature review). This study focused on processing the data collected by the panel-specific instruments as well as adapting the global test results to detailed study of the panels. For the data pertaining to the global test specimen, NEEShub datasets provide both unprocessed data and derived data (for inter-story drift and floor accelerations). The derived data are developed from the unprocessed data, and taken at the geometric center of the building. The derived data were produced by the Nevada-Reno research team. The author used the derived data available from the NEEShub repository and manipulated the values to determine acceleration and displacement of points of the support structure closer to the connection points of the panels.

5.1 Project 571 Fixed-Based Derived Inter-Story Drift

Dao & Ryan (2012) determined the derived inter-story drift data at the center of mass of the structure by interpolating the unprocessed data from the four transducers

located at the Southeast and Northwest corners of floors 2-5. Specifically, Equations 5.1 and 5.2 were used by the researchers at Nevada-Reno to produce the derived inter-story drift data. Figure 5.1 shows the distances L_1 and L_2 for interpolation in the global X direction. The transducer nomenclature as well as the values for L_1 and $L_2$are shown in Tables 5.1 and 5.2, respectively.

$$\delta_{XC} = \delta_{XSE} + \frac{L_1}{L_2} \times (\delta_{XNW} - \delta_{XSE}) \tag{5.1}$$

$$\delta_{YC} = \delta_{YNW} + \frac{L_1}{L_2} \times (\delta_{YSE} - \delta_{YNW}) \tag{5.2}$$

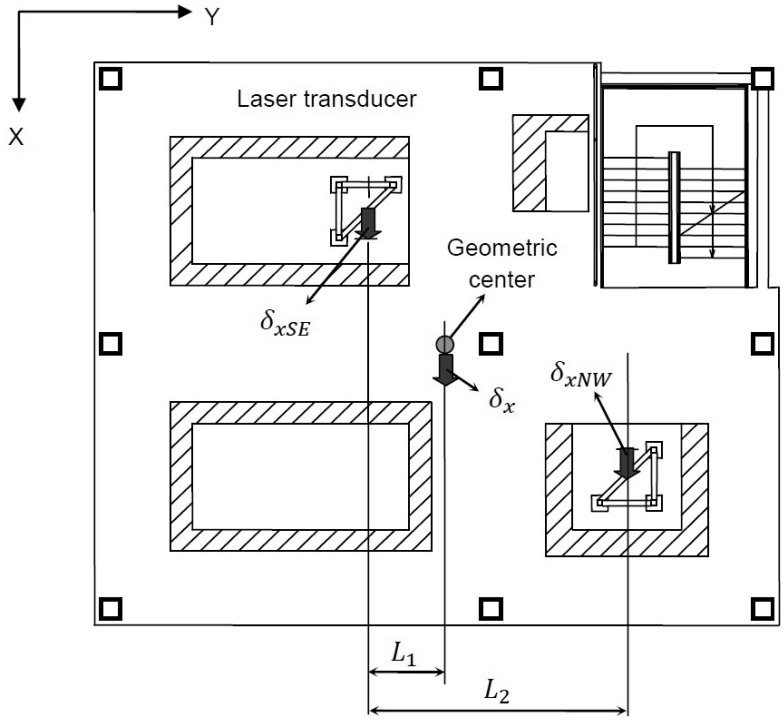

Figure 5.1. L1 and L2 for Interpolation of Raw Data to Compute Derived Drift at the Geometric Center (Ryan, n.d.)

Table 5.1. *Channels for Computing Horizontal Drift at Geometric Center*

Story	Drift	Channel Number	Name
1	δ_{xSE}	1313	SD23X1_DRIFT
	δ_{ySE}	1314	SD24Y1_DRIFT
	δ_{xNW}	1315	SD25X1_DRIFT
	δ_{yNW}	1316	SD26Y1_DRIFT
2	δ_{xSE}	1317	SD27X2_DRIFT
	δ_{ySE}	1318	SD28Y2_DRIFT
	δ_{xNW}	1319	SD29X2_DRIFT
	δ_{yNW}	1320	SD30Y2_DRIFT
3	δ_{xSE}	1321	SD31X3_DRIFT
	δ_{ySE}	1322	SD32Y3_DRIFT
	δ_{xNW}	1323	SD33X3_DRIFT
	δ_{yNW}	1324	SD34Y3_DRIFT
4	δ_{xSE}	1325	SD35X4_DRIFT
	δ_{ySE}	1326	SD36Y4_DRIFT
	δ_{xNW}	1327	SD37X4_DRIFT
	δ_{yNW}	1328	SD38Y4_DRIFT
5	δ_{xSE}	1329	SD39X5_DRIFT
	δ_{ySE}	1330	SD40Y5_DRIFT
	δ_{xNW}	1331	SD41X5_DRIFT
	δ_{yNW}	1332	SD42Y5_DRIFT

Note. Data from Ryan (n.d.).

Table 5.2. *Length L1 and L2 for Computing Inter-Story Drift at Center of Geometry*

	For Computing δ_{xC}		For Computing δ_{yC}	
Story	L_1 (mm)	L_2 (mm)	L_1 (mm)	L_2 (mm)
1	5365	10730	4635	9310
2	1310	4808	2950	5900
3	1295	4793	2940	5890
4	1300	4803	2950	5900
5	1300	4805	2950	5900

Note. Data from Ryan (n.d.).

5.2 Project 571 Fixed-Based Derived Acceleration

Dao & Ryan (2012) determined the derived floor acceleration data at the center of mass of the structure by interpolating the unprocessed data from the accelerometers attached to the columns located at the Southeast, Northwest, and Northeast corners of floors 2 to 5. Specifically, Equations 5.3 to 5.5 were used by researchers at Nevada-Reno to produce the derived floor acceleration data. Figure 4.7 shows the layout and positioning of the accelerometers. The accelerometer nomenclature is summarized in Table 5.3.

$$a_{XC} = \frac{1}{2} \times \left(\frac{a_{XSE} + a_{XNE}}{2} + a_{XNW}\right) \tag{5.3}$$

$$a_{YC} = \frac{1}{2} \times \left(\frac{a_{YNW} + a_{YNE}}{2} + a_{YSE}\right) \tag{5.4}$$

$$a_{ZC} = \frac{1}{3} \times \left(a_{ZNW} + a_{ZNE} + a_{ZSE}\right) \tag{5.5}$$

Table 5.3. *Channels for Computing Horizontal Acceleration at Geometric Centers*

Floor	Acceleration	Channel Number	Name
4	a_{XSE},	0328	SA14X4_COLUMN
	a_{YSE}	0329	SA14Y4_COLUMN
	a_{XNW}	0331	SA15X4_COLUMN
	a_{YNW}	0332	SA15Y4_COLUMN
	a_{XNE}	0334	SA16X4_COLUMN
	a_{YNE}	0335	SA16Y4_COLUMN
	a_{ZSE}	0330	SA14Z4_COLUMN
	a_{ZNW}	0342	SA15Z4_COLUMN
	a_{ZNE}	0345	SA16Z4_COLUMN
5	a_{XSE}	0337	SA17X5_COLUMN
	a_{YSE}	0338	SA17Y5_COLUMN
	a_{XNW}	0340	SA18X5_COLUMN
	a_{YNW}	0341	SA18Y5_COLUMN
	a_{XNE}	0343	SA19X5_COLUMN
	a_{YNE}	0344	SA19Y5_COLUMN
	a_{ZSE}	0339	SA17Z5_COLUMN
	a_{ZNW}	0342	SA18Z5_COLUMN
	a_{ZNE}	0345	SA19Z5_COLUMN

Note. Data from Ryan (n.d.).

5.3 Local Coordinates of Connection Links

Defining the local coordinates of the support points for the APC panel was necessary. Panel behavior was more closely related to the relative orientation of the panel to the structural frame, than to the structure foundation. Hence, a local coordinate system for panels was defined based upon the orientation of the panel to the supporting frame. Each panel had a separate local coordinate system. Figure 5.2 illustrates the local coordinate system defined for APC panels. Local coordinate U1 represents out-of-plane behavior where the plane is defined by the four connections supporting the panel. The

U2 direction is taken as acting upward. The U3 direction is in-plane shear movement and is the cross-product of U1 and U2. Since the panels tested were on adjoining elevations of the building these local coordinates align with different global coordinates. Table 5.4 depicts the local and corresponding global coordinates of both panels as well as their positive and negative directions.

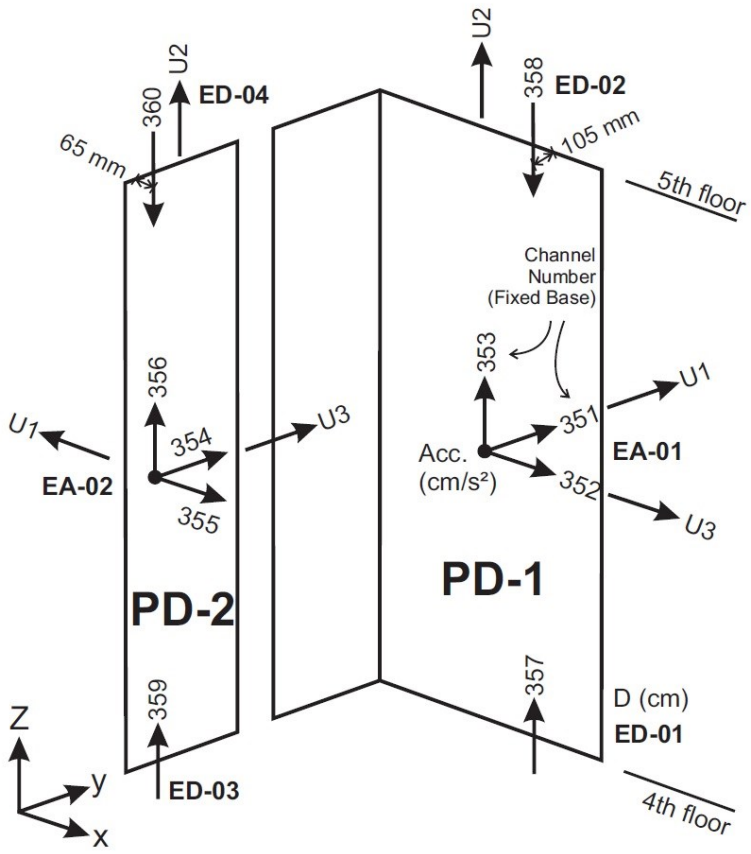

Figure 5.2. Local and Global Coordinates of the Building and APC Panels

Table 5.4. *Local and Global Coordinates for PD-1 Return Panel and PD-2 Flat Panel*

	Local Coordinates	Corresponding Global Coordinates
PD-1 Return Panel	U1	(+) Y
	U2	(+) Z
	U3	(+) X
PD-2 Flat Panel	U1	(-) X
	U2	(+) Z
	U3	(+) Y

6 Displacement and Drift Data

The primary research question for the study was how modern APC systems behave in major earthquakes. Deflection of the panel could be determined using either the inter-story drift of the floor center or of the floor corner where the panels were located. One hypothesis was that the center inter-story drift equaled the corner inter-story drift. The other hypothesis was that center and corner inter-story drifts would differ significantly enough from one another that they would need to be considered separately. If the latter possibility was true, then the center inter-story drift of the building should not be modeled as equivalent to the drift of the panel.

6.1 Center Inter-Story Drift Ratios

Table 6.1 lists the peak center inter-story drifts recorded during all five fixed-base motions at E-Defense. Published data from researchers indicate peak inter-story drift ratio demands ranging from 0.0036 to 0.0438 radians (Hokmabadi et al., 2012; Zona et al., 2008; Sabelli et al., 2003). Peak inter-story drift results for each publication are reported in Table 6.2. The 35Rinaldi ground motion input produced a maximum center floor inter-story drift of 0.903%. Thus the peak story drift demands achieved during the experimental study at E-Defense were generally smaller, but still fell within this range, compared to the demands published by various researchers. This was expected as the response of the E-Defense experiment was restricted to remain in the linear elastic region. The drift ranges suggest that the input intensities of the scaled fixed-based experiments at E-Defense were relatively smaller than the input intensities of the experiments of Sabelli

et al. (2003), Zona et al. (2008), & Hokmabadi et al. (2012) studied in the literature review.

Table 6.1. *Peak Drift Demand from all Five Earthquake Motions run at E-Defense (all stories considered)*

Earthquake Motion	**Inter-Story Drift Ratio at Center of Building (%)**
Westmorland	0.360
35RinaldiXY	0.896
35Rinaldi	0.903
88Rinaldi	0.887
Iwanuma	0.857

Table 6.2. *Peak Drift Demand from Literature Review – Reported Drift (all stories considered)*

Building No.	**Earthquake Motion**	**Inter-Story Drift Ratio at Center of Building (%)**
1	50% 50-year probability exceedance	1.00
1	10% 50-year probability exceedance	1.38
1	2% 50-year probability exceedance	4.38
2a	1994 Northridge	1.70
2b	1994 Northridge	1.72
2c	1994 Northridge	1.72
2d	1994 Northridge	1.71
3	1995 Kobe	1.27
3	1994 Northridge	0.970
3	1940 El Centro	0.360

Note. Data from Sabelli et al. (2003), Zona et al. (2008), & Hokmabadi et al. (2012).

6.2 Corner Inter-Story Drift Ratios

Of primary interest to the present study is how the corners of the building moved as these were the support points of the APC panels. The panels were mounted on the corner of the building with the floor opening of the staircase. This corner allowed for the panels to be installed without interaction with other components of the building. At this corner column, it was possible that non-rigid diaphragm behavior could occur since the slab did not reach this corner column (X1/Y3) and the flexibility of the floor beams might allow non-rigid diaphragm behavior to occur. However, the relative size of the floor opening and the stout beams used for the steel superstructure limited the potential flexibility of the floor and all calculations were made with the expectation that the floor diaphragm was rigid. Thus, combining the contribution of the story torsion with the inter-story drift of the building allowed for the determination of the corner movement.

Corner movement was reported in the U1 or U3 directions of each panel. The design intent of using four vertically slotted connections was expected to allow for significant in-plane (U3) inter-story drift to occur without damage to the panels. Inter-story deflection in the U1 direction was expected to have limited influence on the performance of the panel. The connections were not designed for "rocking" in the U1 direction, so the limited influence is because the panel connections were spaced a story level apart thus allowing movement out-of-plane.

Global building movement was calculated and reported by Dao & Ryan (2012). Dao converted the recorded data of story deflection and reported it as movement of the center of the building and torsional twist of the stories. All inter-story drift data were

reported as inter-story drift ratio, the ratio of the inter-story deflection and the relative story height (H). Torsional twist of the building was determined by Dao and calculated based upon the structural geometric properties of the floor plan and the recorded instrument data. Figure 6.1 depicts the final drift (in the X direction) at the SW corner of the structure where the panels were located.

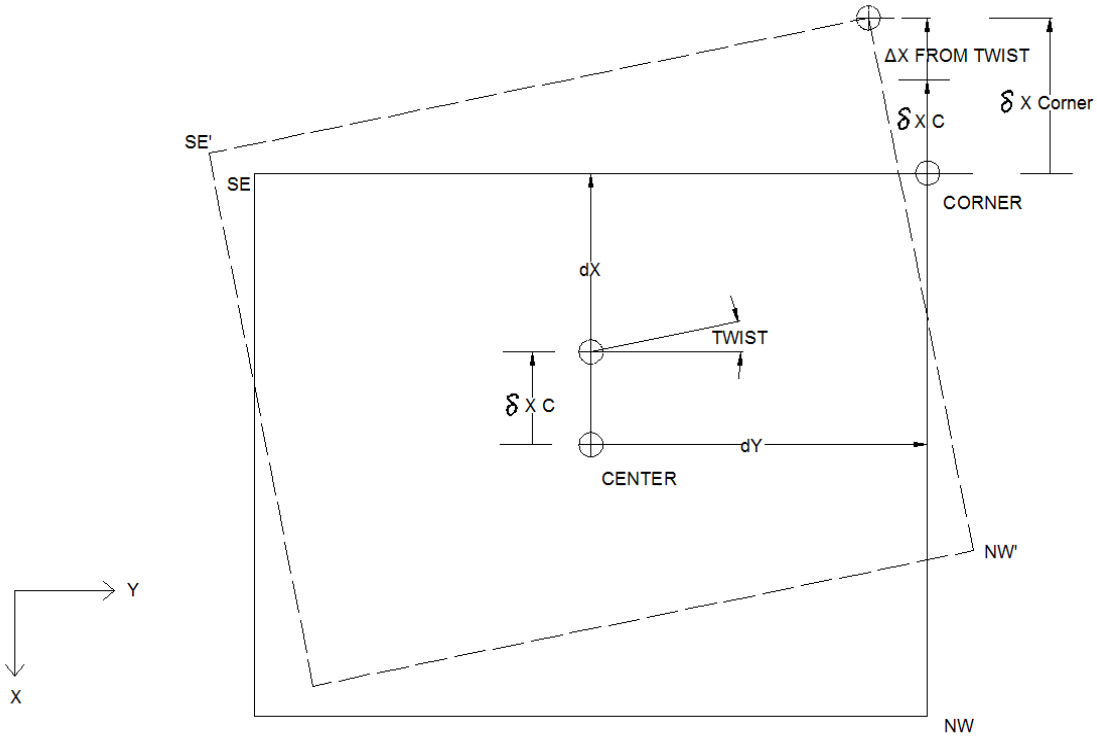

Figure 6.1. Final Drift at the SW Corner of Structure (note that story height (H) is 3 m)

The inter-story twist data were reported in radians, representing the rotation of one floor with respect to the floor above (or below). Therefore, the lateral movement in the X and Y directions at the corner due to twist is the rotation of the floor multiplied by the distance (dY or dX, respectively) to the corner. The drift ratio due to twist is then the lateral movement in the X and Y directions at the corner, caused by the twist, divided by

the story height (H) of 3 m. Figure 6.1 shows the combination of a negative X directional drift, from a positive twist, combined with a negative X directional center drift.

The peak values of each of these vectors of data (center drift data and twist drift data) are listed in Tables 6.3 and 6.4. It is notable that each of these peak values of drift is a function of time. It is likely that the peak value of either drift ratio occurs at a time step that is unique compared to the other drift ratio. Thus the critical time steps were identified for the two distinct points: (1) the maximum value of the inter-story drift occurring at the center of the building and (2) the maximum value of the inter-story drift occurring due to twist or torsion of the floor. All of these critical time steps for each trial are listed in Tables 6.3 and 6.4 as well. Tables 6.3 and 6.4 show that the ratios of peak 4th story torsional drift to peak center drift were as much as 0.43. It was therefore determined that drift from torsion was significant enough to be considered, and corner drift would need to be calculated for the analysis.

Table 6.3. *Peak Displacement and Twist Data – Inter-Story Drift Ratios of Levels 4 and 5 – Global X Direction*

Earthquake Motion	**Peak Inter-story Drift Ratio at Center of Building**	**Peak Inter-story Drift Ratio from Twist**	**Ratio of Peak Twist Drift to Peak Center Drift**
	% (seconds)	**% (seconds)**	
Westmorland	0.264 (18.135)	0.0582 (18.41)	0.220
35RinaldiXY	0.330 (8.911)	0.105 (8.903)	0.318
35Rinaldi	0.337 (8.890)	0.112 (8.843)	0.332
88Rinaldi	0.335 (8.900)	0.145 (8.845)	0.433
Iwanuma	0.511 (75.266)	0.157 (111.108)	0.307

Table 6.4. *Peak Displacement and Twist Data – Inter-Story Drift Ratios of Levels 4 and 5 – Global Y direction*

Earthquake Motion	**Peak Inter-story Drift Ratio at Center of Building** **% (seconds)**	**Peak Inter-story Drift Ratio from Twist** **% (seconds)**	**Ratio of Peak Twist Drift to Peak Center Drift**
Westmorland	0.280 (22.422)	0.0485 (18.41)	0.173
35RinaldiXY	0.603 (8.972)	0.088 (8.903)	0.146
35Rinaldi	0.619 (8.953)	0.093 (8.843)	0.150
88Rinaldi	0.652 (8.941)	0.121 (8.845)	0.186
Iwanuma	0.653 (77.456)	0.131 (111.108)	0.200

At any time step, the orthogonal component of drift due to twist/torsion was combined with the corresponding drift due to translation, to determine a total drift at the corner. Thus, the corner inter-story drift ratios in both the X and Y directions were calculated using Equations 6.1 and 6.2 (visually depicted in Figure 6.1).

$$\delta_{XCorner} = \delta_{XC} + \frac{\theta_t \times d_Y}{H} \qquad \text{(where } \theta_t \text{ in radians)} \qquad (6.1)$$

$$\delta_{YCorner} = \delta_{YC} + \frac{\theta_t \times d_X}{H} \qquad \text{(where } \theta_t \text{ in radians)} \qquad (6.2)$$

The inter-story drift differed significantly depending upon whether torsional effects were considered or not. Hence, the two directions or components of drift (linear and torsional) needed to be considered separately. Tables 6.5 and 6.6 show the peak center and corner inter-story drift ratios calculated for each earthquake. Twist and center drift counteracted one another in the global X direction, whereas they complemented one another in the global Y direction. The largest difference between corner and center inter-

story drift in the global X direction occurs in the 35RinaldiXY trial, where the corner inter-story drift is ~32% less than the center inter-story drift. The largest difference between corner and center inter-story drift in the global Y direction occurs during the 88Rinaldi trial, where the corner inter-story drift is ~16% greater than the center inter-story drift.

Table 6.5. *Peak Panel Displacement Considering Twist – Inter-Story Drift Ratios of Levels 4 and 5 – Global X Direction*

Earthquake Motion	**Time Step (seconds)**	**Inter-Story Drift Ratio at Center of Building (%)**	**Inter-Story Drift Ratio at Column X1/Y3 (%)**	**Panel PD-1 U3 (in-plane) Deflection (mm)**	**Panel PD-2 U1 (out-of-plane) Deflection**
Westmorland	18.583	0.248	0.239	7.17	
35RinaldiXY	8.911	0.330	0.224	6.72	
35Rinaldi	8.889	0.336	0.233	6.99	
88Rinaldi	8.895	0.334	0.241	7.23	
Iwanuma	75.258	0.508	0.436	13.1	

Table 6.6. *Peak Panel Displacement Considering Twist – Inter-Story Drift Ratios of Levels 4 and 5 – Global Y Direction*

Earthquake Motion	Time Step (seconds)	Inter-Story Drift Ratio at Center of Building (%)	Inter-Story Drift Ratio at Column X1/Y3 (%)	Panel PD-1 U1 (out-of-plane) Deflection (mm)	Panel PD-2 U3 (in-plane) Deflection
Westmorland	22.426	0.280	0.282	8.46	
35RinaldiXY	8.965	0.602	0.679	20.4	
35Rinaldi	8.93	0.609	0.693	20.8	
88Rinaldi	8.936	0.651	0.756	22.7	
Iwanuma	76.565	0.636	0.746	22.4	

6.3 Panel Deflection Performance

As center and corner inter-story drift differed significantly, the corner inter-story drift was considered more appropriate for determining the deflection of the panel. Therefore inter-story deflection of the panel was determined by Equation 6.3:

$$Panel_{Deflection} = Drift_{CornerX1/Y3} * Height_{Panel/Floor} \quad (6.3)$$

The value $Drift_{CornerX1/Y3}$ is the corner drift determined from Equations 6.1 and 6.2. The value of $Height_{Panel/Floor}$ is 3 m (as the panels span the story depth). With 4th story corner inter-story drift ratios as high as 0.756% (22.7 mm panel deflection), there was no damage detected the APC panels or their connections. Complete drift and deflection data of the panels are also summarized in Tables 6.5 and 6.6.

When appropriate, engineers conventionally report drift at the center of mass of a building (for simplicity and convenience of design). However, as discussed previously, the difference between drift at the center of the structure and the corner was found to be significant. This may be especially apparent when considering irregular building geometries. Determining this critical difference of when it becomes inappropriate to use the center of mass drifts will be a necessary task for future research.

6.4 Uplift and Rocking Behavior of Panels

Panel displacement data were used to examine the "rocking" behavior of both panels for the Iwanuma earthquake motion. Peaks in vertical acceleration were expected to occur when the bottom of the panel returned to the floor. Vertical panel displacement uplift time-history data of the bottom connections of the return panel is found in Figure 6.2 and for the flat panel in Figure 6.3. The peak vertical displacements experienced by the return panel and flat panel were 2.43 mm and 1.19 mm, respectively. These displacements are quite small, particularly in comparison to the size of the panel. Both of these peaks occurred around the 75 second time step of the earthquake motion.

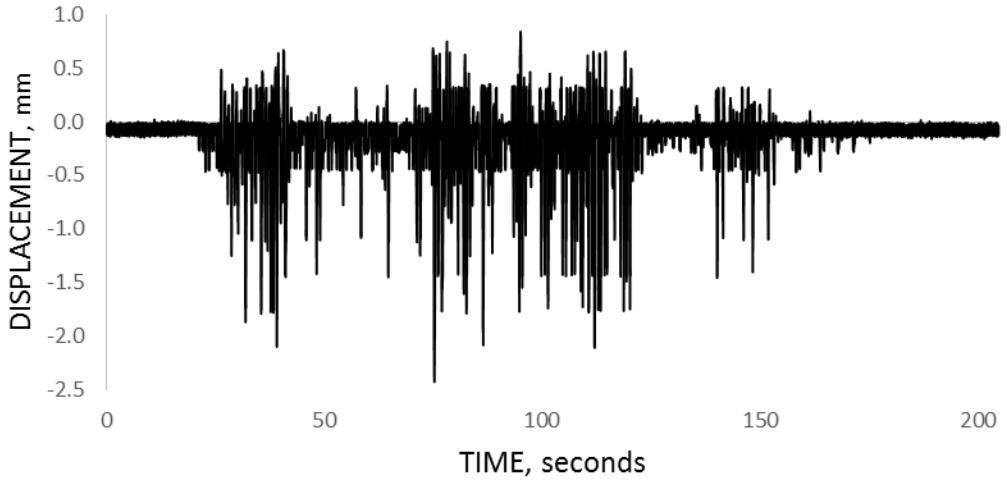

Figure 6.2. Return Panel Uplift Displacement Plot (bottom connection)

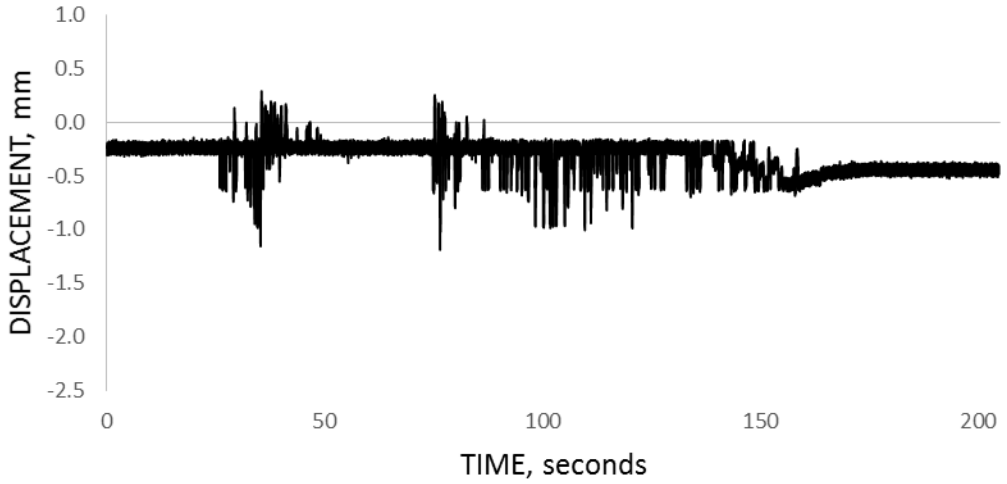

Figure 6.3. Flat Panel Uplift Displacement Plot (bottom connection)

7 Acceleration Data

7.1 Floor Acceleration Data

Floor acceleration data collected during the 70 IWA fixed-base experiment were tabulated and plotted in time histories to detect trends and develop relationships. All peak accelerations occurred around the 75 second time step mark of the earthquake. The 5 second time interval, from 75 to 80 seconds, was chosen specifically because each floor experienced peak center and corner accelerations within this time frame.

The X and Y components of the floor accelerations were measured using accelerometers at the SE, NE, and NW corners of the building. As reported by Ryan (2013), Equations 5.3 and 5.4 were derived to determine the floor center accelerations from the unprocessed data in the X and Y directions. This study used the same accelerometers for extrapolating the floor corner accelerations. As the floors were assumed rigid, the X component of acceleration from the NW accelerometer readings were equal to the SW corner components of acceleration in the X direction. Similarly, the Y component of acceleration from the SE accelerometer readings were equal to the SW corner components of acceleration in the Y direction. Using this extrapolation, Equations 7.1 and 7.2 were used for the acceleration at the SW corner of the structure (at the panel connection points). The accelerometer nomenclature is listed in Table 5.3.

$$a_{SW,\ X-\ Corner} = a_{XNW} \tag{7.1}$$

$$a_{SW,\ Y-\ Corner} = a_{YSE} \tag{7.2}$$

7.1.1 Horizontal acceleration.

Horizontal acceleration of the 4th and 5th stories was of interest in observing the behavior of the panels. The difference in peak value of each acceleration time history was quite apparent when comparing center and corner accelerations in their respective directions. Figures 7.1 to 7.4 are time histories comparing center and corner floor accelerations, for both the 4th and 5th floors. Though Figures 7.2 and 7.4 do show that Y direction accelerations are similar for the 4th and 5th floors, there are noticeable acceleration differences in the X direction as shown in Figures 7.1 and 7.3. Insufficient data were available to suggest that the variation was a result of instrumentation placement, instrumentation error, building geometry, panel weight or any other factors that may contribute. Regardless, Figures 7.1 and 7.3 demonstrate that significant differences in acceleration can occur between center and corner floor geometric location.

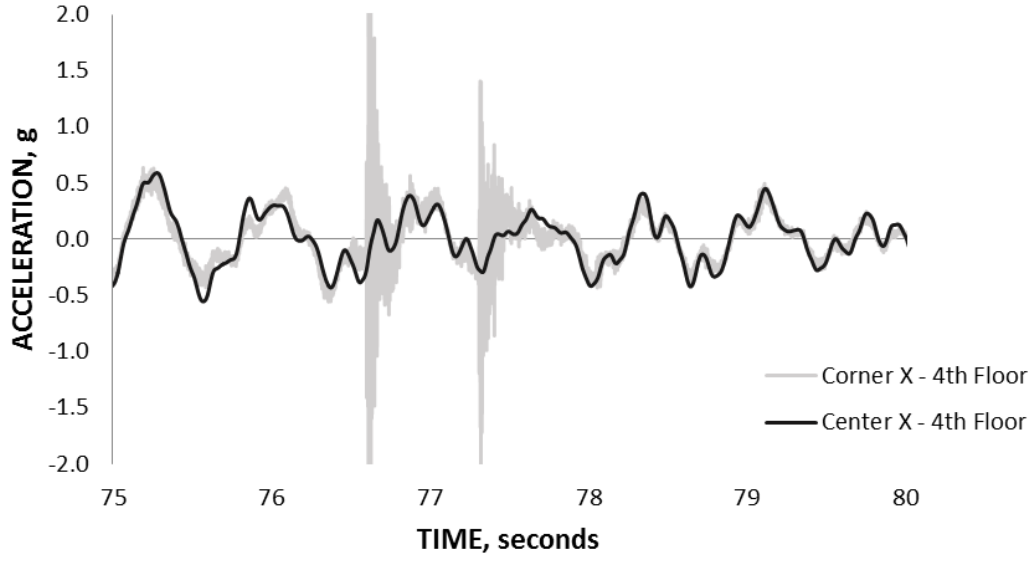

Figure 7.1. 4th Floor Acceleration - Center and Corner of Floor - X Direction

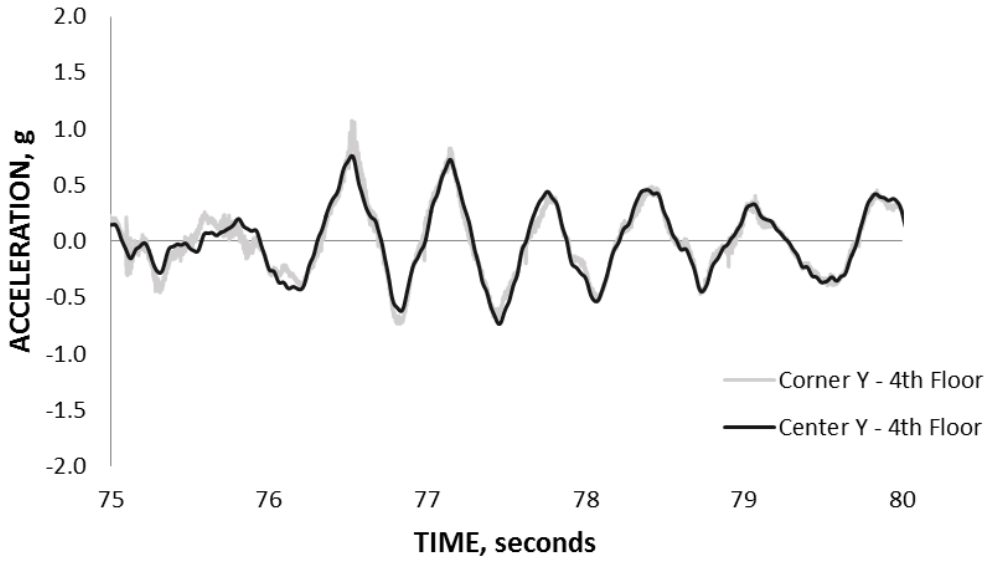

Figure 7.2. 4th Floor Acceleration - Center and Corner of Floor - Y Direction

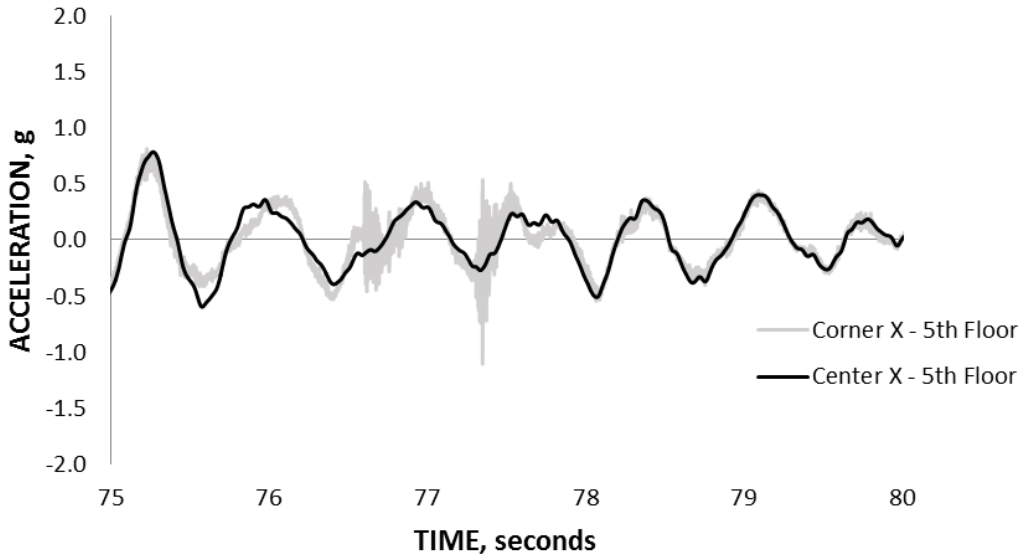

Figure 7.3. 5th Floor Acceleration - Center and Corner of Floor - X Direction

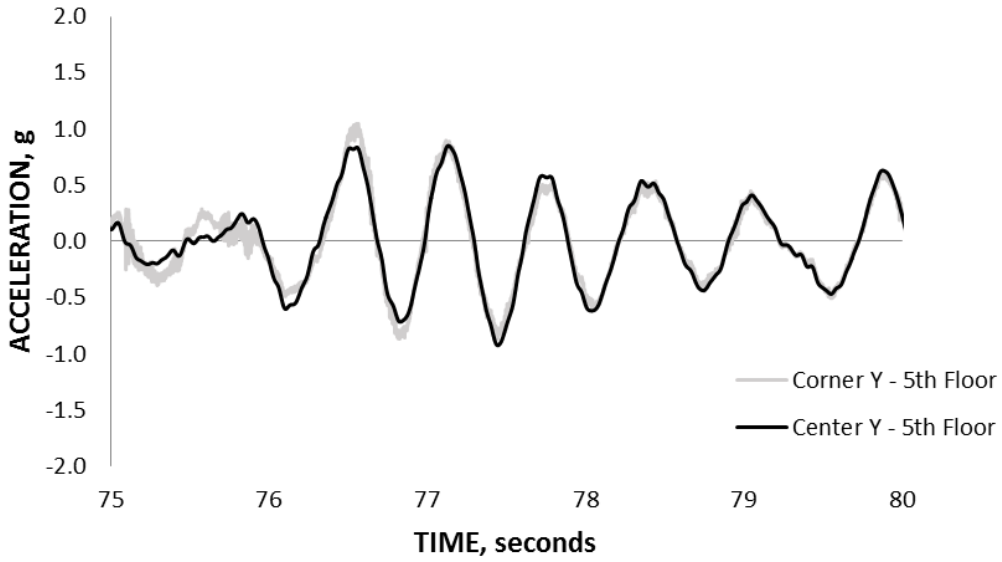

Figure 7.4. 5th Floor Acceleration - Center and Corner of Floor - Y Direction

Had the peak acceleration time histories at the center and corner been similar in each direction at each time step, then perhaps center and corner data could both be used interchangeably to depict the behavior of the panels. During some time frames, the plots show variation far greater than 5% g, such as at the ~77.3 time step of Figure 7.3. As the accelerations do vary by location, it is in fact appropriate to determine the acceleration at the location of the panels. Therefore the corner accelerations should be considered when discussing the panel behaviors. These values are used for acceleration amplification in Section 7.3.

Tables 7.1 to 7.4 show center and corner accelerations of the 4th and 5th floors in the global X and Y directions. The peak floor accelerations are listed as well as the floor accelerations corresponding to the peak panel acceleration responses. Fourth floor peak corner accelerations were greater than fifth floor peak accelerations at the corner, for both

the X and Y directions. However, this trend was opposite for the center of the floor plan. Fourth floor peak corner accelerations were smaller than fifth floor peak accelerations at the center, in both the X and Y directions. Though the accelerations differed in this manner, the ranges were still similar. The 4^{th} and 5^{th} floors experienced similar ranges of acceleration in both X and Y directions at the center and likewise at the corner. The exception is 4^{th} and 5^{th} floor peak accelerations in the X direction of 2.93 g and 1.10 g, respectively. Corner peak accelerations were larger than center floor accelerations for both the 4^{th} and 5^{th} floors, in both X and Y directions. Specifically, fourth floor corner acceleration in the X direction of 2.93 g was greater than fourth floor center acceleration in the X direction of 0.59 g by a factor of about five.

Table 7.1. *Iwanuma Acceleration Data – 4th and 5th Floor Corner (X) and Panels (U1, U2, U3)*

Time Step (sec)	**Level 4 Corner X** (g)	**Level 5 Corner X** (g)	**Panel PD-1 U3** (g)	**Panel PD-2 U1** (g)	**Panel PD-1 U1** (g)	**Panel PD-2 U3** (g)	**Panel PD-1 U2** (g)	**Panel PD-2 U2** (g)
35.271	0.11	0.11	0.14	0.70	0.56	1.73	0.19	**1.11**
35.276	0.10	0.14	0.13	**2.01**	0.36	1.36	0.04	0.03
37.111	0.03	0.10	0.26	0.08	0.12	0.13	**0.40**	0.00
75.178	0.44	0.51	**1.21**	0.73	0.24	0.15	0.08	0.11
76.505	0.15	0.13	0.04	0.70	0.97	**3.37**	0.01	0.20
76.512	0.15	0.07	0.07	1.53	**1.48**	0.41	0.03	0.07
76.627	**2.93**	0.21	0.02	0.12	0.27	0.84	0.02	0.04
77.350	0.63	**1.10**	0.59	0.16	0.37	0.26	0.20	0.10
Max. Value	2.93	1.10	1.21	2.01	1.48	3.37	0.40	1.11

Note. Floor X direction is in-plane with PD-1 and out-of-plane with PD-2 (see Figure 5.2).

Table 7.2. *Iwanuma Acceleration Data – 4th and 5th Floor Corner (Y) and Panels (U1, U2, U3)*

Time Step (sec)	**Level 4 Corner Y (g)**	**Level 5 Corner Y (g)**	**Panel PD-1 U1 (g)**	**Panel PD-2 U3 (g)**	**Panel PD-1 U3 (g)**	**Panel PD-2 U1 (g)**	**Panel PD-1 U2 (g)**	**Panel PD-2 U2 (g)**
35.271	0.53	0.70	0.56	1.73	0.14	0.70	0.19	**1.11**
35.276	0.51	0.66	0.36	1.36	0.13	**2.01**	0.04	0.03
37.111	0.09	0.15	0.12	0.13	0.26	0.08	**0.40**	0.00
75.178	0.12	0.19	0.24	0.15	**1.21**	0.73	0.08	0.11
76.505	0.78	0.90	0.97	**3.37**	0.04	0.70	0.01	0.20
76.512	0.97	0.94	**1.48**	0.41	0.07	1.53	0.03	0.07
76.524	**1.07**	0.99	0.58	0.60	0.19	1.23	0.13	0.14
76.565	0.78	**1.05**	1.00	0.21	0.07	0.25	0.08	0.04
Max. Value	1.07	1.05	1.48	3.37	1.21	2.01	0.40	1.11

Note. Floor Y direction is out-of-plane with PD-1 and in-plane with PD-2 (see Figure 5.2).

Table 7.3. *Iwanuma Acceleration Data – 4th and 5th Floor Center (X) and Panels (U1, U2, U3)*

Time Step (sec)	**Level 4 Center X (g)**	**Level 5 Center X (g)**	**Panel PD-1 U3 (g)**	**Panel PD-2 U1 (g)**	**Panel PD-1 U1 (g)**	**Panel PD-2 U3 (g)**	**Panel PD-1 U2 (g)**	**Panel PD-2 U2 (g)**
35.271	0.12	0.16	0.14	0.70	0.56	1.73	0.19	**1.11**
35.276	0.11	0.14	0.13	**2.01**	0.36	1.36	0.04	0.03
37.111	0.08	0.02	0.26	0.08	0.12	0.13	**0.40**	0.00
75.178	0.45	0.53	**1.21**	0.73	0.24	0.15	0.08	0.11
75.27	**0.59**	**0.78**	0.27	1.06	0.12	0.28	0.06	0.08
75.28	0.59	0.78	0.71	0.53	0.45	0.38	0.08	0.10
76.505	0.20	0.26	0.04	0.70	0.97	**3.37**	0.01	0.20
76.512	0.22	0.25	0.07	1.53	**1.48**	0.41	0.03	0.07
Max. Value	0.59	0.78	1.21	2.01	1.48	3.37	0.40	1.11

Note. Floor X direction is in-plane with PD-1 and out-of-plane with PD-2 (see Figure 5.2).

Table 7.4. *Iwanuma Acceleration Data – 4th and 5th Floor Center (Y) and Panels (U1, U2, U3)*

Time Step (sec)	**Level 4 Center Y** (g)	**Level 5 Center Y** (g)	**Panel PD-1 U1** (g)	**Panel PD-2 U3** (g)	**Panel PD-1 U3** (g)	**Panel PD-2 U1** (g)	**Panel PD-1 U2** (g)	**Panel PD-2 U2** (g)
35.271	0.53	0.67	0.56	1.73	0.14	0.70	0.19	**1.11**
35.276	0.51	0.68	0.36	1.36	0.13	**2.01**	0.04	0.03
37.111	0.03	0.13	0.12	0.13	0.26	0.08	**0.40**	0.00
75.178	0.05	0.16	0.24	0.15	**1.21**	0.73	0.08	0.11
76.505	0.72	0.82	0.97	**3.37**	0.04	0.70	0.01	0.20
76.512	0.74	0.83	**1.48**	0.41	0.07	1.53	0.03	0.07
76.525	**0.76**	0.82	0.89	0.47	0.11	0.66	0.06	0.21
77.446	0.73	**0.93**	0.55	0.71	0.03	0.21	0.05	0.03
Max. Value	0.76	0.93	1.48	3.37	1.21	2.01	0.40	1.11

Note. Floor Y direction is out-of-plane with PD-1 and in-plane with PD-2 (see Figure 5.2).

The acceleration time history for the 4th floor in the X direction is shown in Figure 7.5. The magnitude of these readings is large (a peak of 2.93 g), significantly larger than other acceleration readings reviewed for other portions of the experiment. There are several possible reasons for this large reading, including the possibility that the instrument was damaged or had some other failure. On further review of Figure 7.5, it was noted that the fluctuations of the acceleration were significantly

increased near the 76.6 second time interval. This odd pattern increased the concern about some type of instrumentation error. While it is possible that the accelerations were actually this high, the research team did not have sufficient time to evaluate the situation to make a determination of the accuracy of the reading. Thus limited use was made of this data channel.

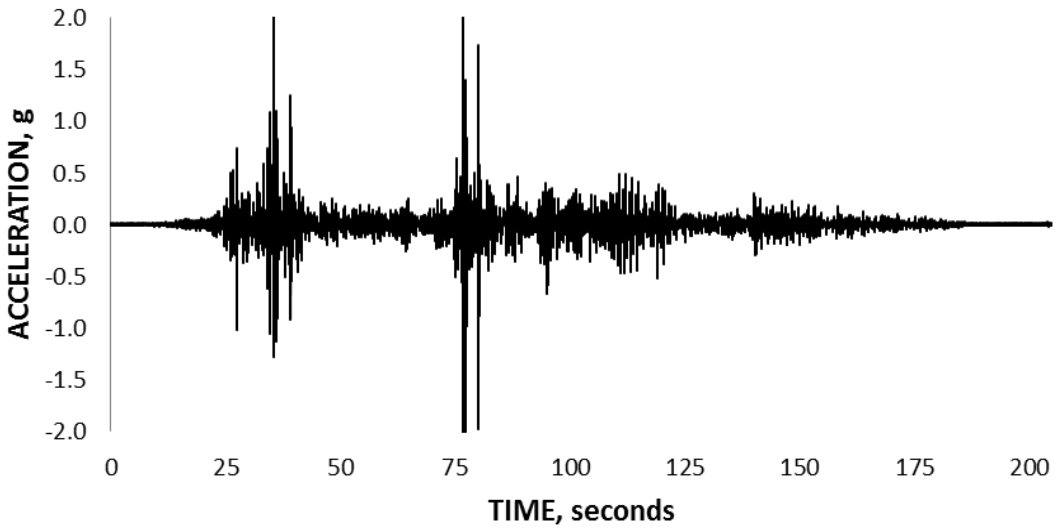

Figure 7.5. Acceleration – Corner of 4th Floor – X Direction (note that 2.93 g exceeds the axis range and is therefore not displayed on the graph)

7.1.2 Vertical acceleration.

There were no floor accelerometers placed at the corner of interest (column X1/Y3). The researchers had to decide if determining the vertical acceleration at this SW corner was necessary. Based upon the insignificant size of the derived (center) vertical

acceleration, no algorithm was developed to determine the Z direction acceleration at column X1/Y3.

As discussed in Section 5.2, the derived center floor vertical acceleration, a_{ZC}, was taken as the average of the NW, NE, and SE corner column vertical accelerations. Since the 4th and 5th floor values of a_{ZC} were in the range of 5% g, as shown in Figures 7.6 and 7.7, the vertical accelerations of the floors were considered negligible (relative to the building response and input intensity). In other words, the researchers decided that the 5% g center floor acceleration ranges obtained by Equation 5.5 indicated insignificant vertical accelerations at the corners, including insignificant vertical acceleration at the SW corner where the panels were mounted. It is also important to note that the floor corner accelerations could have varied significantly but still have averaged to 5% g by Equation 5.5, possibly indicating considerable floor rotation about the X and Y axes; however, this concept is beyond the scope of the current research and was not assessed.

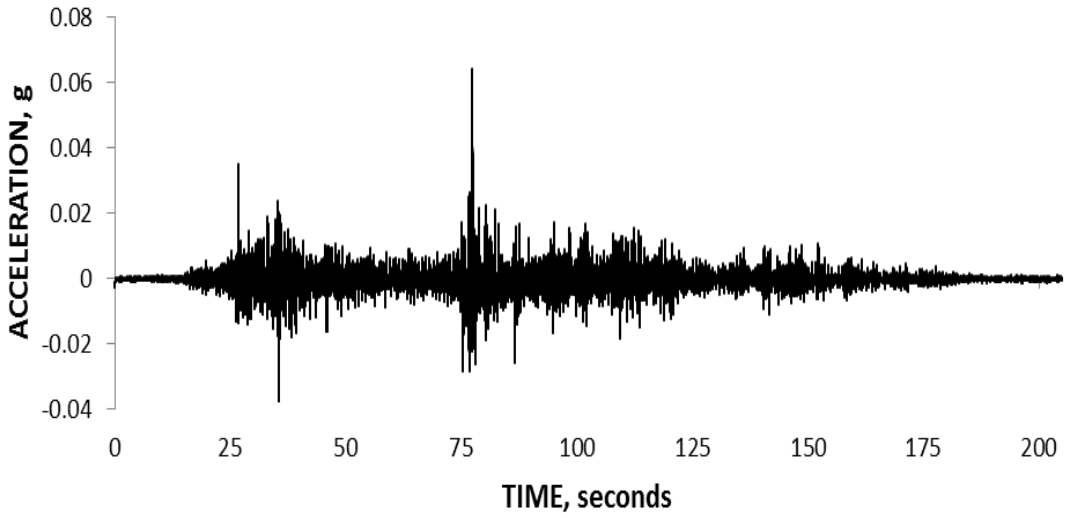

Figure 7.6. Acceleration – Center of 4th Floor – Z Direction

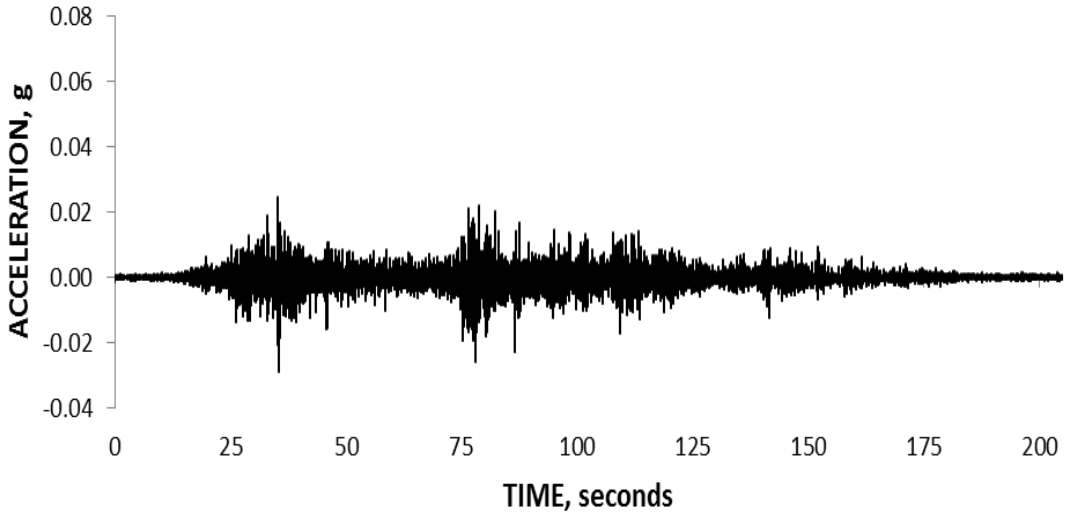

Figure 7.7. Acceleration – Center of 5th Floor – Z Direction

7.2 Panel Acceleration Data

Tables 7.1 to 7.4 list accelerations of both the return and flat panels. Data are reported for each time step associated with a peak acceleration value of either the floor or the panel. The flat panel experienced larger peak accelerations in all three global directions. The tables also show that the peak panel responses occurred before the peak floor responses, except for the in-plane flat panel response of 3.37 g and out-of-plane return panel response of 1.48 g, which occurred before the peak center floor accelerations in the X direction (see Table 7.3). The 3.37 g reading is particularly high and the research team was unable to verify the reading, so limited use was made of the instrument data.

The panel response in relation to the floors above and below was also of interest. The author expected that the 4th floor corner acceleration should control the movement of both panels. Figures 7.5 to 7.15 are time history comparisons of the in-plane panel acceleration to the 4th and 5th floor corner and center accelerations. The five second interval chosen contains all peak panel and floor element accelerations. Figures 7.5 to 7.12 each show that the corner floor accelerations of the 4th and 5th floors were in-phase with the in-plane accelerations of both panels, as one might expect. It is not apparent however from these graphs that the 4th floor corner was a better gauge of the panel response in comparison to the 5th floor corner. It is also not apparent that the 4th floor center was a better gauge of the panel response in comparison to the 5th floor center.

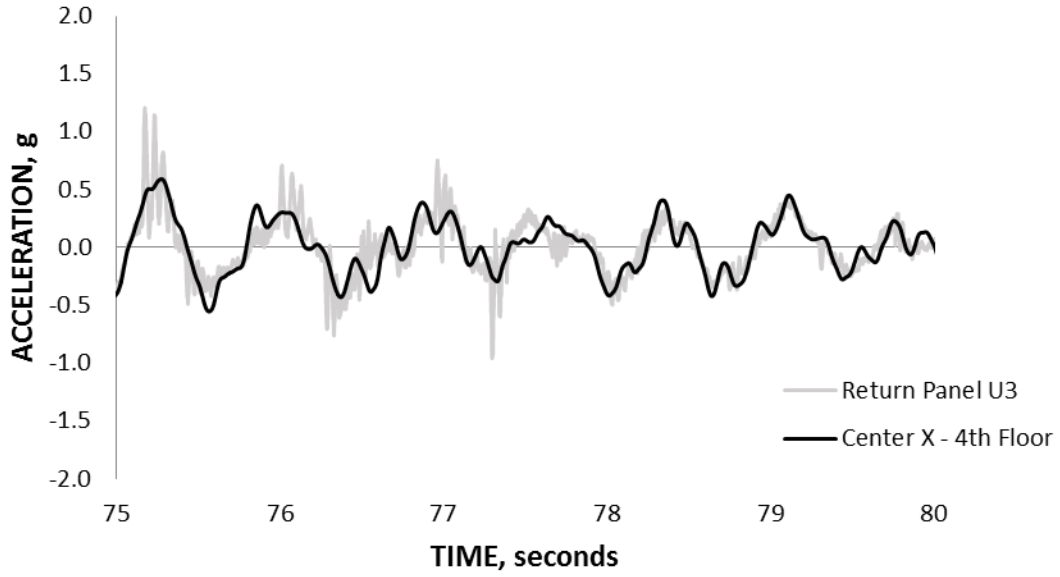

Figure 7.8. Acceleration – Center of 4th Floor and Return Panel U3 – X Direction

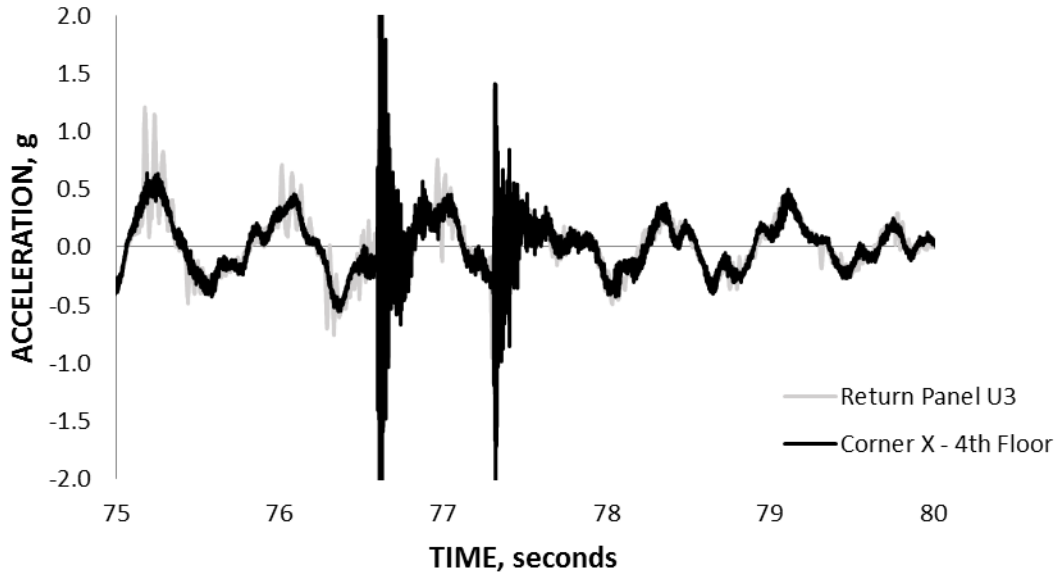

Figure 7.9. Acceleration – Corner of 4th Floor and Return Panel U3 –- X Direction

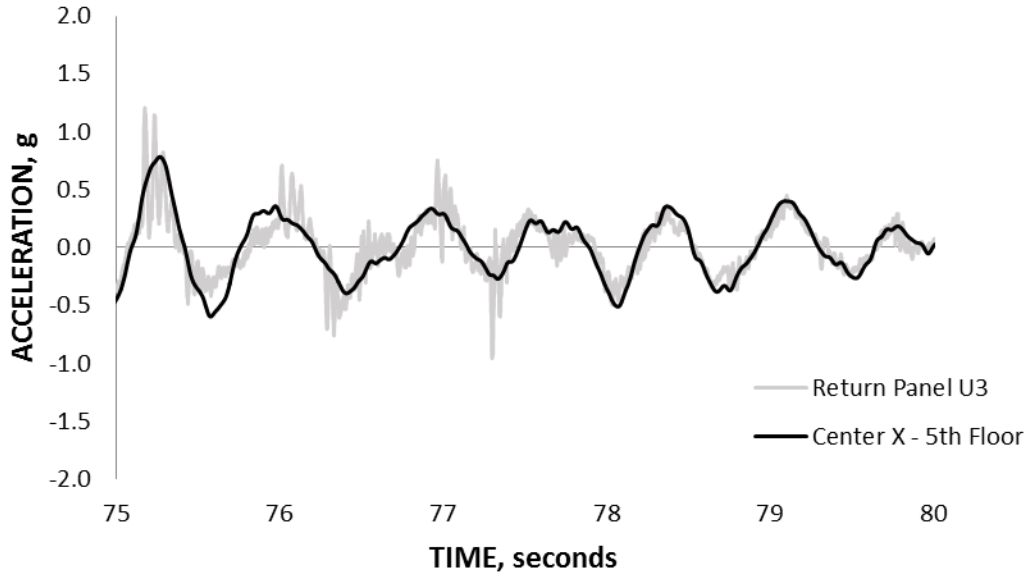

Figure 7.10. Acceleration – Center of 5th Floor and Return Panel U3 – X Direction

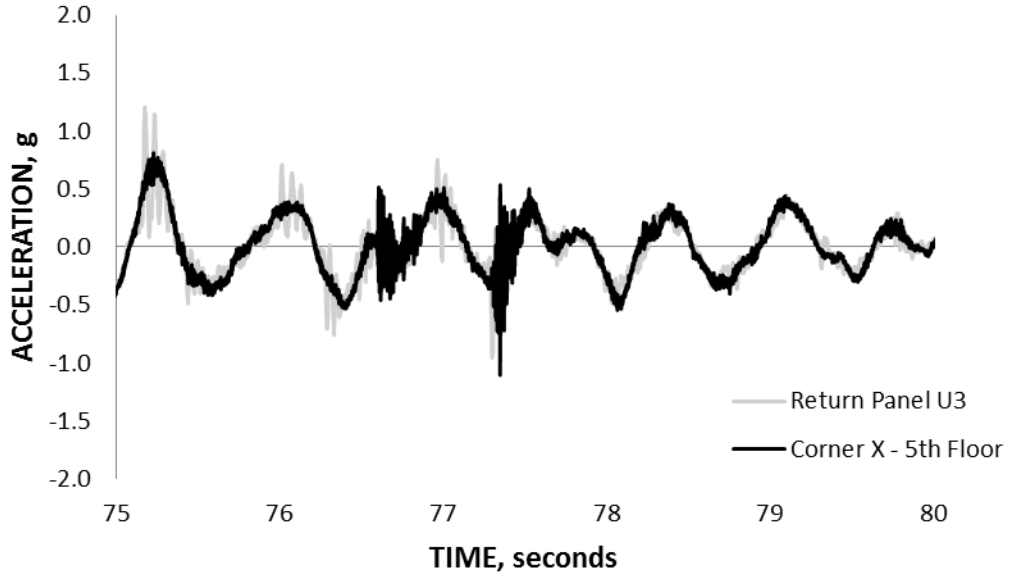

Figure 7.11. Acceleration – Corner of 5th Floor and Return Panel U3 – X Direction

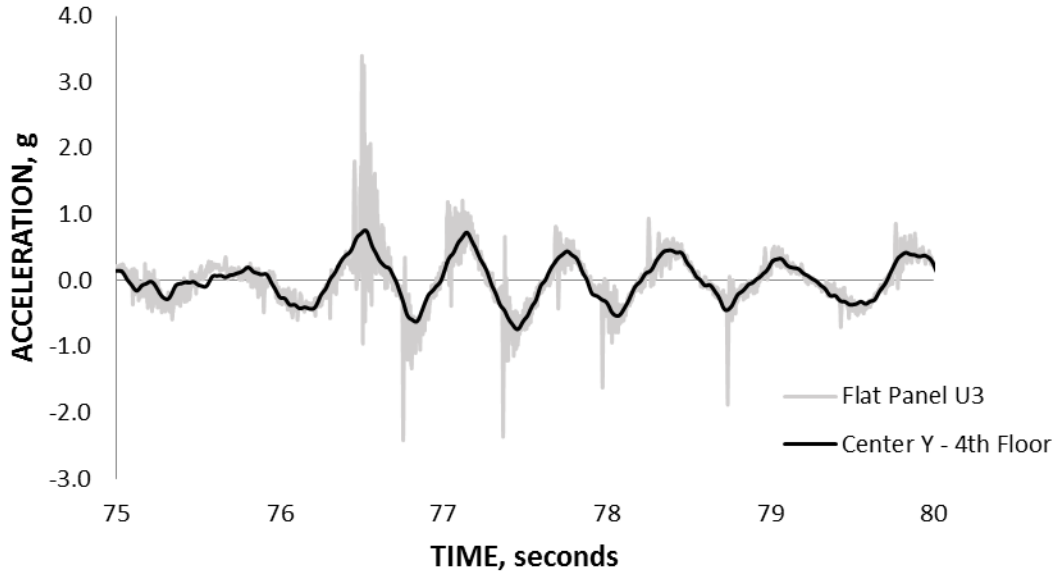

Figure 7.12. Acceleration – Center of 4th Floor and Flat Panel U3 – Y Direction

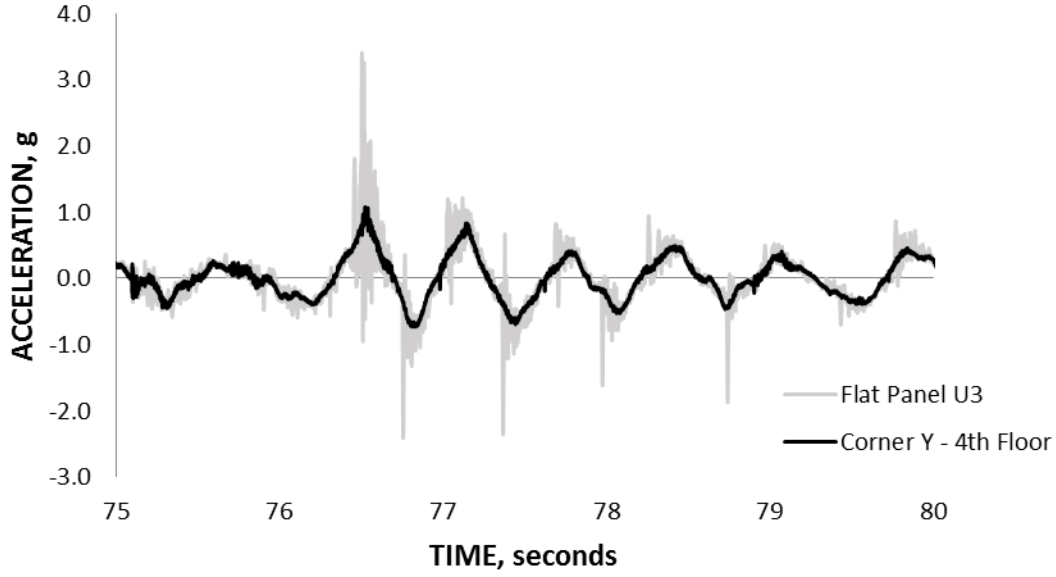

Figure 7.13. Acceleration – Corner of 4th Floor and Flat Panel U3 – Y Direction.

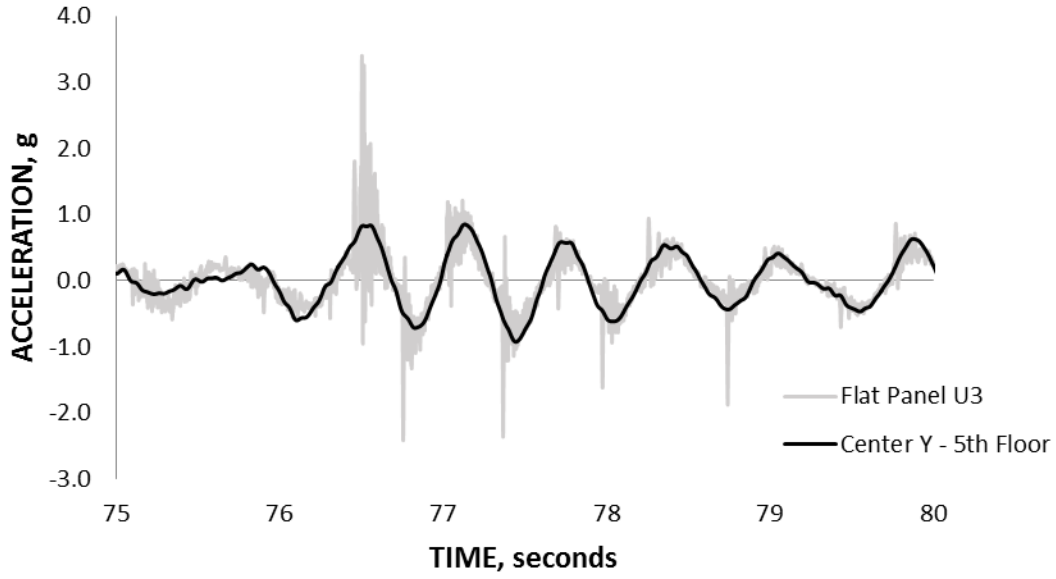

Figure 7.14. Acceleration – Center of 5th Floor and Flat Panel U3 – Y Direction

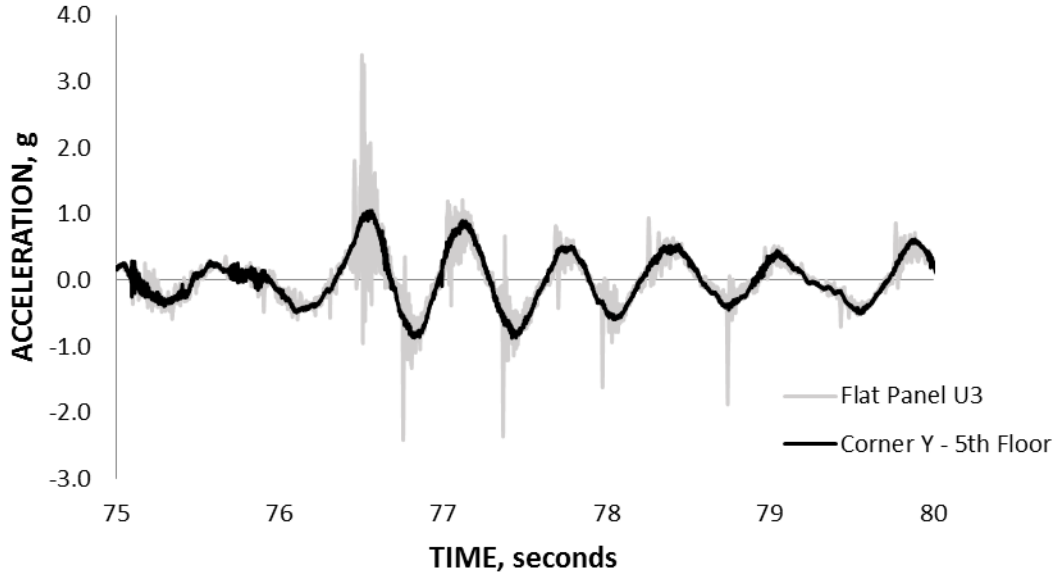

Figure 7.15. Acceleration – Corner of 5th Floor and Flat Panel U3 – Y Direction

There are slight phasing discrepancies when comparing floor center plots (Figures 7.8, 7.10, 7.12, and 7.14) to floor corner plots (Figures 7.9, 7.11, 7.13, and 7.15) at around the 75.5 second time step interval. Phasing differences indicate that the panels were cyclically accelerating differently than the floors, i.e. the floor reached peak acceleration before or after the panel and vice versa. A probable reason for this trend could be the non-rigid connection of the rocking design allowing the panels to move independently of the floor. However, as this out-of-phase trend did not occur for the corner of floor time histories; it is more likely an indication that the corner floor movements were a better representation of the behavior of the panels. Again, it appears that corner and center floor accelerations were different. There were no time frames when the panels were completely out-of-phase with the floor, but these phasing trend characteristics between center and corner of floor data are certainly noticeable in the plots.

Figures 7.16 to 7.23 are time history comparisons of the out-of-plane panel acceleration to the 4^{th} and 5^{th} floor corner and center accelerations. Floor accelerations were expected to be more similar to the out-of-plane panel accelerations than the in-plane panel accelerations, as the connections were rigid in the out-of-plane direction and not slotted. The panels should accelerate and displace with the floor as the bolts and welds prevent them from moving independently in the panel out-of-plane directions. However, compared to the in-plane data of Figures 7.8 to 7.15, the out-of-plane plots do not show a better correlation as far as less phasing discrepancy. In fact, the same slight out-of-phase trends can be observed. Also there are significant differences in acceleration between the

panel and floor, even though the panels were rigidly connected to the floors in this direction.

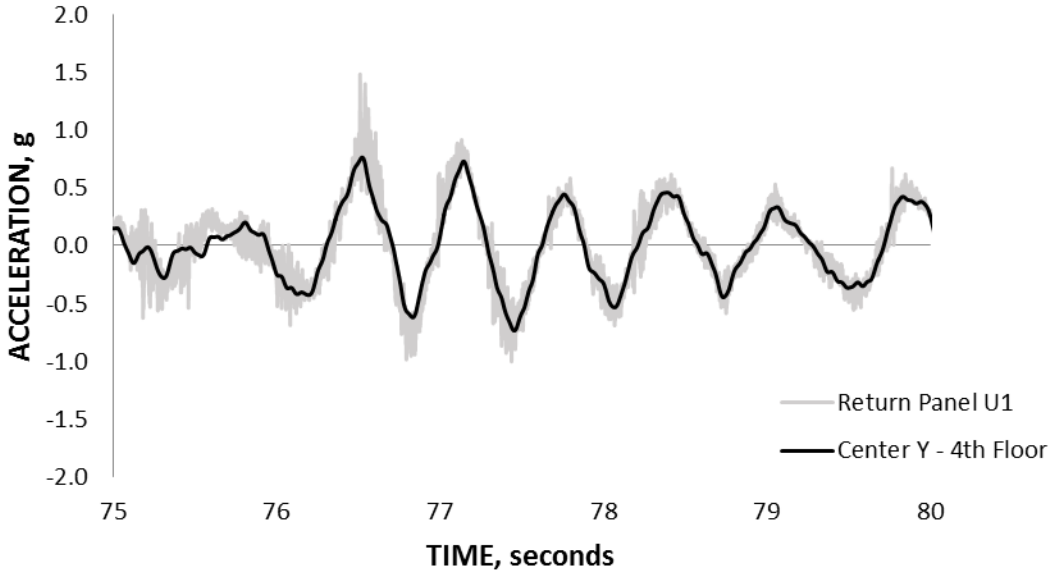

Figure 7.16. Acceleration – Center of 4th Floor and Return Panel U1 – Y Direction

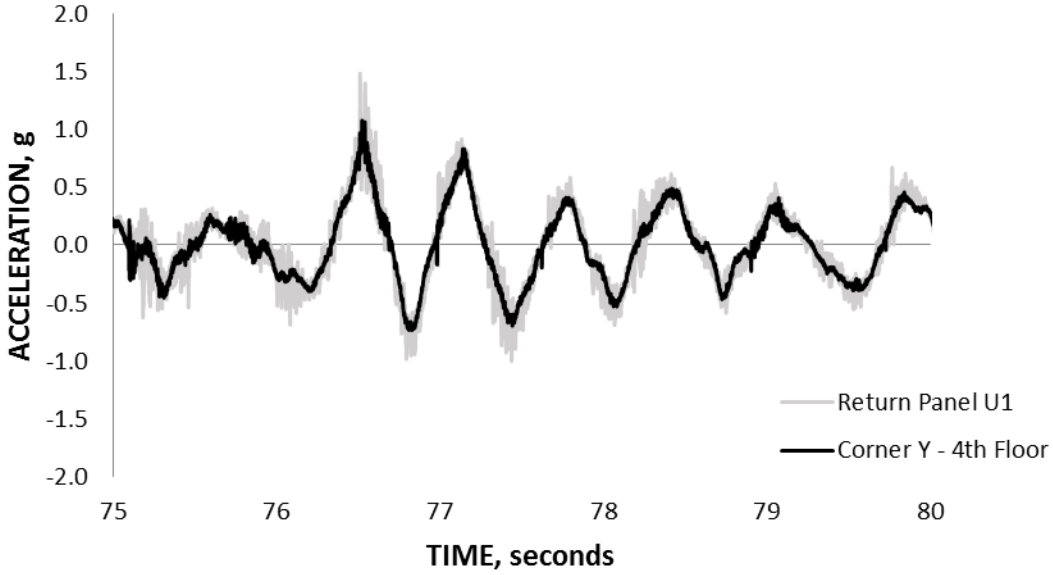

Figure 7.17. Acceleration – Corner of 4th Floor and Return Panel U1 – Y Direction

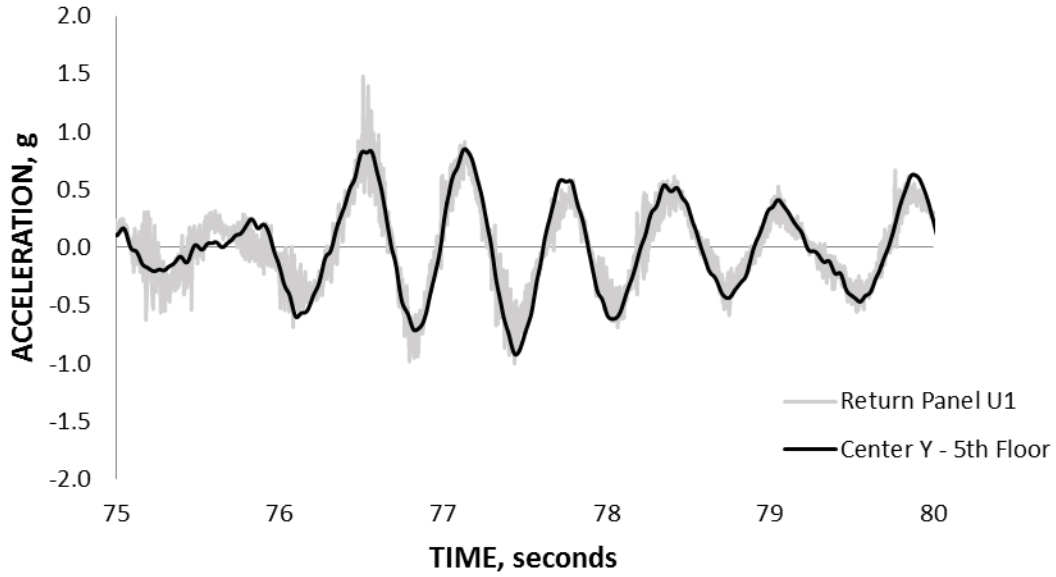

Figure 7.18. Acceleration – Center of 5th Floor and Return Panel U1 – Y Direction

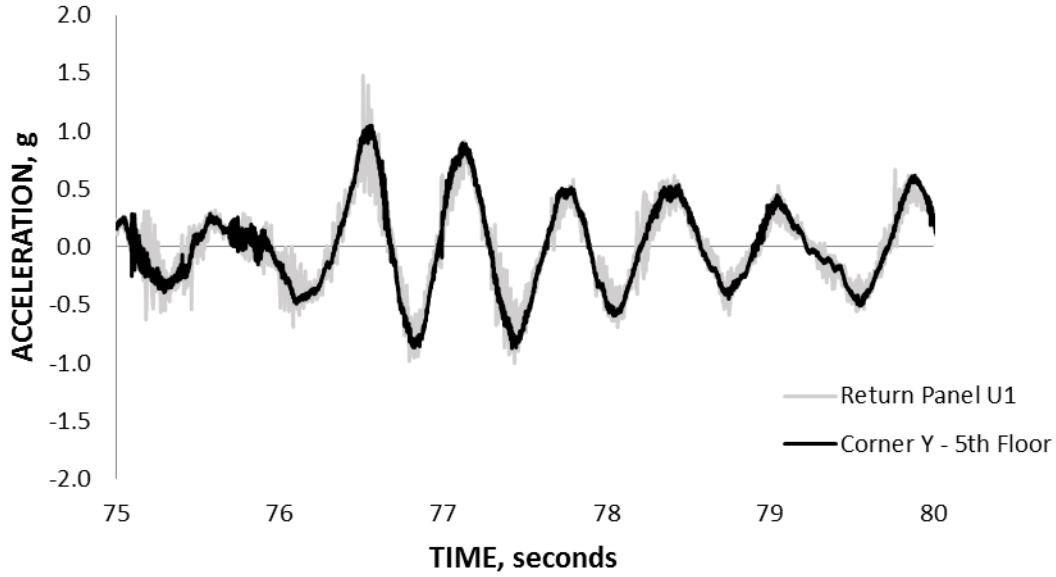

Figure 7.19. Acceleration – Corner of 5th Floor and Return Panel U1 – Y Direction

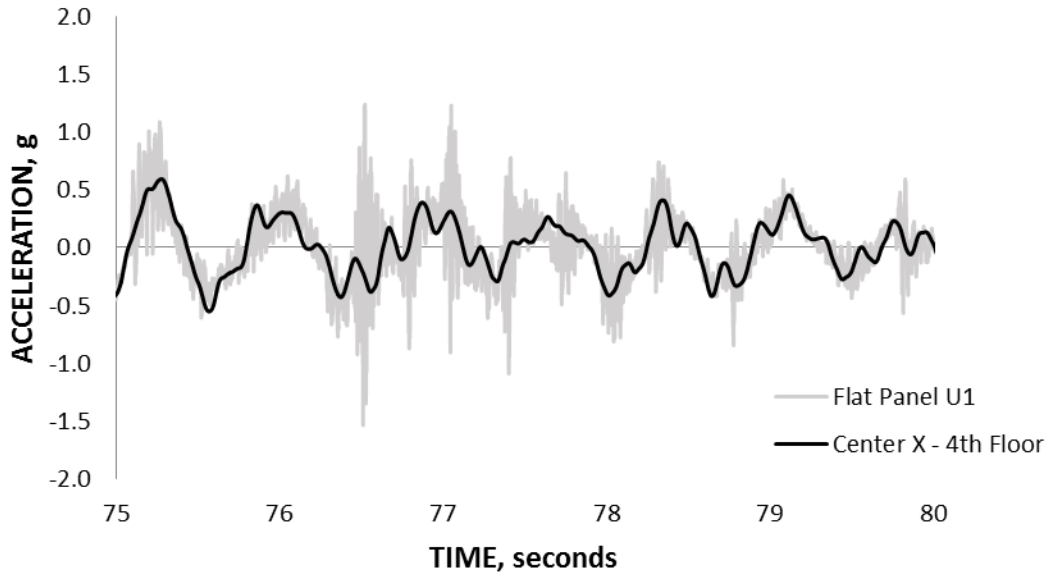

Figure 7.20. Acceleration – Center of 4th Floor and Flat Panel U1 – X Direction

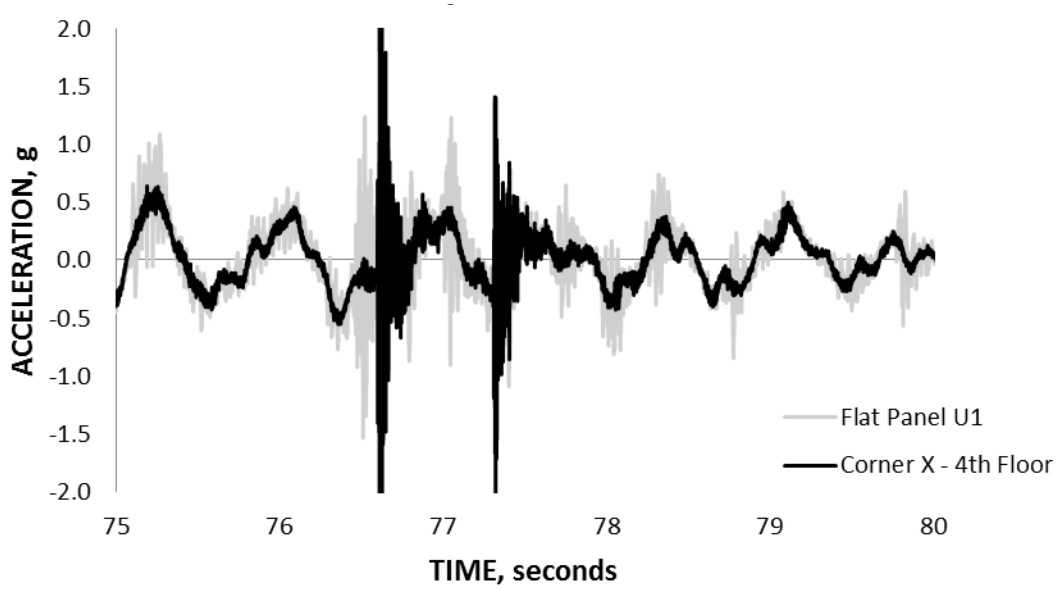

Figure 7.21. Acceleration – Center of 4th Floor and Flat Panel U1 – X Direction

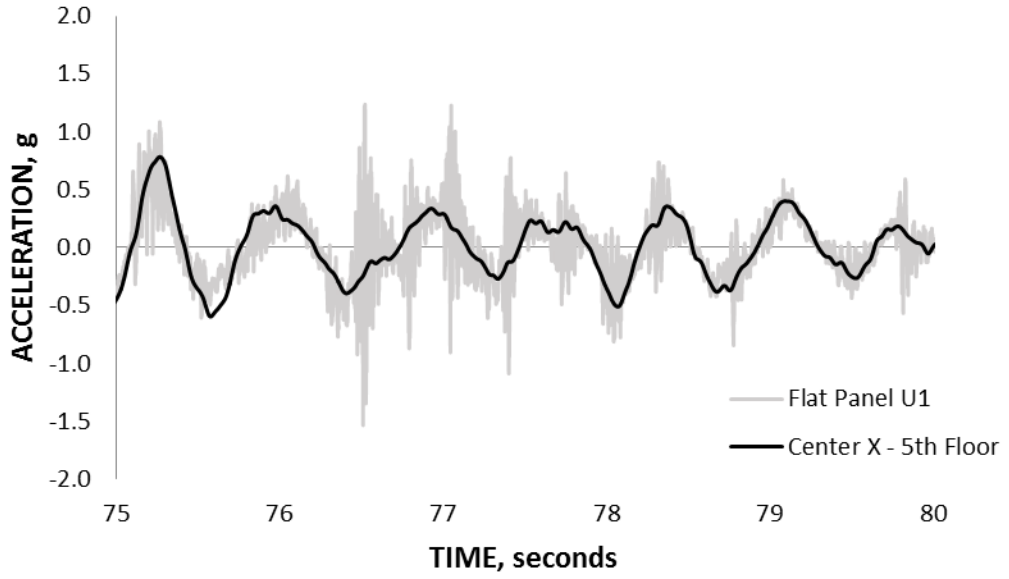

Figure 7.22. Acceleration – Center of 5th Floor and Flat Panel U1 – X Direction

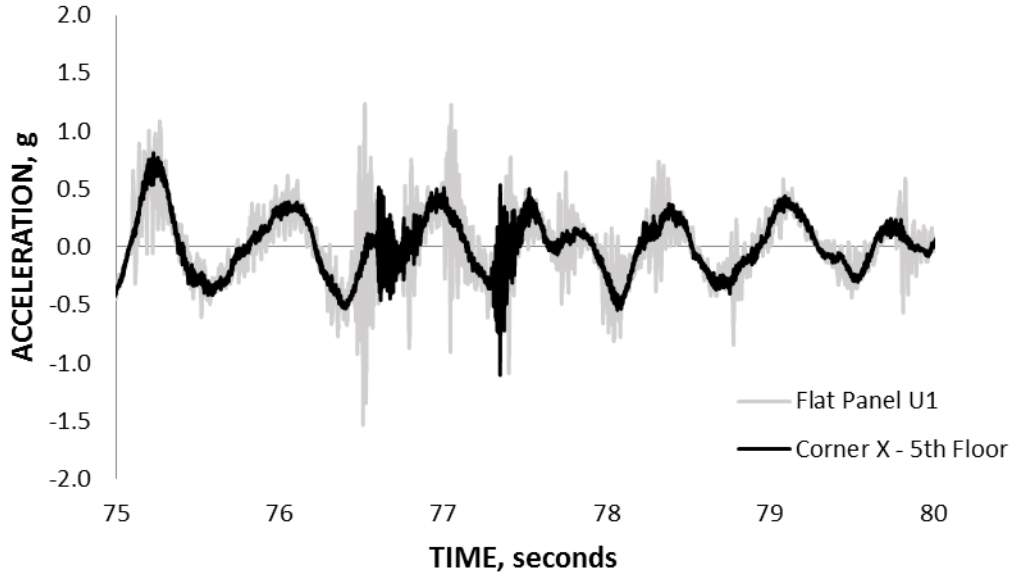

Figure 7.23. Acceleration – Corner of 5th Floor and Flat Panel U1 – X Direction

Though there are slight phasing differences, the plots generally do show that the panel accelerations coincided with the floors in both in-plane and out-of-plane directions (though sometimes with large amplification). As the panels generally accelerated in-phase with the floors, it was appropriate to quantify the true panel acceleration by taking the weighted-average of the floor accelerations (above and below at the floor connections) and the acceleration of the panel itself (Equation 7.3):

$$a_{panel} = \tfrac{1}{2}\{\tfrac{1}{2}(a_{5th} + a_{4th}) + a_{recorded}\} \quad (7.3)$$

This method integrates the acceleration across the entire panel (see Figure 7.24). This method also implies that the top half of the panel was more controlled by the 5th floor and the bottom half was more controlled by the 4th floor, which is an accurate assumption for these types of panel connections. The 5th floor connections are still expected to have an equal influence on panel acceleration, even as only the 4th floor panel connections support the gravitational load of the panels.

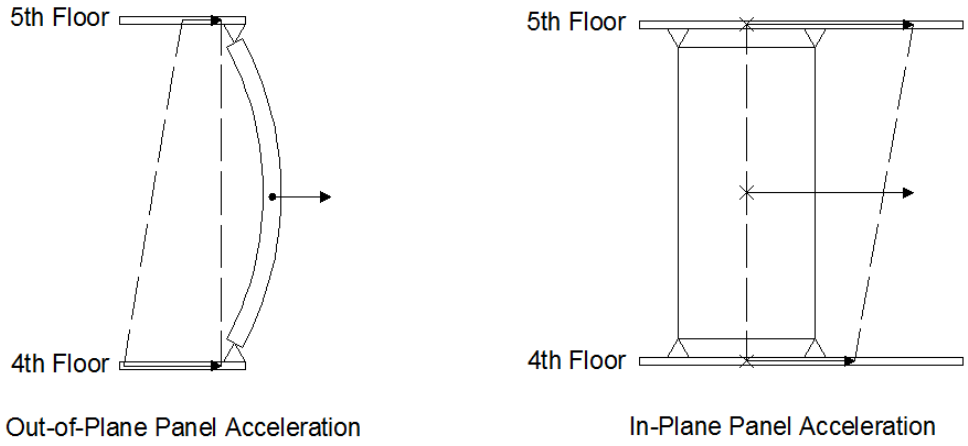

Figure 7.24. Sketch of Out-of-Plane (U1) and In-Plane (U3) Panel Acceleration – Contributions from the Floors Above and Below

The panel acceleration approximated by Equation 7.3 was assumed for both the in-plane and out-of-plane directions. Section 7.4 considers this approximation of the panel acceleration when developing inertial forces of the panels. To verify Equation 7.3, the author also compared the panel acceleration to the acceleration of the 4th and 5th floors averaged together. As the floors above and below the panels accelerate, the acceleration at the center of the panel might more closely follow this averaged acceleration of both floors, as opposed to the acceleration of just one of the floors. Figures 7.25 to 7.28 compare the average of the 4th and 5th floor accelerations to the in-plane accelerations of both panels. Figures 7.29 to 7.32 are the out-of-plane panel accelerations compared to the 4th and 5th floor accelerations averaged together. Again the five second time interval was chosen as the panels and floor experience peak accelerations during this time frame. It is not clear from these plots that using Equation 7.3 is more appropriate or a better approximation of the panel acceleration, when compared to developing an algorithm favoring one of the floor accelerations individually. In other words, the panel acceleration does not seem to be controlled by one floor more than the other. Ultimately, a single panel acceleration is required by Equation 3.2, and Equation 7.3 is the author's best estimation for developing this single panel acceleration. This single panel acceleration is a weighted-average using the data available from the three recording instruments pertaining to the panel's acceleration: the 4th floor accelerometer, the 5th floor accelerometer, and the panel accelerometer itself.

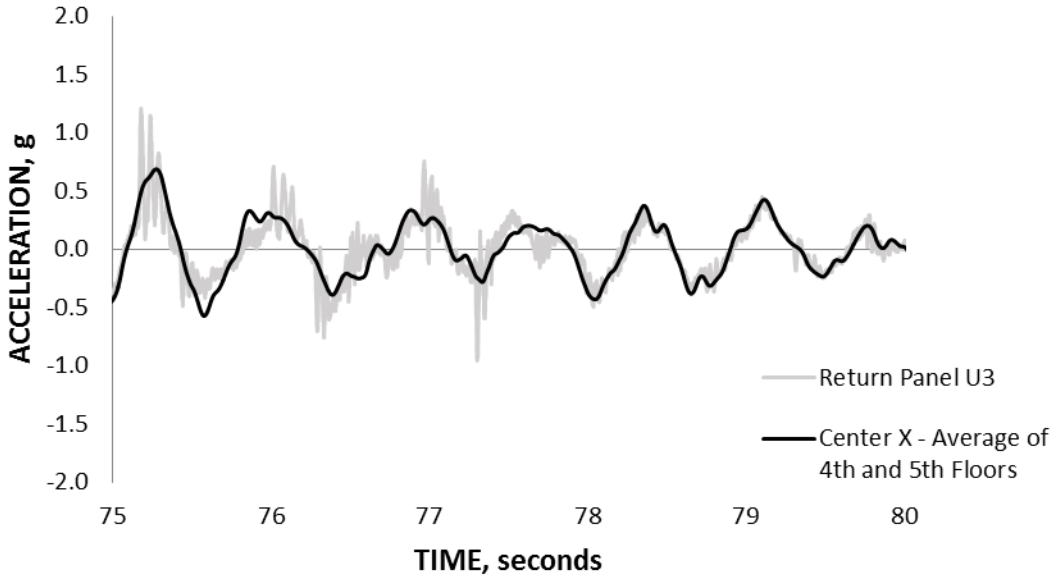

Figure 7.25. Accelerations – Average of 4th & 5th Center Floor and Return Panel U3 – X Direction

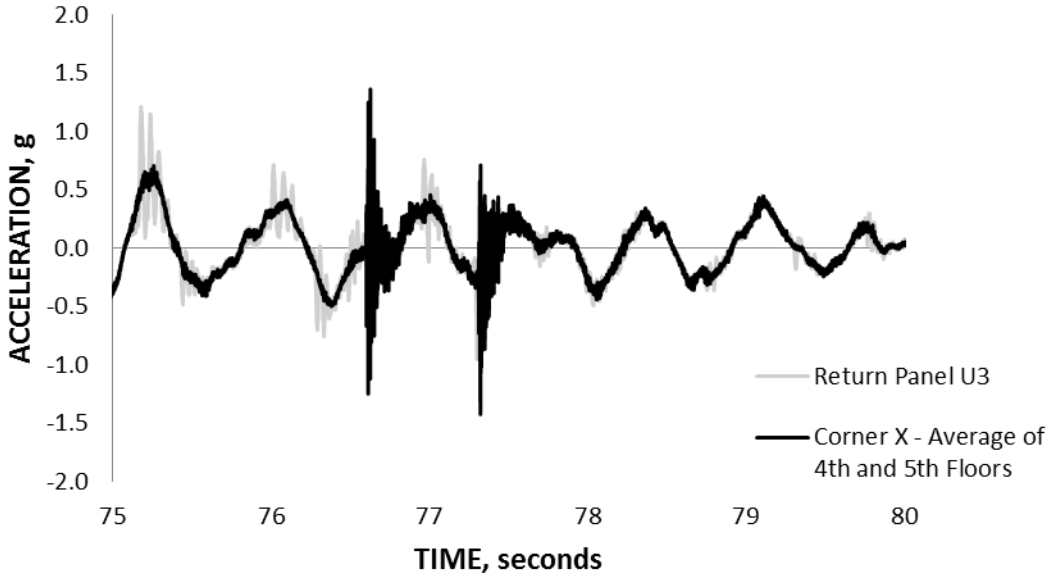

Figure 7.26. Accelerations – Average of 4th & 5th Corner Floor and Return Panel U3 – X Direction

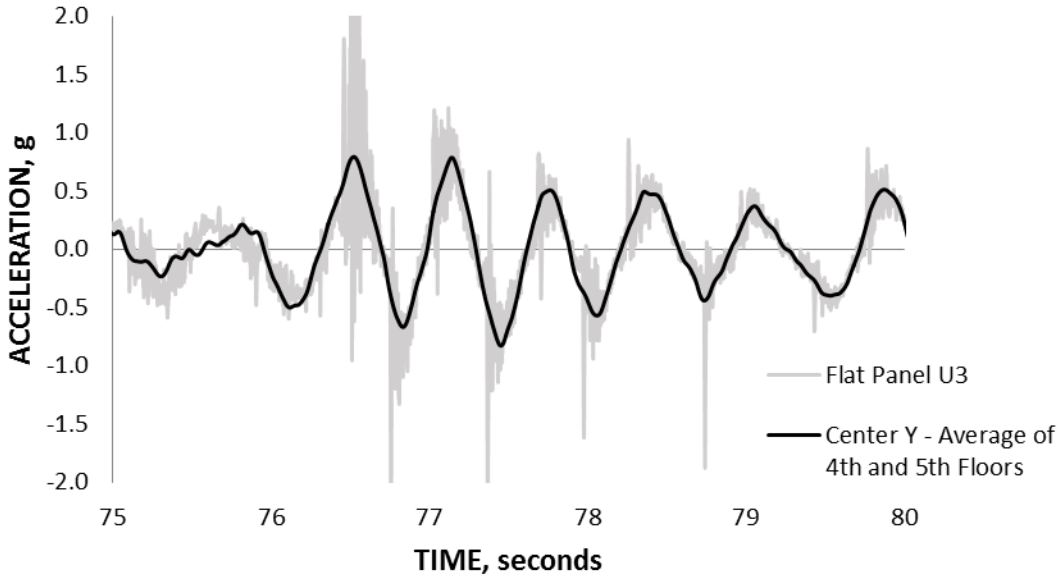

Figure 7.27. Accelerations – Average of 4th & 5th Center Floor and Flat Panel U3 – Y Direction

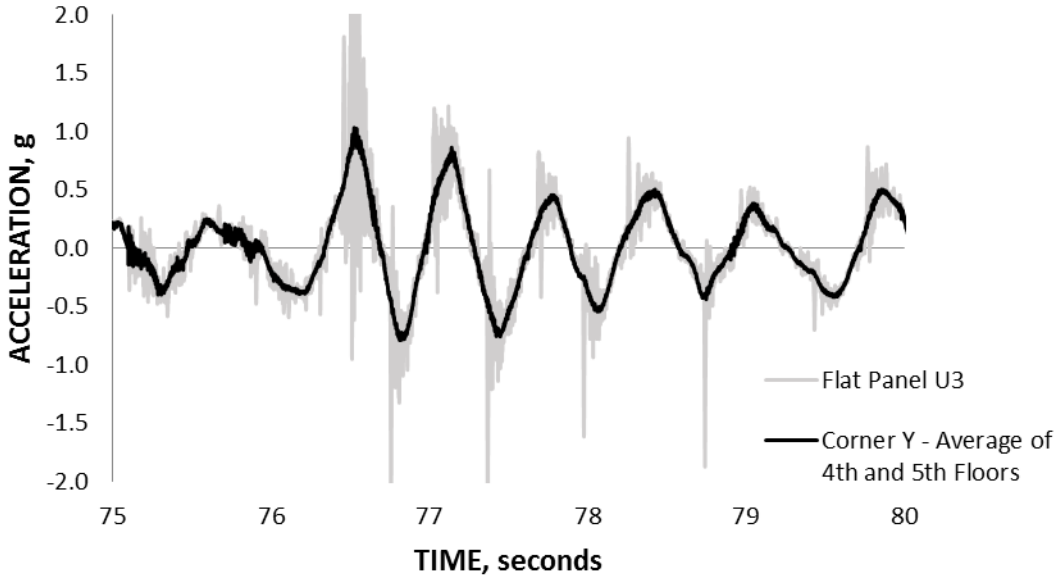

Figure 7.28. Accelerations – Average of 4th & 5th Corner Floor and Flat Panel U3 – Y Direction

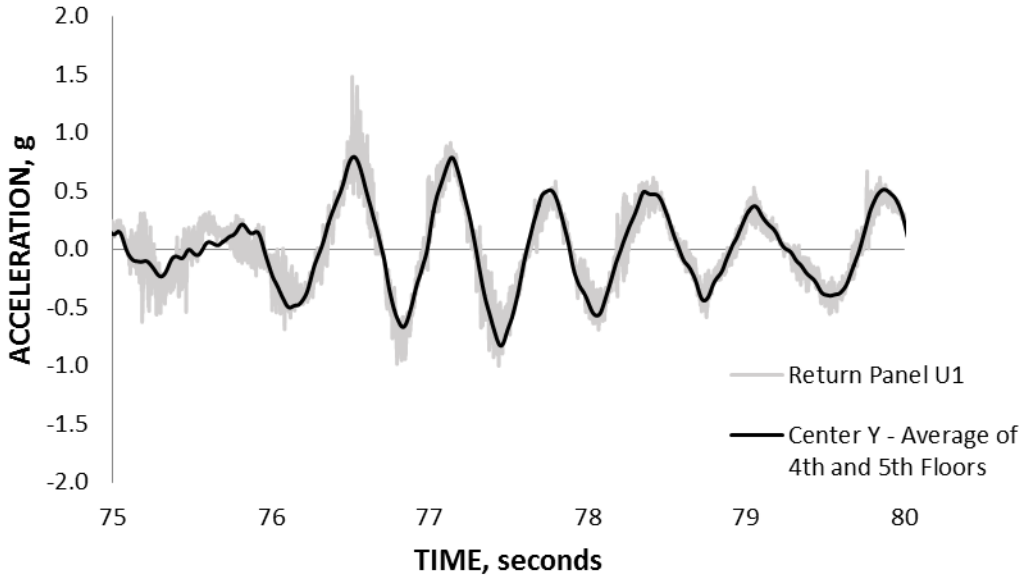

Figure 7.29. Accelerations – Average of 4th & 5th Center Floor and Return Panel U1 – Y Direction

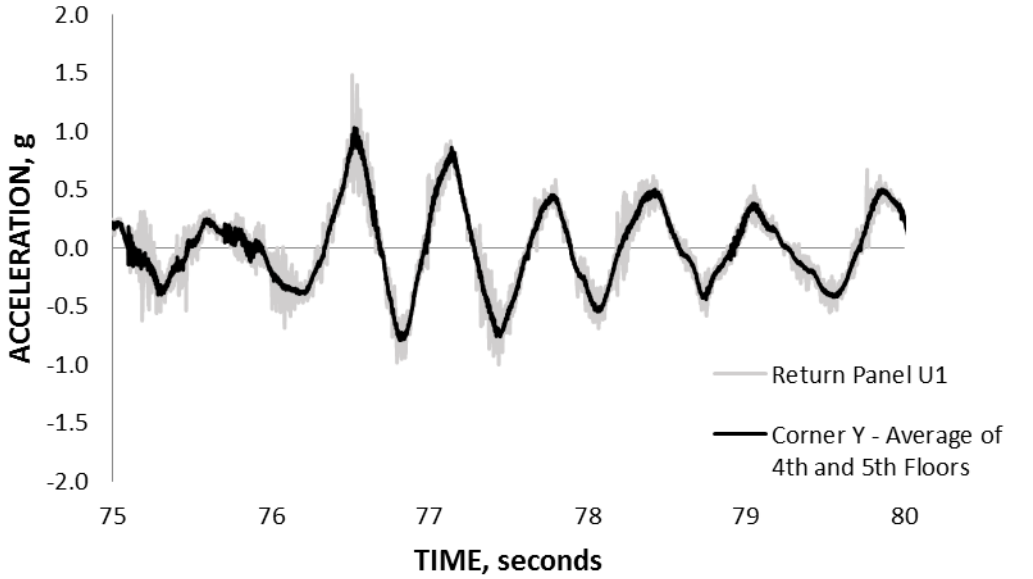

Figure 7.30. Accelerations – Average of 4th & 5th Corner Floor and Return Panel U1 – Y Direction

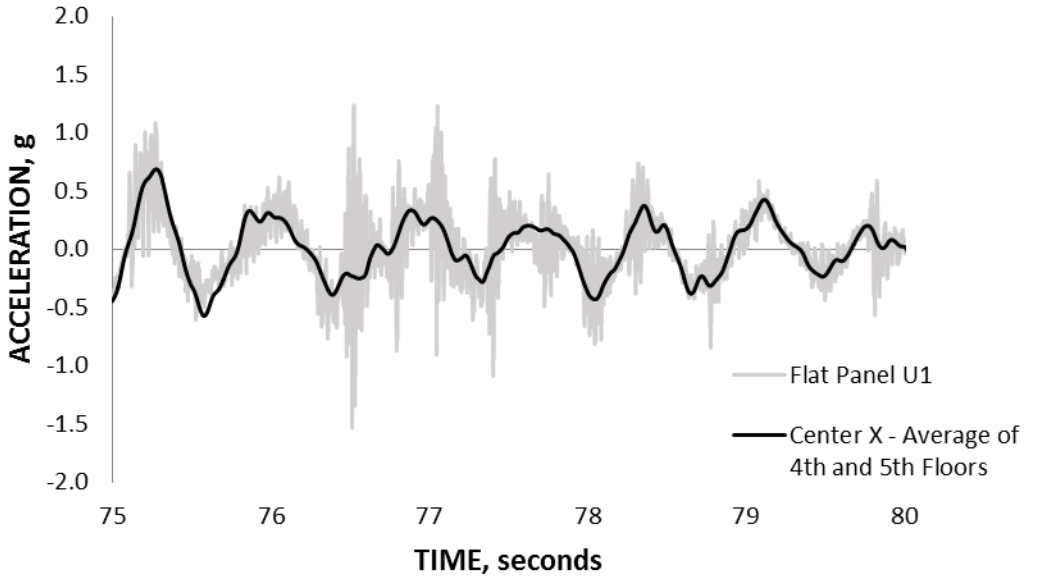

Figure 7.31. Accelerations – Average of 4th & 5th Center Floor and Flat Panel U1 – X Direction

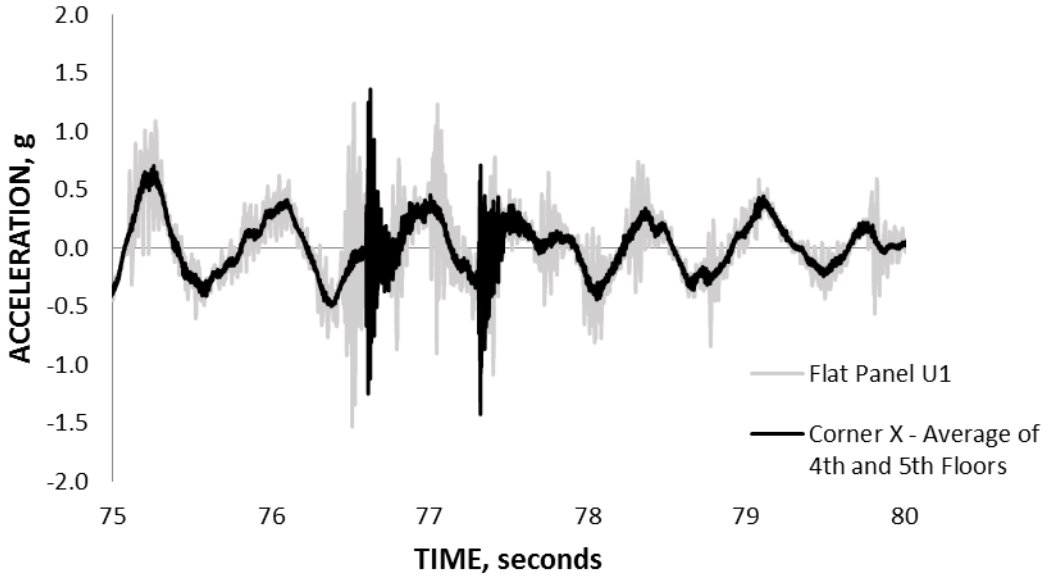

Figure 7.32. Accelerations – Average of 4th & 5th Corner Floor and Flat Panel U1 – X Direction

Tables 7.5 to 7.8 highlight the comparison of the recorded in-plane panel acceleration to corresponding accelerations of the 4th and 5th floors averaged together (for both the floor center and corner). Rarely is this floor average within 0.10g of the recorded panel acceleration at any specific time step. The ratio of the 4th and 5th floor averaged accelerations to the panel's recorded acceleration is observed at the time steps of each of their peaks. The ratios differ drastically enough to indicate that correlation is unlikely.

Table 7.5. *Iwanuma Comparison of 4th and 5th Floor Corner Averaged Accelerations to the Corresponding In-Plane Return Panel Acceleration*

Time Step	**Level 4 Floor Corner X**	**Level 5 Floor Corner X**	**Average acceleration of floors**	**Panel PD-1 U3 $a_{recorded}$**	**Ratio of peak panel acceleration to average acceleration of floors**
(sec)	**(g)**	**(g)**	**(g)**	**(g)**	
75.178	0.44	0.51	0.47	1.21	2.55
76.627	2.93	0.21	1.57	0.02	0.01
77.35	0.63	1.10	0.87	0.59	0.68
Maximum Value	2.93	1.10		1.21	
Avg of Floor Maximums			2.02		
Accel Amplification of Peak Panel to Avg of Floor Maximums:					0.60

Table 7.6. *Iwanuma Comparison of 4th and 5th Floor Corner Averaged Accelerations to the Corresponding In-Plane Flat Panel Acceleration*

Time Step	**Level 4 Floor Corner Y**	**Level 5 Floor Corner Y**	**Average acceleration of floors**	**Panel PD-2 U3 $a_{recorded}$**	**Ratio of peak panel acceleration to average acceleration of floors**
(sec)	**(g)**	**(g)**	**(g)**	**(g)**	
76.505	0.78	0.90	0.84	3.37	4.03
76.524	1.07	0.99	1.03	0.60	0.59
76.565	0.78	1.05	0.92	0.21	0.23
Maximum Value	1.07	1.05		3.37	
Avg of Floor Maximums			1.06		
Accel Amplification of Peak Panel to Avg of Floor Maximums:					3.18

Table 7.7. *Iwanuma Comparison of 4th and 5th Floor Center Averaged Accelerations to the Corresponding In-Plane Return Panel Acceleration*

Time Step	**Level 4 Floor Center X**	**Level 5 Floor Center X**	**Average acceleration of floors**	**Panel PD-1 U3 $a_{recorded}$**	**Ratio of peak panel acceleration to average acceleration of floors**
(sec)	**(g)**	**(g)**	**(g)**	**(g)**	
75.178	0.45	0.53	0.49	1.21	2.47
75.27	0.59	0.78	0.69	0.27	0.40
75.28	0.59	0.78	0.68	0.71	1.04
Maximum Value	0.59	0.78		1.21	
Avg of Floor Maximums			0.69		
Accel Amplification of Peak Panel to Avg of Floor Maximums:					1.75

Table 7.8. *Iwanuma Comparison of 4th and 5th Floor Center Averaged Accelerations to the Corresponding In-Plane Flat Panel Acceleration*

Time Step	Level 4 Floor Center Y	Level 5 Floor Center Y	Average acceleration of floors	Panel PD-2 U3 $a_{recorded}$	Ratio of peak panel acceleration to average acceleration of floors
(sec)	(g)	(g)	(g)	(g)	
76.505	0.72	0.82	0.77	3.37	4.35
76.525	0.76	0.82	0.79	0.47	0.59
77.446	0.73	0.93	0.83	0.71	0.86
Maximum Value	0.76	0.93		3.37	
Avg of Floor Maximums			0.85		
Accel Amplification of Peak Panel to Avg of Floor Maximums:					3.96

Using the maximum floor accelerations to determine a_{panel} may be appropriate. For instance if only the peak acceleration data of each floor is available, averaging these peaks should serve as a reasonable approximation without having to look at individual time data. The average of the floor maximums is quite comparable to the averaged acceleration of the floors in Tables 7.6 to 7.8. The exception is Table 7.5 where the average of the floor maximums at 2.02 g is not close to any of the averaged floor values of 0.47 g, 1.57 g, or 0.87 g. This may be a result of instrumentation inaccuracy error as the 4th floor corner acceleration of 2.93 g is unusually high. Again, this suggests that the maximum panel accelerations (a_{panel}) calculated using Equation 7.3 can be analyzed using the peak floor acceleration values, rather than the values of a_{5th}, a_{4th}, and $a_{recorded}$ together along an individual time step.

The last row of each of Tables 7.5 to 7.8 gives the acceleration amplification of the peak panel to the average of the floor maximums. Comparing this maximum amplification value (from the last row of Tables 7.5 to 7.8) to the maximum ratio value determined at a time step (from the last column of Tables 7.5 to 7.8), illustrates that using the floor maximums solely may not be appropriate for this specific amplification (this amplification is not to be confused with the amplification discussed in Section 7.3). For instance 3.18, 1.75, and 3.96 are not quite comparable to 4.03, 2.47, and 4.35, respectively (the values differ by 27%, 41%, and 10%, respectively). For this particular assessment, the research team considered any difference greater than 10% to be non-comparable. However, it is also important to note that Tables 7.5 to 7.8 consider only three time step locations, so they are certainly not conclusive.

Figures 7.33 and 7.34 show that acceleration of the panels in the Z direction have larger magnitudes than the 5% g range of the floors in the Z direction (see Section 7.1.2). This difference between panel and floor acceleration also demonstrates that the panels are fully slotted, allowing panel movement different than the floor. Had the panel connections been designed as rigid connections, the author would expect peak panel accelerations closer to 5% g.

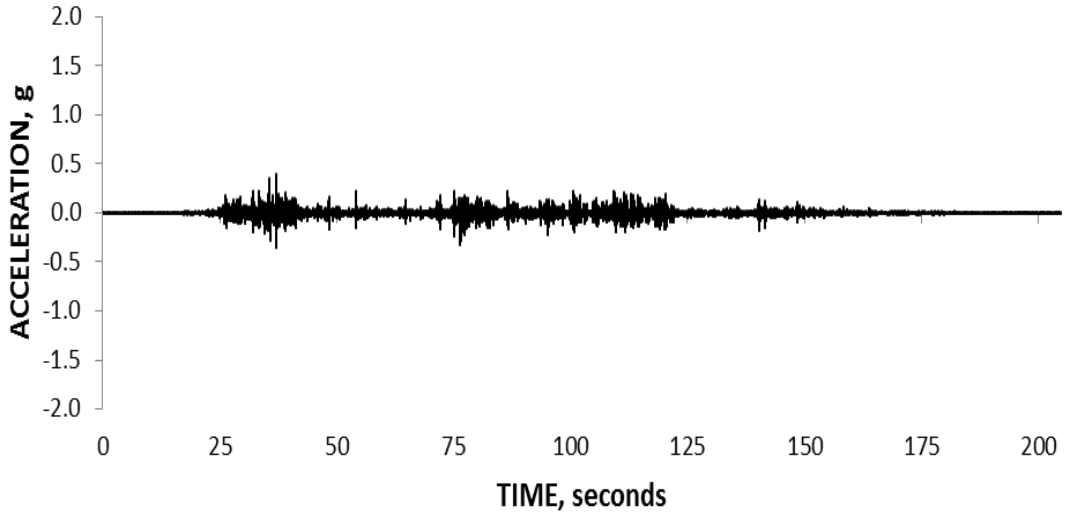

Figure 7.33. Acceleration – PD-1 – U2, Z Direction

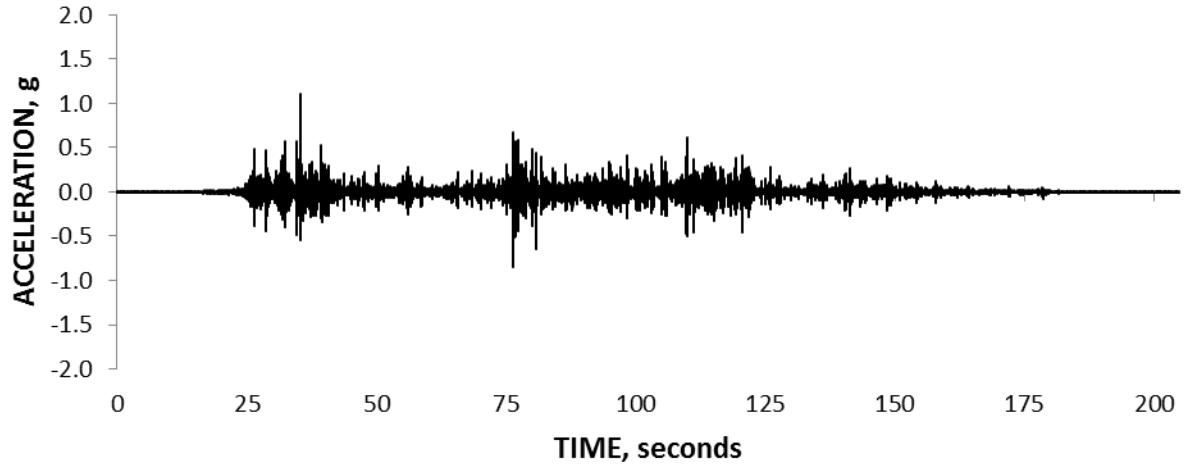

Figure 7.34. Acceleration – PD-2 – U2, Z Direction

7.3 Discussion of High Floor and Panel Accelerations

Peak acceleration response data of both the floor and panel are high enough to raise concern pertaining to the accuracy of the data. Specifically, the 4th floor corner X direction peak acceleration of 2.93 g and the flat panel X direction peak acceleration of 3.37 g seem to be higher than the overall building can respond. Time history plots also show other high response values occurring during time intervals where the peaks are achieved. It should be noted that these high values of acceleration, including the individual peaks, exist for only a few milliseconds. The fact that the concrete received no apparent damage at such high response is yet another cause of concern.

One possible explanation of these larger accelerations is that there is an instrumentation error, but since the remainder of the data seems appropriate, that lessens this possibility. Furthermore, the researchers suspect that the concrete could not have reacted to such high accelerations over such short time frames. Especially for the panel, it appears that if these few spikes are removed, plots would show accelerations closer to 1.5 g, which would seem to align closer to the researcher's expectations. This filtering would produce a more 'averaged' curve which would be more in line with expectations. Contrarily however, one has to consider that the panel is a relatively small mass of concrete which is being supported by a large mass, and there may in fact exist higher frequency motion. This kind of filtering may be more appropriate for the floor due to the floor's larger mass. Resonance of both the panel and floor is also a possibility, requiring greater insight of the structures dynamic properties.

Evaluating the effects of filtering and the accuracy of the readings in this regard is beyond the scope of the current project. The data has not been filtered by the research team, nor is it apparent that the data has been filtered by the researchers at Nevada, Reno. The researchers decided not to alter/filter the data, but to be definitive about what was calculated. The findings of this thesis do not pertain to all panel systems, nor do the researchers intend to imply that the design and construction of these systems need to be altered based upon the findings of this thesis.

The goal of the research is to develop a better understanding of how APC panels perform in earthquakes so that industry professionals may benefit from the research findings. Building designers and precast fabricators will be unlikely to quantitatively model such detail as individual panels, so obtaining experimental data about peak values of panel acceleration response may not be of much value to them. Perhaps the current state of the art is to concentrate on tying research findings to building floor motion parameters, mostly because these are the values that industry professionals can calculate.

7.4 Acceleration Amplification

Acceleration amplification ratio in this thesis is a measure of how the vibrational characteristics of an item compares to the vibration of the item's supporting structure. Typical dynamic amplification comparing the structure's acceleration (item) to the table base input acceleration (supporting structure) is an amplification of interest. The author also developed amplification relationships between the peak acceleration of the panel (item) and the peak acceleration of the supporting floors (supporting structures). Comparing this definition to a traditional structural dynamics system, the APC panel is

comparable to the structure, and the floors are comparable to the table base at ground level. The relationship of corner floor acceleration to center floor acceleration was explored as well.

For the panels of these experiments, acceleration amplification ratio is the ratio of the peak acceleration of the panel to another acceleration recorded on the structure. The complexity comes from defining the acceleration of the supporting structure. Amplification based upon the peak acceleration of the base of the structure, or in the case of experimental testing, the shake table allows a quick estimate of the panel acceleration in comparison with the expected peak acceleration of a building site. The concern about this ratio is that it is likely heavily dependent upon the height and dynamic characteristics of the building, not the panel.

Determining amplification based upon the peak acceleration of the center of the floor on which the panel sits removes much of the dynamic characteristics of the structure from the resulting value. In addition, acceleration of the center of mass of a floor is a common output from many structural analysis programs used by design engineers. However, the floor of the structure can have significantly different accelerations at different locations of the floor based upon the torsional characteristics of the structure.

Determining amplification using the acceleration of the portion of the structure directly connected to the panel is expected to be the best 'predictor' of the behavior of a panel. The damage of a cladding system is likely to be distributed around the perimeter of a structure depending upon the variation of the structure movement at any given point. Therefore, this ratio should allow for the prediction of acceleration related damage

distributed over the height, width and depth of a structure. The disadvantage of this more reliable estimate is that most design engineers do not evaluate such detailed analytical output of their structures.

Similar to the traditional item-to-support ratio, floor accelerations can be compared amongst themselves at varying geometric locations. Though accelerations at different floor locations are not outputs of one another in the traditional amplification sense, their variation is of particular interest, and amplification serves as an effective tool for observing their variation. In other words amplification comparing floor locations was used to interpret differences in building behavior based upon geometry. Without even knowing the panel response, if the amplifications of the floor are known to differ significantly based on location prior, then researchers may be better guided as to which areas or locations are best to focus on for future experimentation.

Therefore to interpret the panel response behavior, four types of accelerations were quantified: (1) floor acceleration at the panel connection points where the gravity load of the panel is supported, (2) acceleration at the floor center which provides the gravity support for the panel (almost always the lower level of the panel), (3) input table acceleration at the base of the structure, and (4) panel acceleration. From these four types of accelerations, five acceleration amplifications were documented (Equations 7.4 to 7.8):

$$[7.4] \quad \text{Amplification (1)} = \frac{\text{Corner Floor Acceleration}}{\text{Center Floor Acceleration}}$$

$$[7.5] \quad \text{Amplification (2)} = \frac{\text{Floor Acceleration}}{\text{Earthquake Input Table Acceleration}}$$

$$[7.6] \quad \text{Amplification (3)} = \frac{\text{Panel Acceleration}}{\text{Earthquake Input Table Acceleration}}$$

$$[7.7] \quad \text{Amplification (4)} = \frac{\text{Panel Acceleration}}{\text{Center Floor Acceleration}}$$

$$[7.8] \quad \text{Amplification (5)} = \frac{\text{Panel Acceleration}}{\text{Corner Floor Acceleration}}$$

Only peak acceleration values are considered for these five amplifications. The peak panel accelerations used for the amplifications came from the data recorded by the panel accelerometers listed in Table 4.1. The peak floor accelerations used for the amplifications came from the data recorded by the accelerometers listed in Table 5.3 (only the 4th and 5th floors were considered). Peak table accelerations were reported by Dao & Ryan (2012) and are summarized in Table 3.8. Only the absolute values of the acceleration data were used. Upon advice from the research advisor, accelerations less than 6% g were not considered. Accelerations in this range and below are considered negligible (about zero) relative to the building response and input intensity. Acceleration amplifications based on these low accelerations would be erratic and therefore impractical. Only coinciding-plane movement amplification was developed, for local and global coordinates. For example the return panel's out-of-plane acceleration was amplified with the floors global Y direction acceleration, but not with the floors global X direction acceleration.

Tables 7.9 to 7.13 show the acceleration amplifications data. The amplification ratios comparing the panel acceleration to the table base input accelerations and the accelerations of the 4th and 5th floors to the table base input accelerations are shown. The amplification ratios developed for the center to corner floor accelerations and panel to floor accelerations are also shown. The floors accelerated more than the table by at least a factor of ~2 and by as much as ~4. As Z direction acceleration of the table and center of floors were near 5% g and considered negligible, amplifications in the U2 direction were not calculated.

Center and corner acceleration amplification data differed noticeably, so it may be inaccurate to use them interchangeably when predicting behavior of an APC panel. Table 7.9 contains the amplification of corner to center floor accelerations, and amplifications as great as 1.41 in the Y direction at the 4th floor, indicate that the floor corner can experience quite different responses than the floor center. Tables 7.10 and 7.11 show significant acceleration amplification of the floor relative to the table. As mentioned previously, due to the concern about the accuracy of the acceleration reading of instrument SA15X4_COLUMN, the amplification values corresponding to 2.93 g (4th floor corner X direction) were not calculated.

Table 7.9. *Iwanuma Floor (Corner):Floor (Center), Peak Acceleration Amplification Data*

	4th Floor Corner		5th Floor Corner	
	X	**Y**	**X**	**Y**
Peak Acceleration (g)	**2.93 g**	**1.07 g**	**1.10 g**	**1.05 g**
Amplification factor				
relative to 4th floor center	-*	1.41	-	-
relative to 5th floor center	-	-	1.40	1.14

* Due to the concern about the accuracy of the acceleration reading of instrument SA15X4_COLUMN, the amplification value corresponding to 2.93 g was not calculated.

Table 7.10. *Iwanuma Floor (Center):Table, Peak Acceleration Amplification Data*

	4th Floor Center		5th Floor Center	
	X	**Y**	**X**	**Y**
Peak Acceleration (g)	**0.592**	**0.761**	**0.783**	**0.925**
Amplification factor				
relative to table	2.19	2.04	2.90	2.48

Table 7.11. *Iwanuma Floor (Corner):Table, Peak Acceleration Amplification Data*

	4th Floor Corner		5th Floor Corner	
	X	**Y**	**X**	**Y**
Peak Acceleration (g)	**2.93**	**1.07**	**1.1**	**1.05**
Amplification factor				
relative to table	-*	2.87	4.07	2.82

* Due to the concern about the accuracy of the acceleration reading of instrument SA15X4_COLUMN, the amplification value corresponding to 2.93 g was not calculated.

Likewise, amplification ratios of the panel compared to the structure are summarized in Tables 7.12 and 7.13. It can be observed that generally the panels experienced greater amplification with respect to the table than to the floor acceleration, as one might expect. The flat panel experienced out-of-plane amplification as great as 7.44. The flat panel amplification of 9.03 in the in-plane direction is particularly high, possibly suggesting instrumentation error. Panel amplifications at the floor corner are generally closer to unity than amplifications at the floor center. This correlation indicates that the accelerations of the floor at the panel support points more closely follow the acceleration of the panels themselves (more so than the center floor acceleration), as expected. The flat panel generally experienced higher amplification than the return panel. For example when comparing the individual panels to their support points on the structure floor (corner accelerations at both the 4^{th} and 5^{th} floors), it is observed that the return panel achieved in-plane amplification of 1.10 and out-of-plane amplification of 1.41, whereas the flat panel achieved in-plane amplification of 3.21 and out-of-plane amplification of 1.91.

Table 7.12. *Iwanuma Peak Panel U1 Acceleration Amplification Data - Panel:Table, Panel:Floor (Center), and Panel:Floor (Corner)*

	Panel U1 Amplification	
	PD-1	**PD-2**
Panel Acceleration (g)	**1.48**	**2.01**
Amplification factor		
relative to table	3.97	7.44
relative to 4th floor center	1.94	3.55
relative to 5th floor center	1.60	2.68
relative to 4th floor corner	1.38	-*
relative to 5th floor corner	1.41	1.91

* Due to the concern about the accuracy of the acceleration reading of instrument SA15X4_COLUMN, the amplification value corresponding to 2.93 g was not calculated.

Table 7.13. *Iwanuma Peak Panel U3 Acceleration Amplification Data - Panel:Table, Panel:Floor (Center), and Panel:Floor (Corner)*

	Panel U3 Amplification	
	PD-1	**PD-2**
Panel Acceleration (g)	**1.21**	**3.37**
Amplification factor		
relative to table	4.48	9.03
relative to 4th floor center	2.04	4.43
relative to 5th floor center	1.55	3.64
relative to 4th floor corner	-*	3.15
relative to 5th floor corner	1.10	3.21

* Due to the concern about the accuracy of the acceleration reading of instrument SA15X4_COLUMN, the amplification value corresponding to 2.93 g was not calculated.

In-plane acceleration amplifications are generally larger than the out-of-plane amplifications for both panels. Tables 7.12 and 7.13 also show that in-plane amplifications can differ by more than a factor of ~2, when comparing the amplifications of PD-1 to the amplifications of PD-2. This factor of ~2 is also observed in the out-of-plane direction when comparing PD-1 amplifications to PD-2 amplifications. One may expect similar magnitudes of in-plane amplification when comparing PD-1 to PD-2 (likewise for the out-of-plane amplifications), but this is not necessarily evident according to the data. This particular lack of correlation could be due to the different geometries of the panels. Though the peak acceleration reading of instrument EA02Y4_PANEL also raised a concern for accuracy, the amplification values corresponding to 3.37 g (in-plane PD-2 acceleration) were still calculated.

7.5 Comparison of IBC Static Code Force to Experimental Force

The *ASCE 7-10* (ASCE, 2010) standard and *IBC* (ICC, 2011) were used as a basis for determining design forces that might be used by engineers when designing the APC panels of the experiment. For the design, the ASCE parameters used for the design spectra were S_{DS} of 1.0g, I_p of 1.0 representing a region of relatively high design accelerations. Table 7.14 provides a summary of the IBC design forces and the Iwanuma recorded peak values. The design forces are reported as the force to the applied to the center of mass of each panel for either the design of the panel body (concrete, reinforcement) or the connection (embeds, welds, bolts, etc…). The peak recorded values are reported for U1, the out-of-plane direction of each panel, or U3, the in-plane direction of each panel. The design force is an integration of the seismic load over the

entire panel. To obtain an estimation of the panel acceleration integrated over the entire panel, it was necessary to combine the peak acceleration recorded at the middle of the panel and the accelerations at the supports using Equation 7.3.

Table 7.14. *Iwanuma Design Loads for APC Panels*

Design/Test Parameter	**APC Panel PD-1 Return Panel**	**APC Panel PD-2 Flat Panel**
Panel weight, lbs.	3278	1192
Design force for concrete panel, lbs.	1276	464
Design force for connections, lbs.	3988	1450
Peak U1 acceleration, g (using Eqn. 7.3)	1.22	1.06
Peak U1 inertial force, lbs	3999	1264
Peak U3 acceleration, g (using Eqn. 7.3)	0.954	2.10*
Peak U3 inertial force, lbs	3127	2503

*Potential instrumentation error (EA02Y4_PANEL).

The peak acceleration of each panel was determined by Equation 7.3. As previously stated, it is expected that the acceleration of the panel at any time step of loading is an average of the acceleration recorded on the panel and the average of the floor accelerations of the two stories supporting the panel. Maximum panel accelerations (a_{panel}) calculated using Equation 7.3 occurred at the time of peak panel recorded accelerations ($a_{recorded}$), except for the in-plane acceleration of the return panel. Though there was concern about the accuracy of the acceleration reading of instrument EA02Y4_PANEL, the peak U3 acceleration using Equation 7.3 was still calculated.

To allow for comparison with the design forces, the inertial force of the panel was calculated as the product of the peak acceleration of the panel and the mass of the panel. The code-based design forces are comparable in magnitude to the experimental forces. Both in-plane and out-of-plane forces experienced by the panels exceeded their corresponding panel design force. The in-plane force of the return panel and the out-of-plane force of the flat panel did not exceed the connection design forces. The out-of-plane design force of the flat panel was within 1% of its connection design force.

7.6 Uplift and Rocking Behavior of Panels

A potential concern when using vertically slotted connections is that high impact forces may be generated when the panel 'seats itself' after uplifting off the leveling bolt. The expected movement of the slotted connection is that as the top of the panel moves laterally, one bottom leveling bolt lifts from the support. When the panel moves back in the opposite direction, this leveling bolt lowers back to the original position. If this occurs quickly, high impact forces may be generated leading to damage.

To explore this potential phenomenon, the data recorded for the movement of the bottom vertical connections, as discussed in Section 6.2, was graphed along with the panel accelerations at times of interest as shown in Figures 7.35 to 7.39. Choosing the time intervals for observing this potential phenomenon consisted of first determining when the panel experienced its maximum negative displacement. At this time, the panels were expected to be returning to the floor. Second, panel acceleration responses at time intervals near the largest negative panel displacement were analyzed. The largest panel displacements occurred during both the time intervals of ~36 seconds and ~76 seconds.

The author then looked at 2 second and 1 second intervals near these time frames to observe the phenomenon.

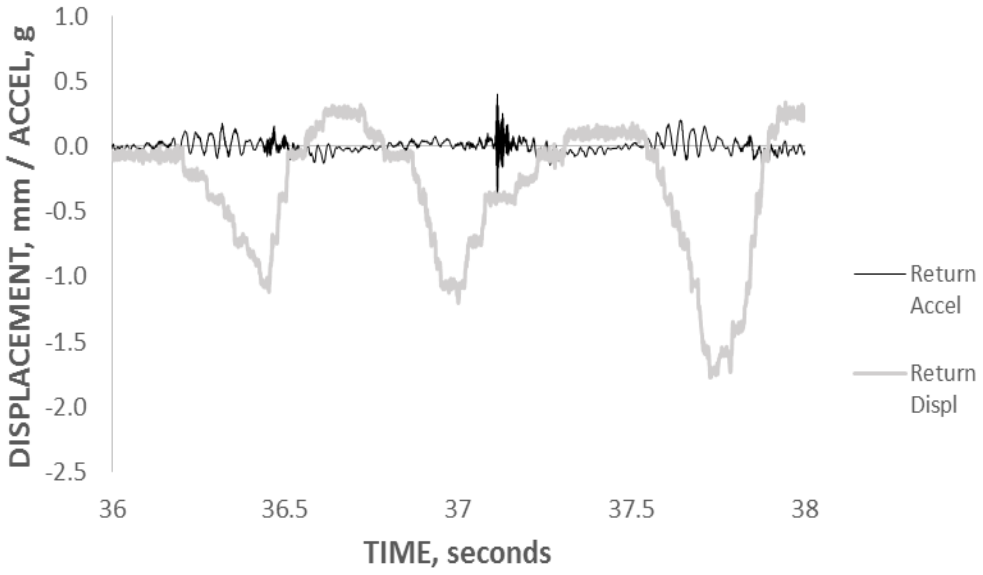

Figure 7.35. PD-1 Bottom Uplift vs. Z Direction Acceleration Time History Plots

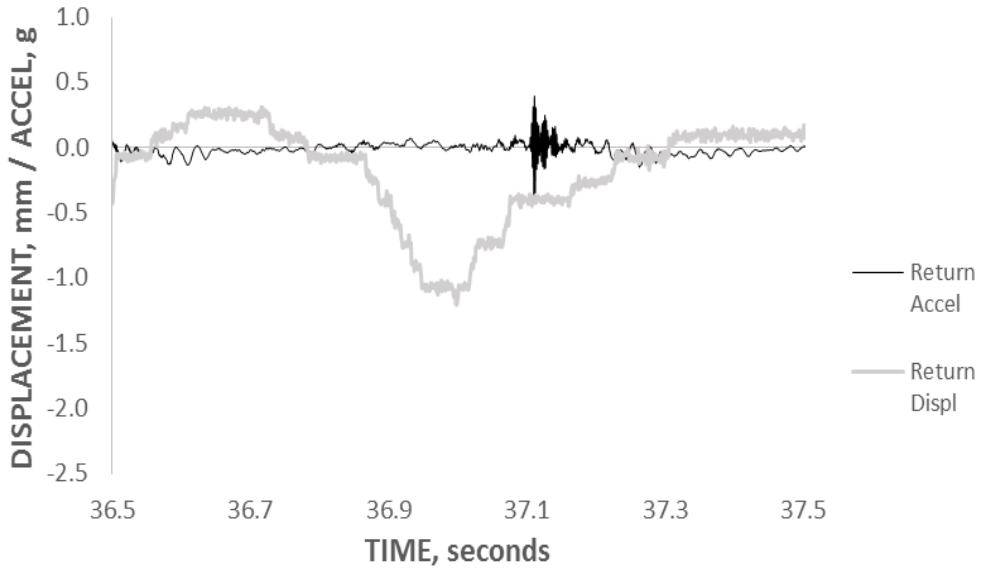

Figure 7.36. PD-1 Bottom Uplift vs. Z Direction Acceleration Time History Plots

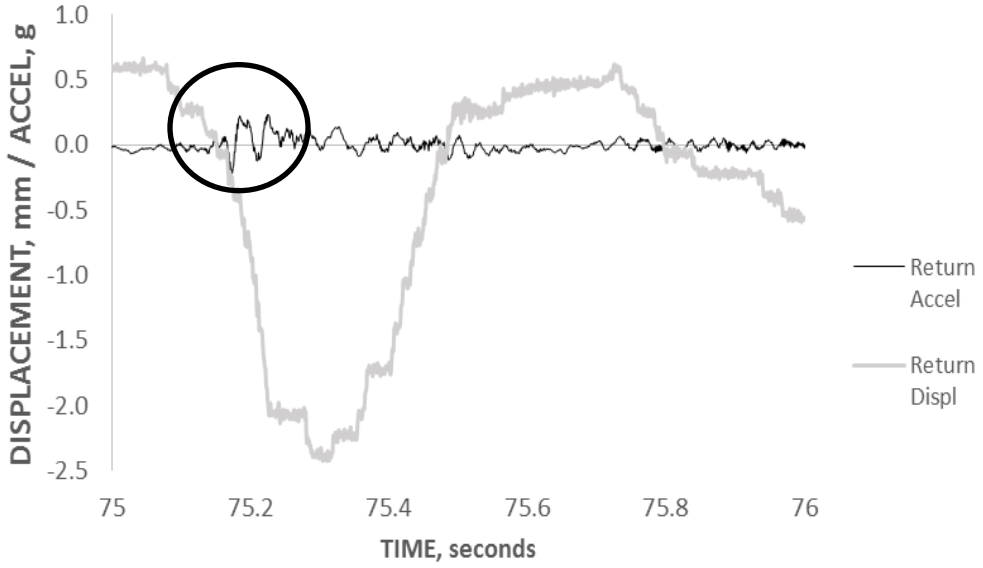

Figure 7.37. PD-1 Bottom Uplift vs. Z Direction Acceleration Time History Plots

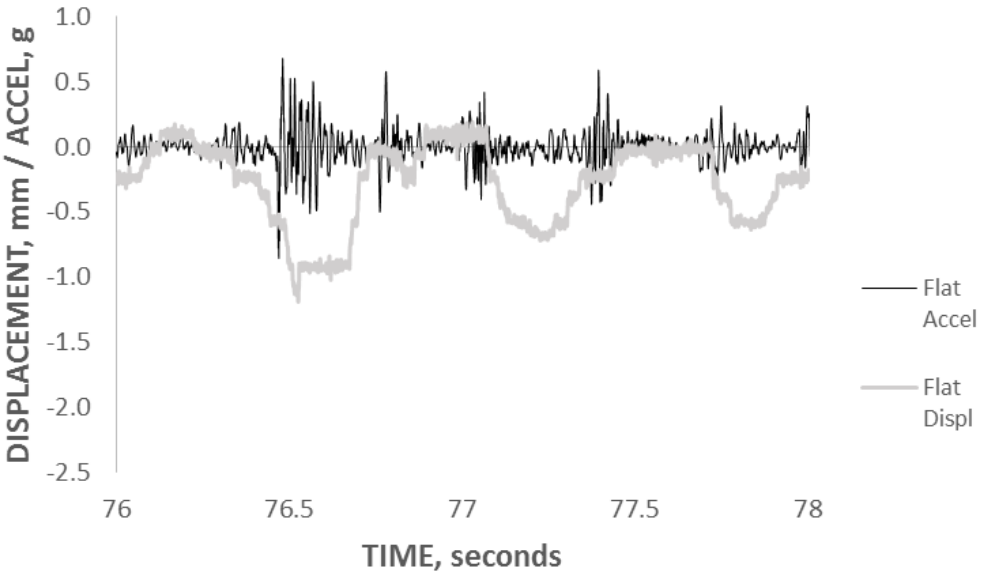

Figure 7.38. PD-2 Bottom Uplift vs. Z Direction Acceleration Time History Plots

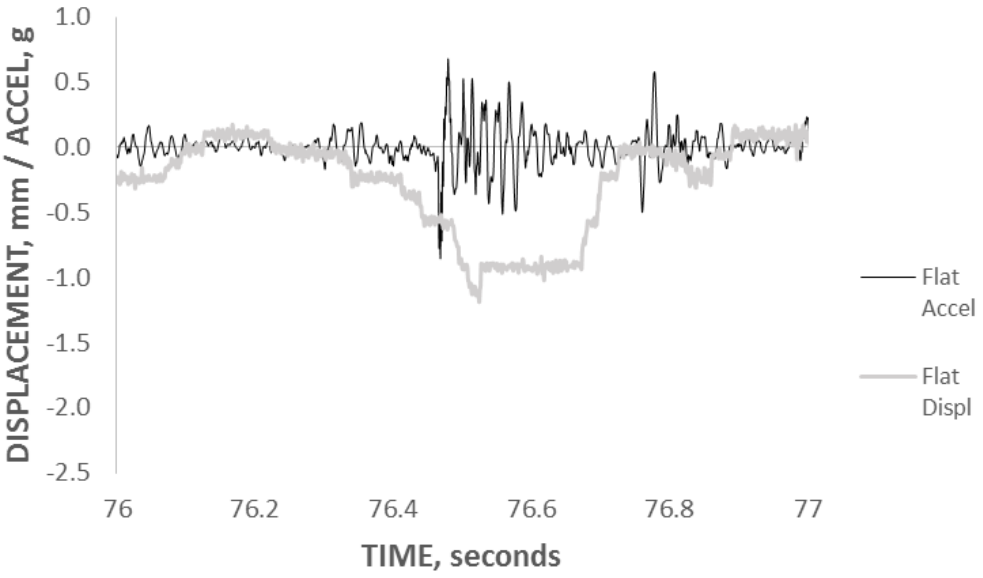

Figure 7.39. PD-2 Bottom Uplift vs. Z Direction Acceleration Time History Plots

Spikes are evident in acceleration throughout the time history for both the return and flat panels. The spikes in acceleration are indicated by the high magnitude and high frequency. Some of the spikes do indeed occur when the displacement of the panel reaches its negative peak. This negative peak should represent the panel returning to the floor and likely causing a spike in vertical acceleration. Figures 7.35 to 7.37 are plots of specific time segments where this phenomenon seems to be prevalent for the return panel. Figures 7.38 and 7.39 are plots of specific time segments where this phenomenon seems to be prevalent for the flat panel. Figures 7.37 and 7.39 include the point of the largest negative displacement response of both the return panel and flat panel, respectively. Figure 7.37 shows a spike in acceleration that is small yet still apparent at the 75.2 second time interval.

To confirm the rocking behavior of the panels as a result of the slotted connections, video footage observed during the time intervals of Figures 7.35 to 7.39 was reviewed. Unfortunately the footage was unable to capture or distinguish the rocking behavior of the panels via the floor cameras because the deflections were too small to visually see uplift within the slots.

It should be noted that there are other reasons as to why the spikes in vertical acceleration may occur. Spikes may be due to impact when the panel returns to the support due to the rocking action, but spikes may also occur due to some other impact, such as the panel against the support or the closing of the gap between the steel slot and the connection bolt. Flexibility of the steel cantilever supporting the panel may also affect the dynamic response of the system. Additionally, the input motion to the table

also includes significant spikes in the ground acceleration. While the large mass of the structure reduces the likelihood of these rapid acceleration changes to affect the entire structure, the possibility of a frequency approaching resonance with a dynamic mode of the panel is possible.

In addition to these physical causes of spikes in acceleration, experimental error may also result from instability of the voltage supplies to the instrument, incorrect attachment of the instrument to the specimen, or computational error in the data logging system. While care was taken to minimize instrumentation error during the testing, it is difficult to remove all such possibilities. For these multiple reasons, more investigation of the dynamic character of the entire system will be necessary before definitive interpretation of the experimental data is possible.

8 Results

Drift data were analyzed for all earthquake motions; however, acceleration data were only considered for the Iwanuma ground motion. The goal of this project was to develop a systematic process that can serve as a model for analyzing all ground motions for future research related to NEES Project 571, Experiment 5 at E-Defense. All research objectives discussed in Section 1.2 were addressed in this project. Each objective is discussed below:

1. Determine the floor acceleration time history records at the connection points of the APC panels to the structure floor.

- Floor acceleration time history records at the connection points of the APC panels to the structure floor were produced. There were accelerometers mounted on each panel, but there were no floor or column triaxial accelerometers at the corner of interest. Based on the assumption that the diaphragm was rigid, accelerations at the NW and SE columns of the building were extrapolated to the corner of interest.

2. Compare the acceleration time history of the individual panels to the support points on the structure floor.

- Acceleration time history records of the individual panels were graphed to compare to the accelerations at the support points on the structure floor. Acceleration peaks for all the functions occurred near time interval of 75 to 77.5 seconds. One issue of interest is whether the individual non-structural elements of a structure experience the same acceleration as the floors that provide their

gravity support. By reviewing the 4th floor, 5th floor, and panel acceleration plots of Figures 7.8 to 7.23, it is not apparent that either floor is better representative of the panel acceleration.

- The plots all show high frequencies and magnitudes during the 35 second and 75 second time intervals.

3. Determine the magnitude of the peak acceleration amplification factor for each panel.

- The magnitudes of the peak acceleration amplification factors for each panel were determined. At the corner where the panels were installed, the flat panel experienced the greatest in-plane corner floor acceleration amplification of 3.21 (Table 7.13). The return panel experienced generally less amplification and in the out-of-plane direction had an acceleration amplification of 1.41 relative to the corner of the floor diaphragm (Table 7.12).
- Panel amplification relative to the corner was closer to unity than panel amplification relative to the center, and therefore may be considered a better predictor of the panel behavior (for example, the floor corner accelerations at the panel connection points may be more comparable to the actual panel accelerations).
- The in-plane amplifications of PD-1 and PD-2 varied significantly (also true for out-of-plane amplifications) and therefore more data are required for predicting panel acceleration as a trend could not be observed. The different panel geometries could be a reason for the amplification variances in similar planes.

- The peak acceleration of the 4th floor corner (where the panels were located) and the peak in-plane acceleration of panel PD-2 were uncharacteristically high, which may be an indication of instrumentation error. Though both of these accelerations may very well be accurate, the authors were unable to determine or verify if there was in fact instrumentation error. The author did not use the peak 4th floor corner acceleration to compute amplifications, but chose to keep the peak in-plane acceleration of panel PD-2.

4. Determine the relationship of the inter-story drift ratio and the rocking behavior of the panels.

- The primary findings related to the overall performance include the observation that slotted connections slide with minimal restraint while the structure and panels are being accelerated in a full scale 3D seismic motion. Algorithms were developed to determine the building drift at the point of the floor where the panels are connected and the drift of the panels themselves. As there was no damage, the author was unable to develop an upper bound on the drift the panels could accommodate before damage occurred.
- Comparison of the panel's vertical acceleration with the panel's vertical displacement did show apparent spikes in acceleration at the vertical displacements representing the panel returning to the floor. Spikes in acceleration were short in duration, thus occurring at higher frequency. This suggested rocking behavior. Video documentation would have been used to verify rocking behavior at the peak vertical accelerations of the panels, when the stringpot

attached to the panel returned to its resting position (representing the panel returning to the floor). The panel movement during the experiment was too small to be captured by the video.

- Also panel acceleration spikes occurred at instances when the panel did not appear to have returned to its support. This was not surprising as spikes in vertical acceleration of the panels could also be the result of other phenomena such as resonance or closing of the gap between the steel slot and connection bolt (without rocking). Again, video footage would have been beneficial to confirm these causes of spikes in vertical acceleration.
- Damage is expected to occur as a result of this rocking. Further research is required to relate drift, displacement, and acceleration to the physical behavior of the panels through damage states. It is premature to establish a relation between drift, displacement, acceleration, and panel damage states.

5. Compare the peak inter-story drift ratios achieved during the shake table testing with structure inter-story drift demands defined in engineering literature.

- Structure inter-story drift demands defined in engineering literature were compared to the peak inter-story drift ratios achieved during the shake table testing. Each structure of the literature review was regular and contained an *ASCE 7-10* (ASCE, 2010) recognized lateral system. Each structure was 5 or more stories (mid to high rise) and subjected to seismic loading. Dynamic inelastic analysis was performed on all buildings and drift ratios varied from 0.0036 to 0.0438 radians. The maximum center inter-story drift ratio of the

structure was 0.903% and occurred during the 35RRS test trial. The peak corner inter-story drift ratio at the 4th story (story of interest) occurred during the IWA test trial and was 0.756%. Both of these peak drifts fall within the lower range of the drifts collected from literature review and expectedly so as the shake table experiments were scaled to limit the frame to elastic response only.

6. Develop an algorithm for determining drift at the corner of the building from data recorded on the global movement of the building.

- Drift was determined considering both the displacement at the center of mass and the displacement caused by twisting of the building. Drift due to twist was deemed significant enough to be considered. Twist data were retrieved from Dao & Ryan (2012). Drift contributions from twist were added to the initial derived center of mass drift to develop a final drift.

7. Develop relationships between drift and acceleration measured at the center of the building to the movement of the APC panel (drift and amplification).

- Common engineering practice is to report drift at the center of mass of a building. For applications such as determining building design forces, this is effective. However, in analyzing the concrete cladding, it is apparent that the floor drifts experienced at the center of the building and the floor drifts reported at the location of the panels can differ significantly. Depending on the length and size of the floor, each building will differ significantly, so it may be inappropriate to report panel drift in reference to floor drift at the center of the building.

- If instrumentation is not placed directly at the panel location, drift at the location of interest may be derived using twist vectors developed from floor geometry or through other methods.
- Center and corner floor accelerations varied significantly as well. Panel to center floor acceleration amplifications were noticeably high in both out-of-plane and in-plane directions (See Tables 7.12 and 7.13).

8. Develop relationships between drift and acceleration measured at the connection points of the panels to the movement of the APC panels (panel deflection and amplification).

- Panel deflection was determined from story drift measured at the connection points of the panels. Both panels experienced maximum deflections in the range of ~13.1 mm and ~22.7 mm. As there was no observed damage to either panel, these ranges cannot be related to damage states.
- The accelerations at the corner of the structure were larger than those at the center. Peak in-plane accelerations of the panels occurred within ~2 seconds of both the center and corner floor acceleration peaks. Panels and floors all had peak accelerations during similar time intervals but no other distinct relationship was developed between the panel and floor accelerations. Amplification data showed variation, but as there was no observed damage, it is unclear whether center and/or corner floor accelerations are valid to produce fragility plots.
- Peaks in panel acceleration, as the panels returned to the supports within the slotted connections, may be a result of rocking.

9. Determine inertial forces generated during an earthquake and compare those values to the design forces assigned by current building codes.

- The panel connection design forces for both the return panel and flat panel were developed using the International Building Code (IBC), for a similar building in San Jose, CA. The design force is applicable for all three directions. The experimental panel forces were derived using the maximum acceleration of the three directions, multiplied by the mass of the panels. When comparing the connection design forces to the inertial forces developed during the experiment, two of the four were found to be larger. The out-of-plane inertial forces of the return panel and in-plane inertial forces of the flat panel both exceeded connection design forces. In-plane inertial forces of the return panel and out-of-plane inertial forces of the flat panel are both lower than the connection design forces. In-plane and out-of-plane inertial forces exceeded panel design forces. As the panels experienced no damage, the code forces used for the design of the panels produced a design with good performance.

9 Conclusions and Recommendations

The purpose of this research project was to evaluate the behavior of architectural precast concrete cladding under seismic loading, using the data from a recent shake table experiment. Ultimately the cladding behavior was examined as a function of building drift and acceleration. Drift and acceleration are fundamental responses of seismic engineering that are useful for gauging the element/component behaviors that they are proportional to.

The acceleration and drift data vary considerably depending upon whether they are measured at the corner of the floor or at the center of mass, so it may be inaccurate to use them interchangeably when discussing behavior of the panels. At the story of interest, when comparing drift at the center of the floor model to drift due to twist at the corner, it was determined that twist drift was as much as 43% of the center drift (significant). Floor accelerations varied between center and corner as well. The peak 4^{th} floor corner acceleration in the global X direction was greater than the peak 4^{th} floor center acceleration by a factor of 4.95. These results suggest that the accelerations and drifts at a building's center-of-mass are not accurate representations of the building's corner behavior. Center and corner responses are not interchangeable when describing the behavior of concrete cladding panels. Building planar geometry plays a significant role in the behavior of cladding, even among regular buildings. The cladding experienced no damage at the building's target maximum response acceleration of 1g. An algorithm was not developed to determine vertical floor acceleration at the corner as

center floor accelerations were taken as the average of three corner column accelerations and were in the range of 5% g (considered negligible).

Amplification ratios of the acceleration were calculated for each panel. The flat panel experienced a maximum in-plane acceleration amplification of 3.21 when compared to the support points on the structure floor, whereas the return panel's peak in-plane acceleration amplification to the floor connections was 1.10. One might expect these values to be more similar, but there are reasons that amplifications in similar planes of motion can differ so drastically. One reason is due to the different geometric properties of the panels themselves. More data are needed to observe a trend as far as predicting panel acceleration. There was also no clear trend between the acceleration of the panel and the average acceleration of floors below and above the panels at the corner other than that their peaks occurred within similar time intervals. Also a relationship could not be determined between panel performance and acceleration as the panels experienced no damage and therefore the acceleration could not be correlated to damage limit states. Drifts also could not be correlated to damage states as there was no recorded damage to the panels.

The absence of damage recorded to the panels may be expected as target experimental drift ratios and accelerations for the building were aimed to be limited to 1% and 1 g (to exhibit linearly elastic behavior only), respectively. It is also important to note that the corner at column X1/Y3 may not be the corner that experienced the highest inter-story drift. In the future, conducting full scale fixed-based experiments will be

beneficial for developing fragility curve plots of damage state levels related to inter-story drift and peak floor acceleration.

Inertial forces generated during the Iwanuma earthquake ground motion were generally higher than the design forces assigned by current building codes. Inertial forces surpassed panel design forces but connection design forces were more comparable. Out-of-plane inertial force of the return panel fell within 1% of the connection design force. Code forces are conservative and are not meant to withstand the full earthquake loads so this may be expected. The absence of damage to either panel only suggests that the code forces worked as intended in the design of the panels. Further testing and research in similar areas may reveal that design codes need to be shifted, but this thesis is not suggesting that.

The video camera footage was clear, but the deflections were too small to establish (or expect) visual confirmation of rocking. Although fragility curves were not developed, future experiments that include higher responses than that of the experiment at E-Defense, should be able to build upon the initial findings of this thesis. For instance had a catch basin been available for the shake table experiment at E-Defense, perhaps a full scale Iwanuma trial could have been conducted resulting in drifts closer to the higher ranged values presented in literature review.

The author further recommends testing more panels in an individual experiment as well as placing more instrumentation at the locations of interest, if at all possible. This will allow researchers to detect more trends and perhaps better trends in the observation of APC panel behavior. Nonetheless, one can use the data reduction methodology

presented in this thesis to predict the acceleration and drift responses at the locations of interest if it is necessary.

References

ASCE. (2010). *Minimum Design Loads for Buildings and Other Structures*. ASCE/SEI Standard 7-10.

Bojórquezl, E., Ruiz-García, J. (2013). Residual drift demands in moment-resisting steel frames subjected to narrow-band earthquake ground motions. *Earthquake Engineering & Structural Dynamics.* Wiley Online Library, DOI: 10.1002/eqe.2288

Carpenter, L. (2004). High-rise building cladding drift accommodation. *The Structural Design of Tall and Special Buildings, 13*, 439-456.

Chopra, A. (2007). *Dynamics of Structures: Theory and Applications to Earthquake Engineering 3rd Edition*. Pearson Education, Inc.

Dao, N. & Ryan, K. (2012). Seismic Response of a Full-Scale Steel Frame Building Isolated with Triple Pendulum Bearings Under 3D Excitation. Network for Earthquake Engineering Simulation (distributor), Dataset, DOI:10.4231/D3NP1WJ3P

Dao, N. & Ryan, K. (2013). Computational simulation of a full-scale, fixed-base, and isolated-base steel moment frame building tested at E-defense. *Journal of Structural Engineering, 140*, A4014005. Network for Earthquake Engineering Simulation (distributor), Dataset, DOI:10.4231/D3NP1WJ3P

Hart, G., Vasdevan, R. (1975). Earthquake Design of Buildings: Damping. *ASCE Journal of the Structural Division, 101*, 11-30.

Heiduschke, A., Kasal, B., & Haller, P. (2009). "Shake table tests of small-and full-scale laminated timber frames with moment connections." *Bulletin of Earthquake Engineering, 7*(1), 323-339. Engineering Village, DOI: 10.1007/s10518-008-9075-4

Hokmabadi, A. S., Fatahi, B. & Samali, B. (2012). Recording inter-storey drifts of structures in time-history approach for seismic design of building frames. *Australian Journal of Structural Engineering*, *13*, 175-180. http://dx.doi.org/10.7158/S11-118.2012.13.2

ICC. (2007). *International Fire Code Section 5607 Blasting*. Falls Church, Virginia: International Code Council.

ICC. (2011). *2012 International Building Code*. Country Club Hills, Ill: International Code Council.

Kamura, H., Katayama, T., Shimokawa, H., & Okamoto, H. (2000, November). Energy dissipation characteristics of hysteretic dampers with low yield strength steel. *Proceedings of the US–Japan Joint Meeting for Advanced Steel Structures, Building Research Institute, Tokyo.*

Kiggins, S., & Uang, C. (2006). Reducing residual drift of buckling-restrained braced frames as a dual system. *Engineering Structures, 28*, 1525-1532. Engineering Village, DOI: 10.1016/j.engstruct.2005.10.023

Krawinkler, H., Medina, R., Alavi, B. (2003). Seismic drift and ductility demands and their dependence on ground motions. *Engineering Structures*, *25*, 637-653. Engineering Village, DOI: 10.1016/S0141-0296(02)00174-8

Lee, S., Ham, H. J., & Kim, H. (2013). Fragility Assessment for Cladding of Industrial Buildings Subjected to Extreme Wind. *Journal of Asian Architecture and Building Engineering, 12*(1), 65-72. http://doi.org/10.3130/jaabe.12.65

Lindeburg, M., McMullin, K. (2011). *Seismic Design of Building Structures: A Professional's Introduction to Earthquake Forces and Design Details 10th Edition*. Belmont, California: Professional Publications, Inc.

Linkute, L., Juocevicius, V., & Vaidogas, E. R. (2013). A probabilistic design of sacrificial cladding for a blast wall using limited statistical information on blast loading. *Mechanika, 19*(1), 58-66. DOI:10.5755/j01.mech.19.1.3621

Maddalena, S. (2003). Realizing the design: Decorative precast cladding. *Concrete*, *37*, 56-58.

McMullin, K. (2013). *CE 267 Advanced Steel Design Reader*. San Jose State University.

McMullin, K. (Photographer). (2011). Miki, Japan.

Medina, R. A. (2005). Evaluation of drift demands for the seismic performance assessment of frames. *Journal of Structural Engineering*, *131*, 1003-1013. Engineering Village, DOI: 10.1061/(ASCE)0733-9445(2005)131:7(1003)

Ohi, K., Shimawaki, Y., Lee, S., & Otsuka, H. (2001). Pseudodynamic tests on pseudo-elastic bracing system made from shape memory alloy. *Bulletin of Earthquake Resistant Structure Research Center*, *34*, 21-8.

Olmati, P., Petrini, F., & Gkoumas, K. (2014). Fragility analysis for the Performance-Based Design of cladding wall panels subjected to blast load. *Engineering Structures, 78*, 112-120. http://dx.doi.org.libaccess.sjlibrary.org/10.1016/j.engstruct.2014.06.004

Ortiz, M. (Photographer). (2011). Miki, Japan.

Ryan, K. (n.d.). Experiment 5: Full Scale 5-story Building in Fixed-Base Condition at E-Defense. Network for Earthquake Engineering Simulation (distributor), Dataset, DOI:10.4231/D3NP1WJ3P

Ryan, K., Dao, N., Sato, E., Sasaki, T., & Okazaki, T. (2012a). *Aspects of isolation device behavior observed from full-scale testing of an isolated building at E-defense*. Paper presented at the 43rd Structures Congress, Chicago, Illinois. Network for Earthquake Engineering Simulation (distributor), Dataset, DOI:10.4231/D3NP1WJ3P

Ryan, K., Dao, N., Sato, E., Sasaki, T., & Okazaki, T. (2012b). *NEES/E-defense base-isolation tests: Interaction of horizontal and vertical response*. Paper presented at the Proc. 15th World Conference on Earthquake Engineering, Lisbon, Portugal. Network for Earthquake Engineering Simulation (distributor), Dataset, DOI:10.4231/D3NP1WJ3P

Ryan, K., Sato, E., Sasaki, T., Okazaki, T., Guzman, J., Dao, N.D., Soroushian, S., Coria, C. (2013). Full Scale 5-story Building in Fixed-Base Condition at E-Defense. Network for Earthquake Engineering Simulation (distributor), Dataset, DOI:10.4231/D3NP1WJ3P

Sabelli, R., Mahin, S., & Chang, C. (2003). Seismic demands on steel braced frame buildings with buckling-restrained braces. *Engineering Structures, 25*, 655-666. DOI: 10.1016/S01410296(02)00175-X

Searer, G., Freeman, S. (2004, May). Seismic Drift and the Design of Claddings. *Proceedings of the 2004 Structures Congress, Nashville, Tennessee*, 1-10. DOI:10.1061/40700(2004)71

Soroushian, S., Ryan, K., Maragakis, M., Wieser, J., Sasaki, T., Sato, E.,. Mosqueda, G. (2012). *NEES/E-defense tests: Seismic performance of ceiling/sprinkler piping non-structural systems in base isolated and fixed-base building*. Paper presented at the 15th World Conference on Earthquake Engineering (15WCEE), Lisbon, Portugal. Network for Earthquake Engineering Simulation (distributor), Dataset, DOI:10.4231/D3NP1WJ3P

Tremblay, R. (2002). Inelastic seismic response of steel bracing members. *Journal of Constructional Steel Research, 58*, 665-701. http://dx.doi.org.libaccess.sjlibrary.org/10.1016/S0143-974X(01)00104-3

USGS. (2016). *U.S. Department of the Interior: USGS Earthquakes Hazards Program*. Retreived from http://earthquake.usgs.gov/earthquakes/

Van Paepegem,W., Palanivelu, S., Degrieck, J., Vantomme, J., Reymen, B., Kakogiannis, D., Wastiels, J. (2014). Blast performance of a sacrificial cladding with composite tubes for protection of civil engineering structures. *Composites Part B: Engineering, 65*, 131-146. http://dx.doi.org.libaccess.sjlibrary.org/10.1016/j.compositesb.2014.02.004

Walker, D., & Kennell, D. (2006). Precast concrete cladding - then and now. *Concrete, 40*, 58-59. Retrieved from http://search.proquest.com.libaccess.sjlibrary.org/docview/204060515?accountid=10361

Zona, A., Barbato, M., & Conte, J. (2008). Nonlinear seismic response analysis of steel–concrete composite frames. *Journal of Structural Engineering, 134*, 986-997. DOI: 10.1061/(ASCE)0733-9445(2008)134:6(986)

Appendix A: Structural Details of the APC Cladding

Care was taken to match the goals of experimental testing with the necessity of meeting construction limitations. APC systems in the US and Japan have similar functions and architectural features but have quite significant differences in engineering detailing and construction. Ideally, the cladding system would be built in the US by an American precast concrete fabricator to fully capture the seismic performance expected from US commercial real estate. However, the prohibitive cost of shipping required the casting to be done in Japan. Since only two panels were to be built, the scope of work did not justify contracting with either a US or Japanese precast fabrication company, so the research team concluded that the general contractor for the construction of the main test specimen would be hired to form and cast the two panels.

Since the expected inelastic behavior of cladding is primarily in the steel connections, care was taken to achieve accurate representation of US construction practice. Hence, the cladding panel was designed and the steel connections were fabricated under the guidance of a major US precast concrete cladding company and the connections were shipped to Japan to be used in the assembly of the test specimen.

Two panels were installed to represent the corner column cover assembly of a building, as previously shown in Figure 4.1. The APC panels were designed according to common U.S. practice for seismic load intended to represent a large seismic event. The APC panels are located on the 4^{th} story in the SW corner of the building at the stairwell. Figures A.1 to A.8 show the structural details and dimensions of the return panel and flat panel, respectively. Steel connections cantilevered from the main steel frame provided

support for the panels. The panel weight was supported by steel components cantilevered from the structural steel frames of Level 4. Figure A.1 is an elevation view of both the return panel and flat panel referred to as PD-1 and PD-2, respectively. The larger panel, PD-1, was a return panel, with a plan view shape of an L with a long leg of 1200 mm and a short leg of 575 mm. The smaller panel, PD-2, was a half-width flat panel with a width of 575 mm. Both full-height column cover panels were 3000 mm tall and 120 mm thick. The panels were installed with a 50 mm seismic joint over the full height of the panels. The seismic gap is shown in Figure A.1 as well.

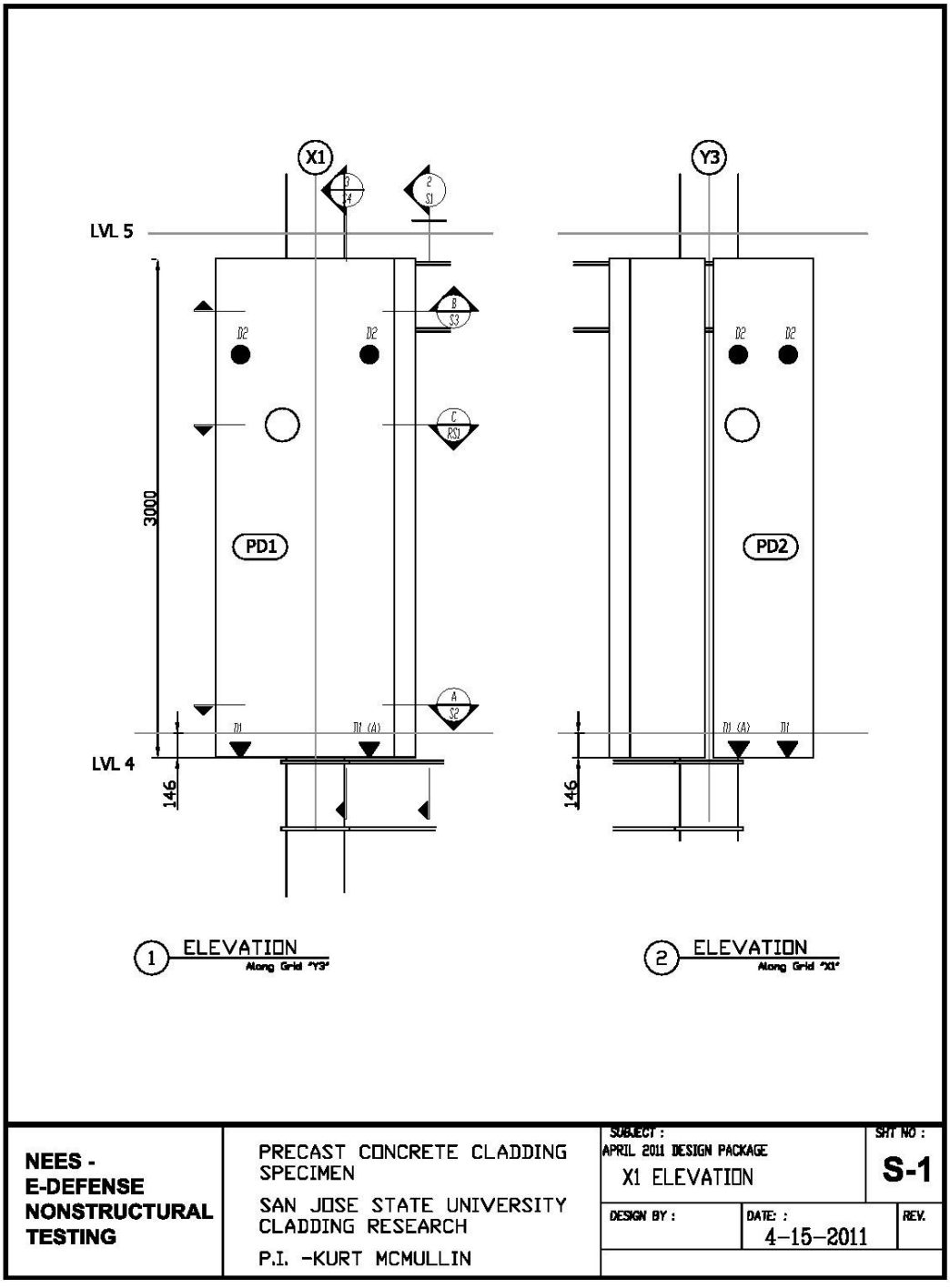

Figure A.1. Elevation View of the Return and Flat Panels with the Location of the Seismic Gap

There are two bearing connections and two slotted connections for every panel. Figures A.2 and A.3 show plan views of the connections at the 4th and 5th floor plans of the SW corner, respectively. Figure A.4 shows the bottom and top panel connections in an elevation view. Figure A.5 highlights the typical bearing connection detail for the bottom of the panels connected to the 4th floor beams. These bearing connections consist of a slot for vertical translation as well as a leveling nut to ensure proper alignment during installation. Figure A.6 highlights the typical slotted connection detail for the top of the panels connected to the 5th floor beams. These slotted connections allow for the vertical translation as well. Essentially each of the panels was supported by four connections forming a plane. These connections allow for the "rocking mechanism" discussed in Section 1.4.3. Figures A.7 and A.8 show construction shop drawing elevations of both the panels PD-1 and PD-2, respectively.

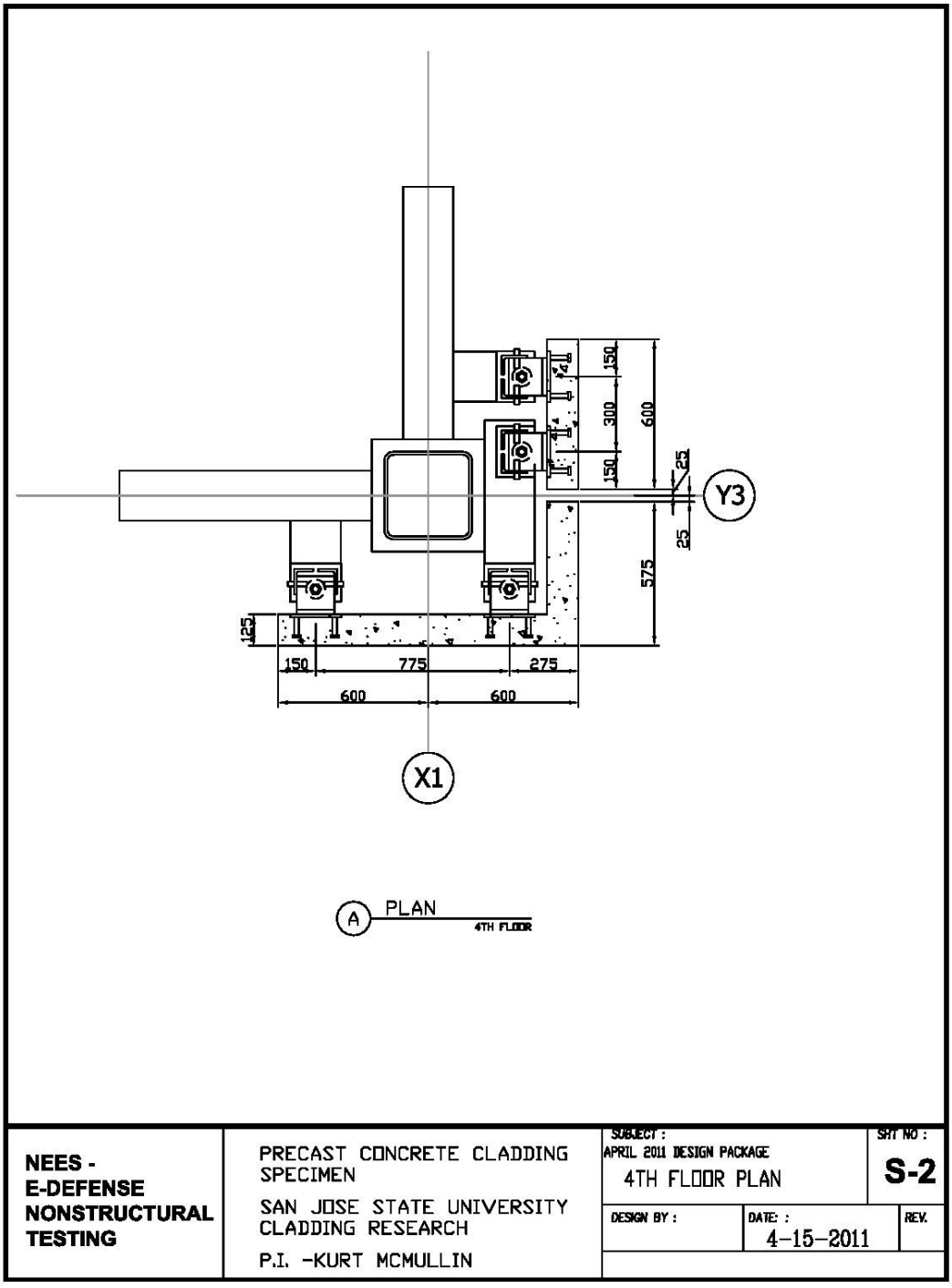

Figure A.2. Plan View of Bottom Bearing Connections for both the Return and Flat Panel

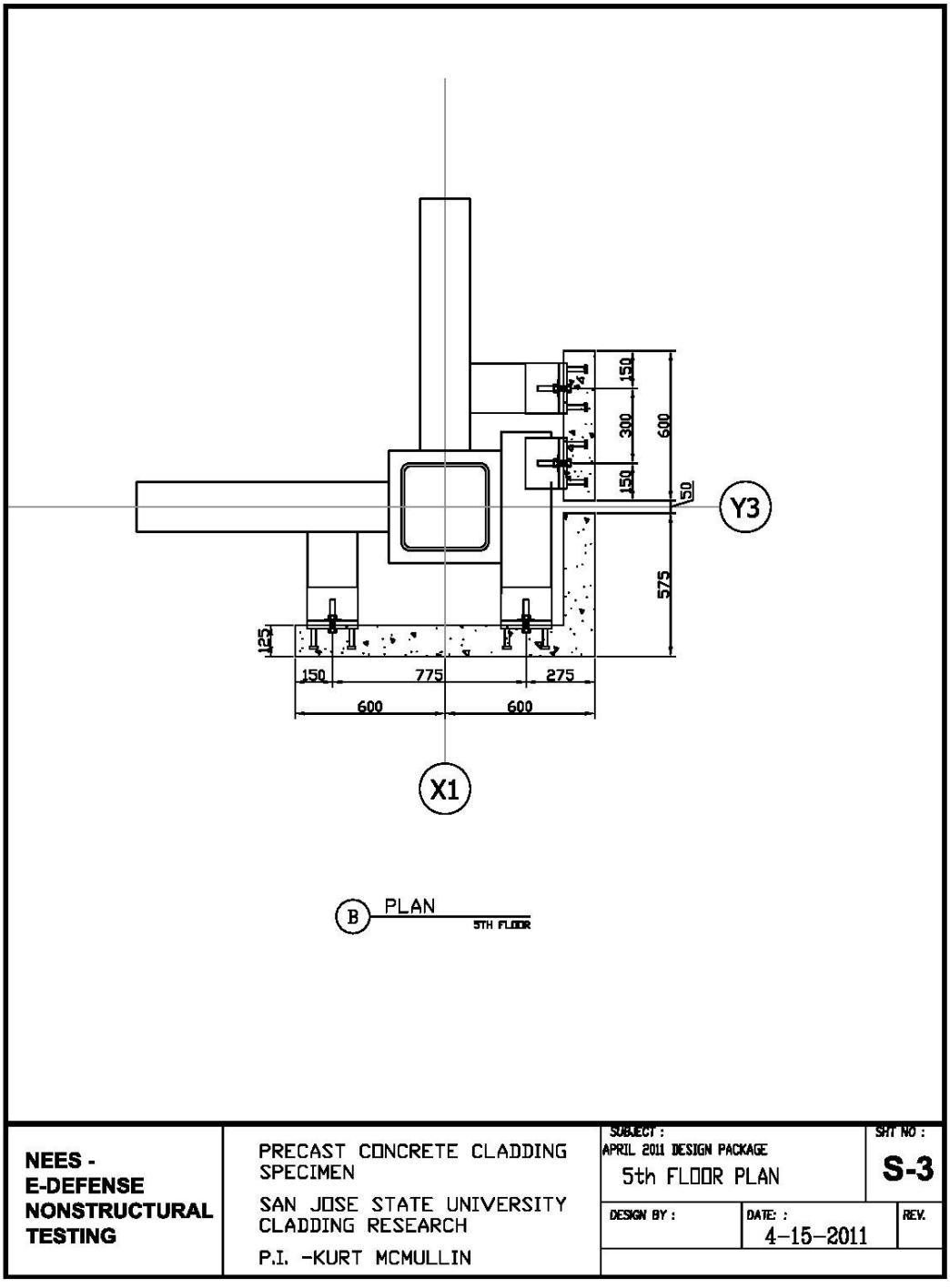

Figure A.3. Plan View of Top Slotted Connections for both the Return and Flat Panel

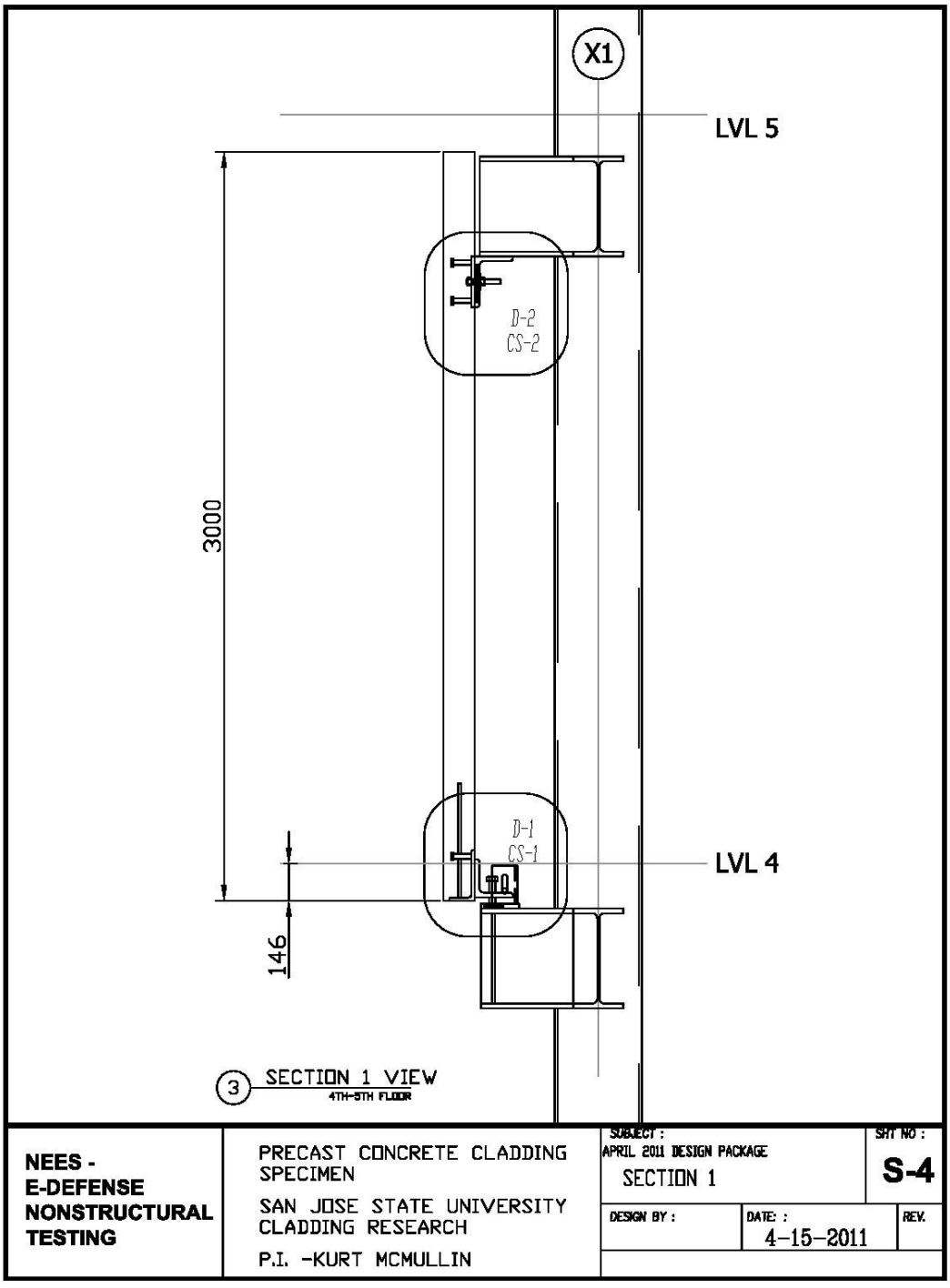

Figure A.4. Elevation Highlighting Top Slotted Connection and Bottom Bearing Connection (layout typical to both panels)

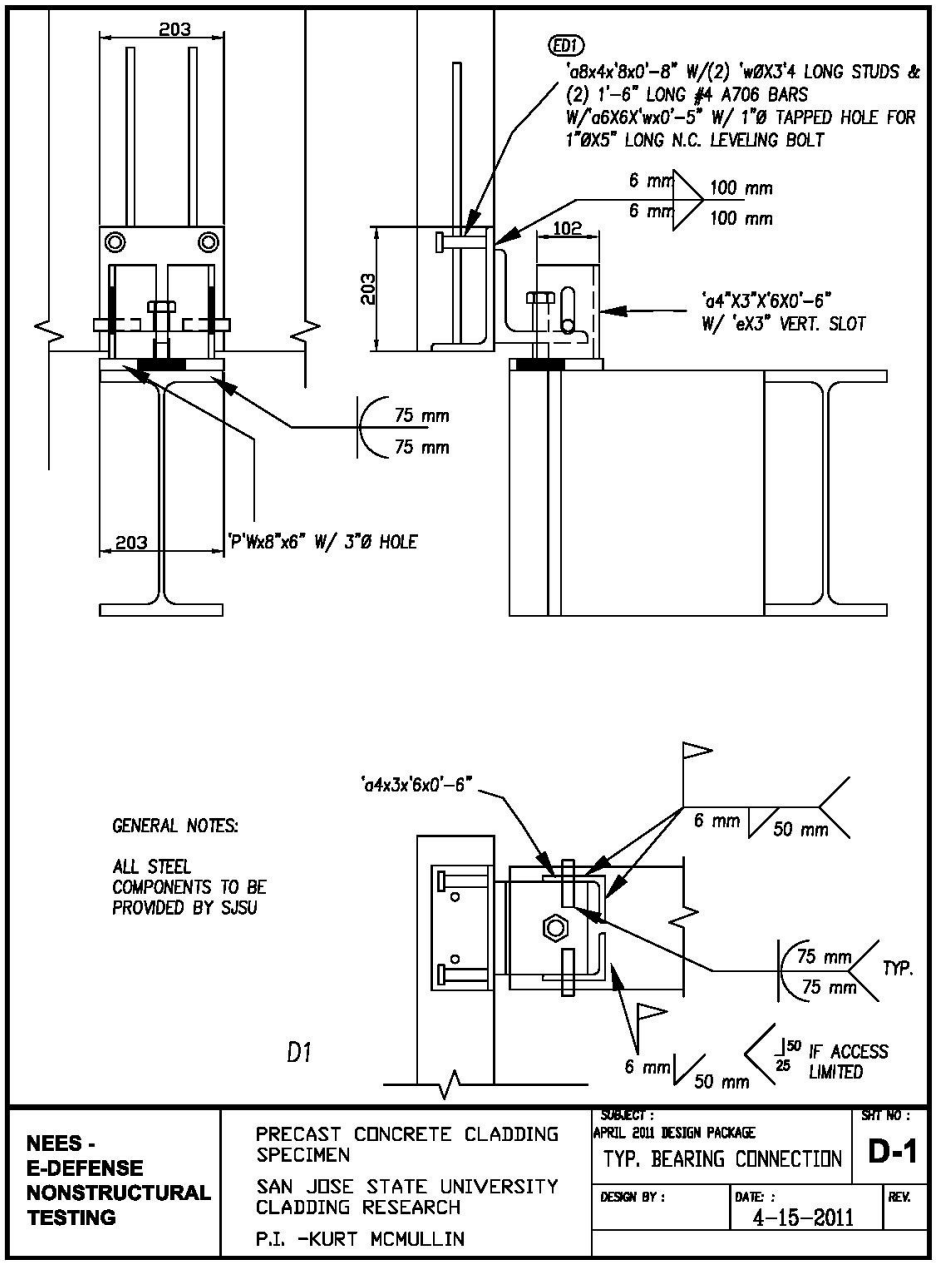

Figure A.5. Blueprint Detail of Typical Bearing Connection at Bottom of each Panel

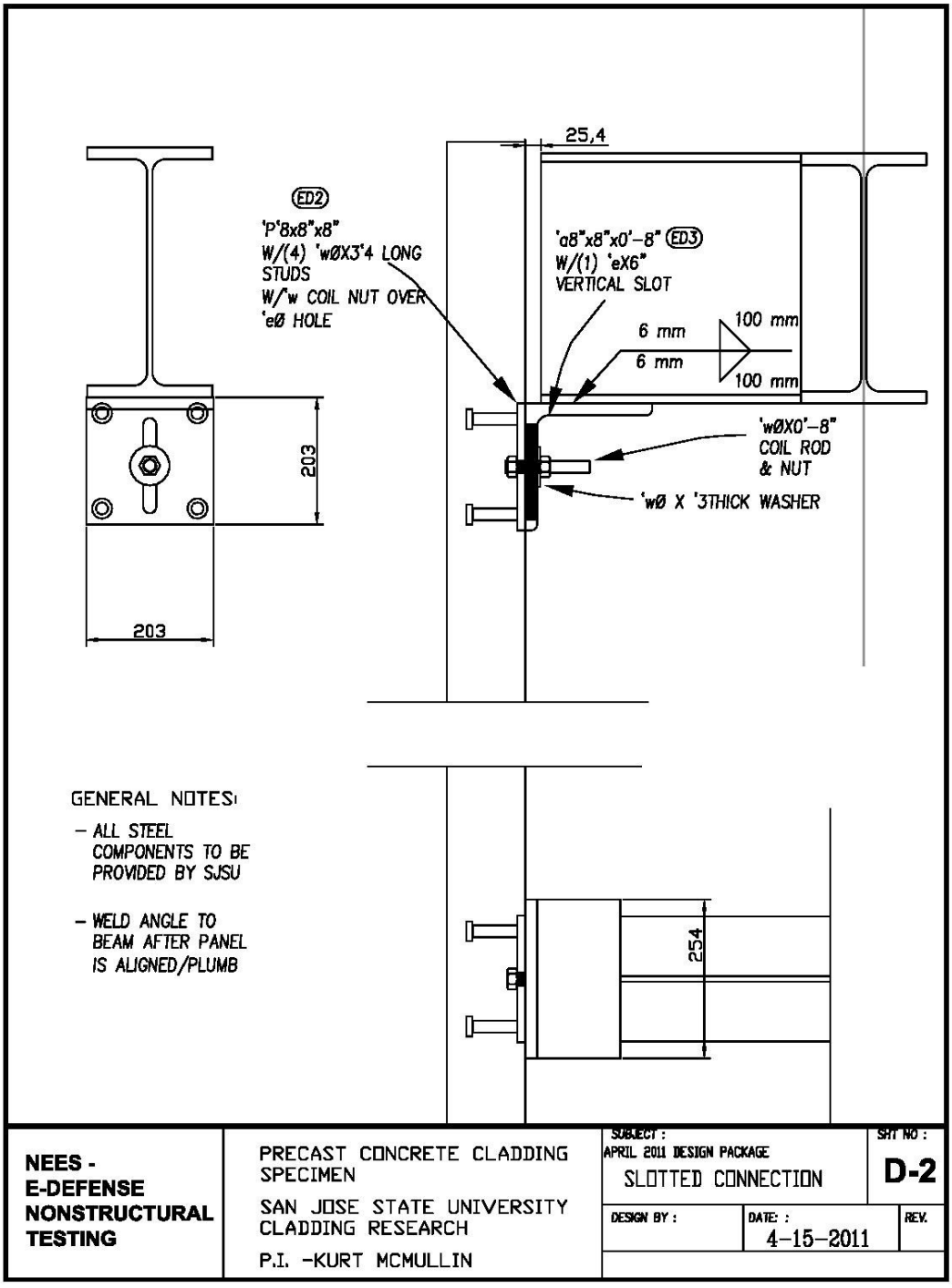

Figure A.6. Blueprint Detail of Typical Slotted Connection at Top of each Panel

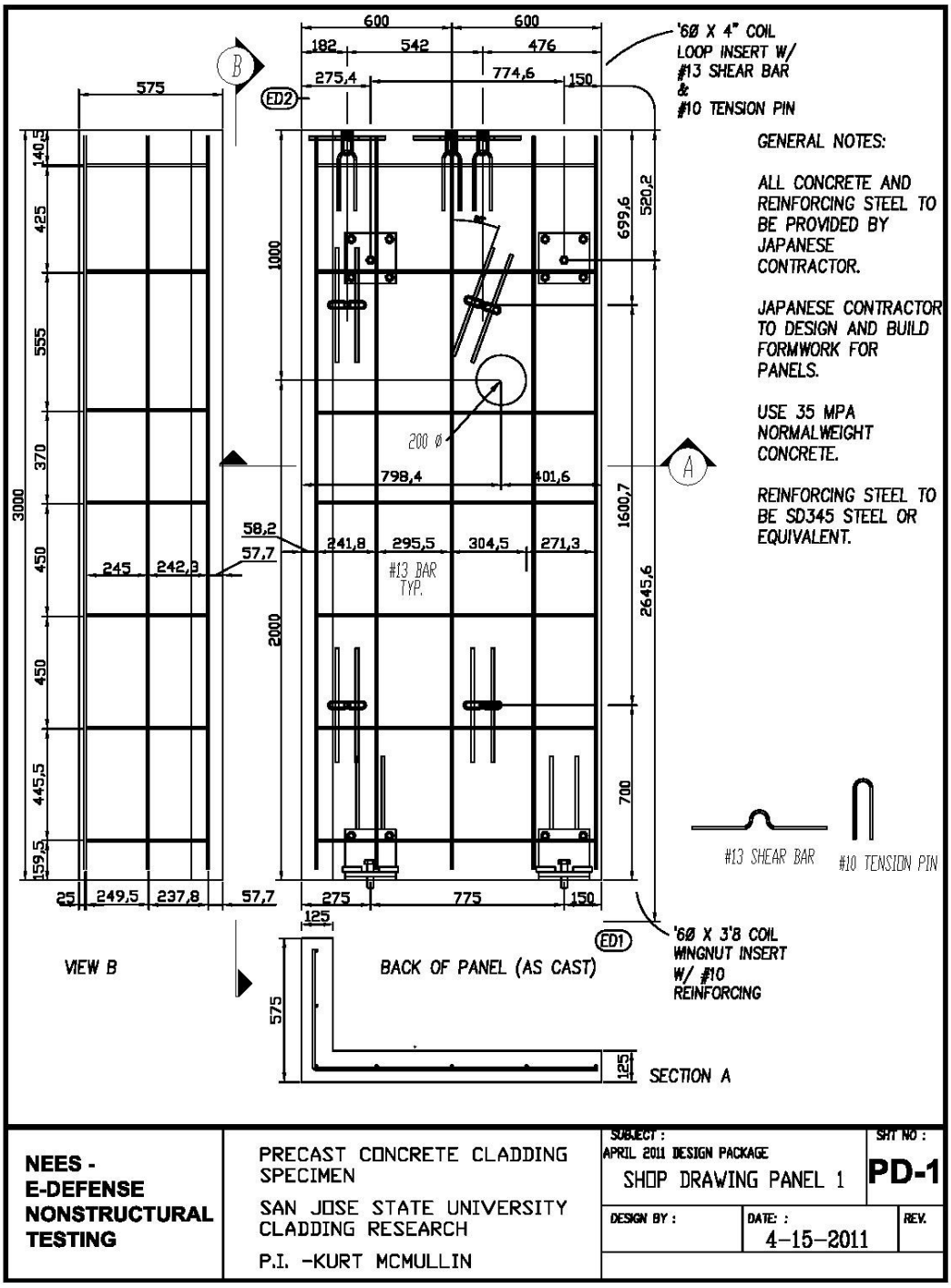

Figure A.7. Shop Drawing Blueprint Detail of the Return Panel PD-1

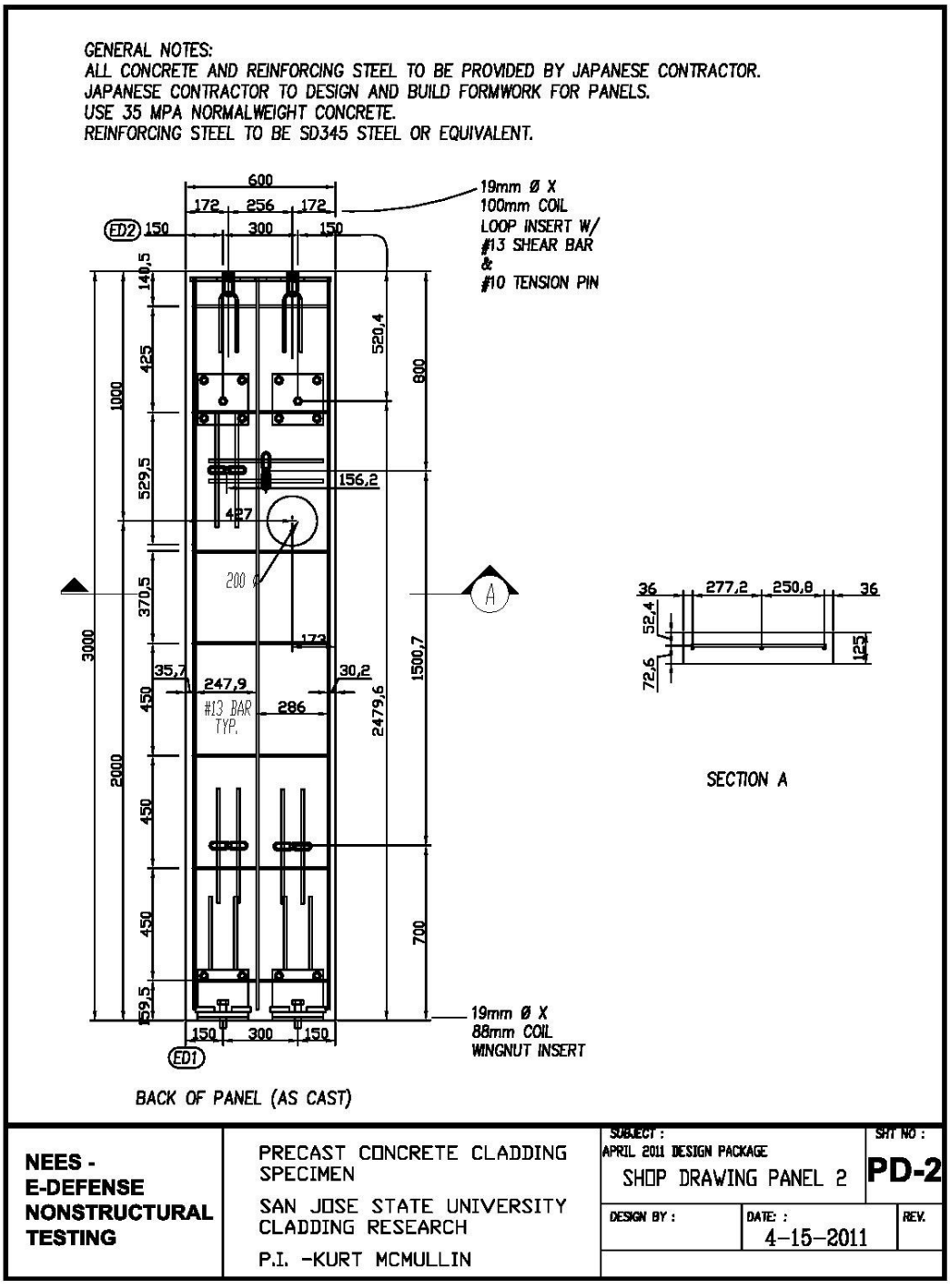

Figure A.8. Shop Drawing Blueprint Detail of the Flat Panel PD-2

Appendix B: Floor and Panel Time History Plots

Figures B.1 to B.6 show the time histories of the 4th and 5th center floor accelerations for the X, Y, and Z directions, respectively. The data were retrieved from the instruments listed in Table 5.3. Figures B.7 to B.10 show the time histories of the 4th and 5th corner floor accelerations for the X and Y directions, respectively. Corner accelerations were derived by the author using Equations 7.1 and 7.2. Equations 7.1 and 7.2 use the data retrieved from the instruments listed in Table 5.3. Figures B.11 to B.16 show the acceleration time histories of the panels. The data were retrieved from the instruments listed in Table 4.4.

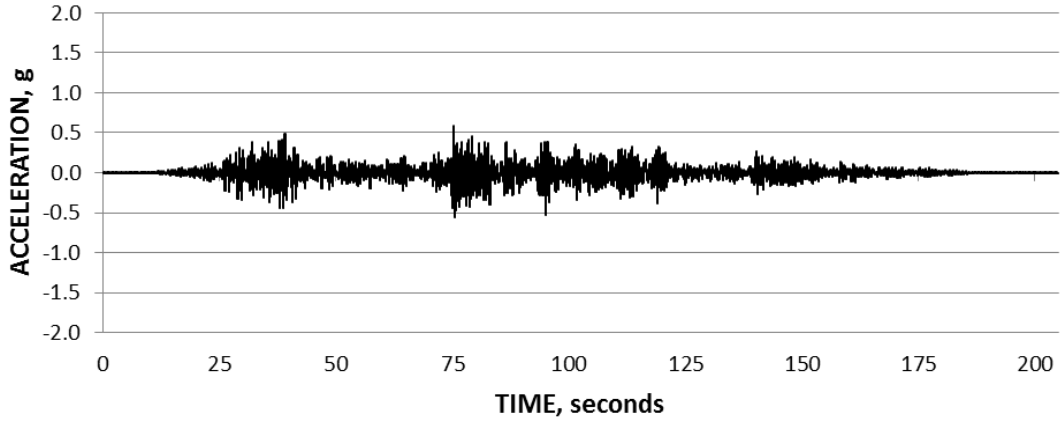

Figure B.1. 4th Floor Center Acceleration Time History, X direction

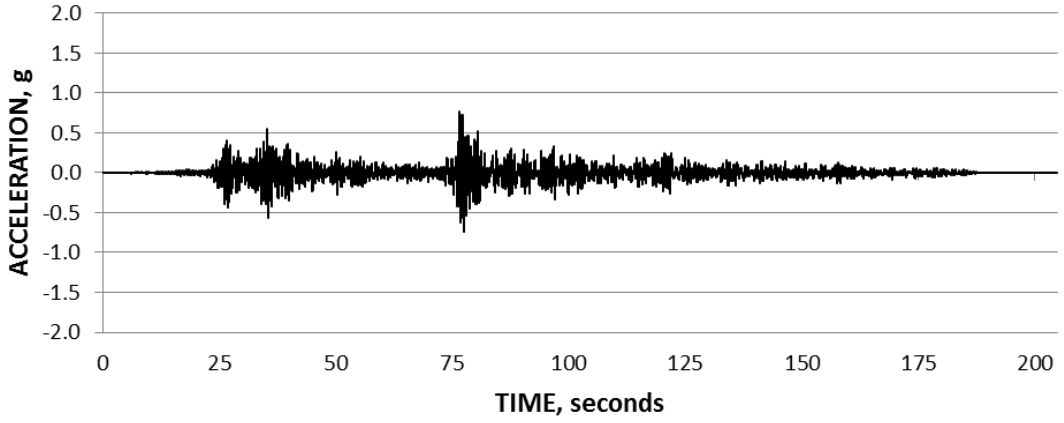

Figure B.2. 4th Floor Center Acceleration Time History, Y direction

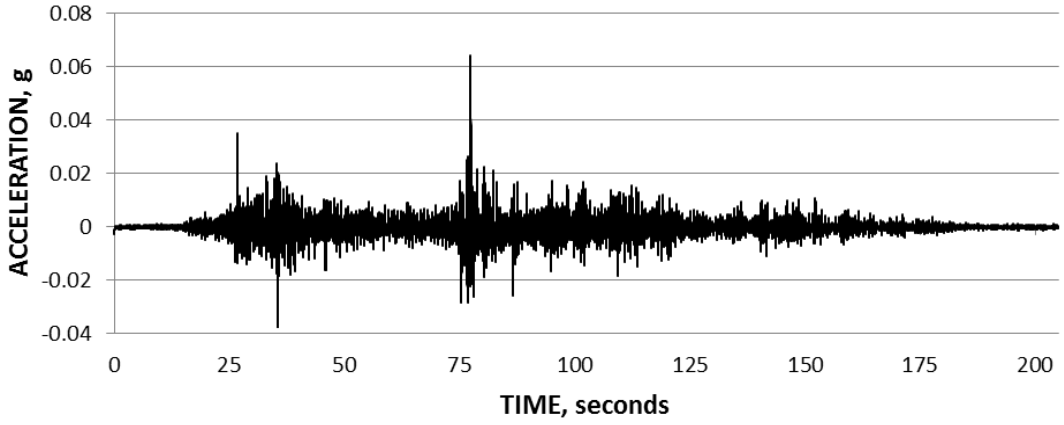

Figure B.3. 4th Floor Center Acceleration Time History, Z Direction

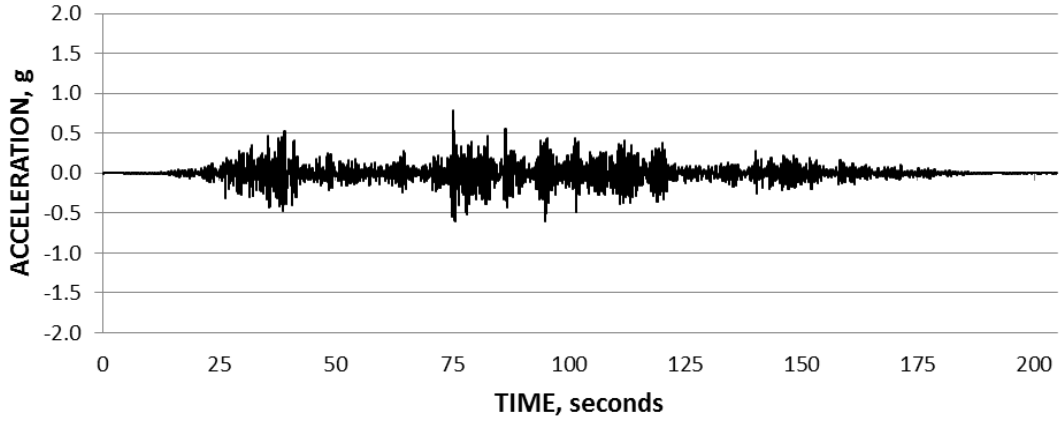

Figure B.4. 5th Floor Center Acceleration Time History, X direction

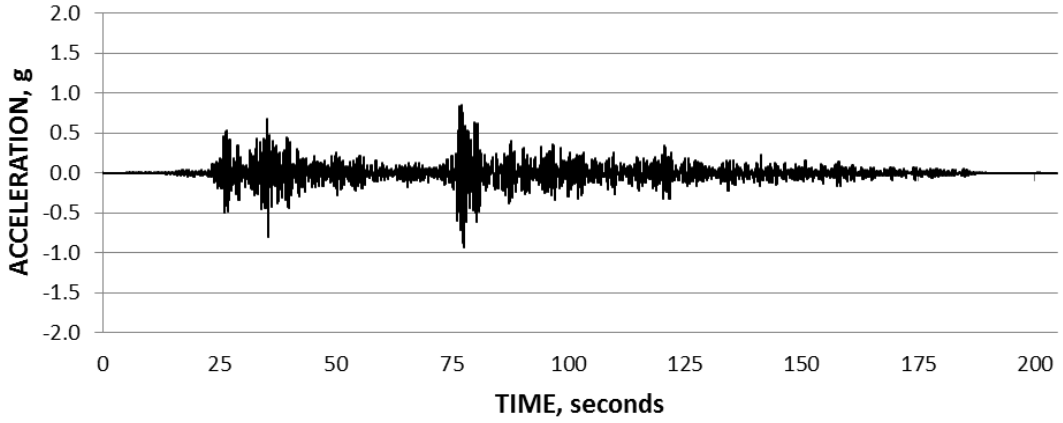

Figure B.5. 5th Floor Center Acceleration Time History, Y direction

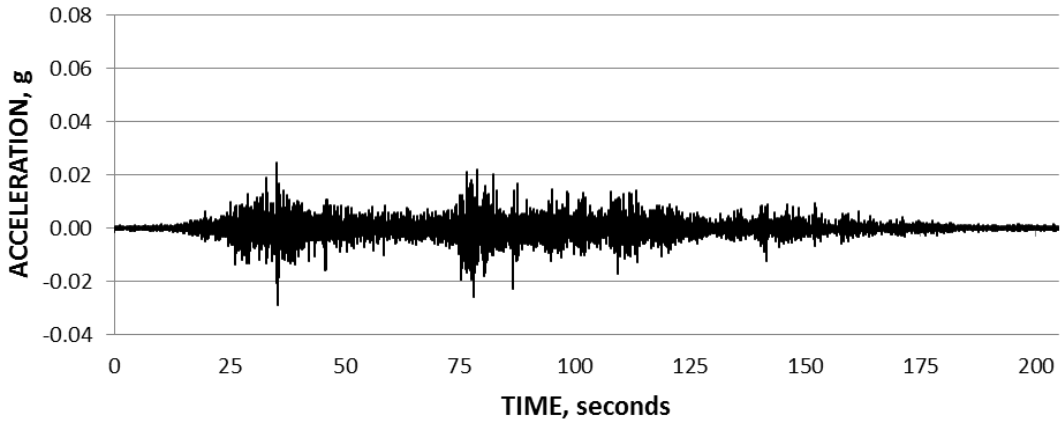

Figure B.6. 5th Floor Center Acceleration Time History, Z Direction

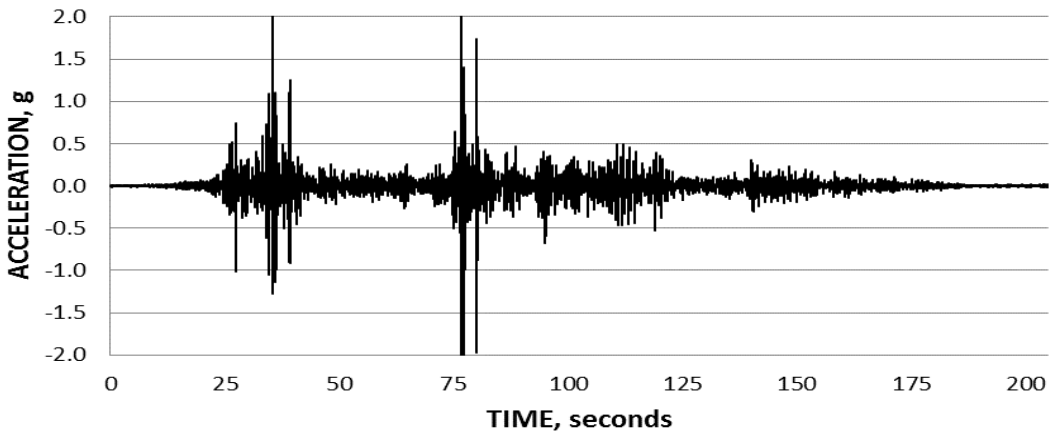

Figure B.7. 4th Floor Corner Acceleration Time History, X direction

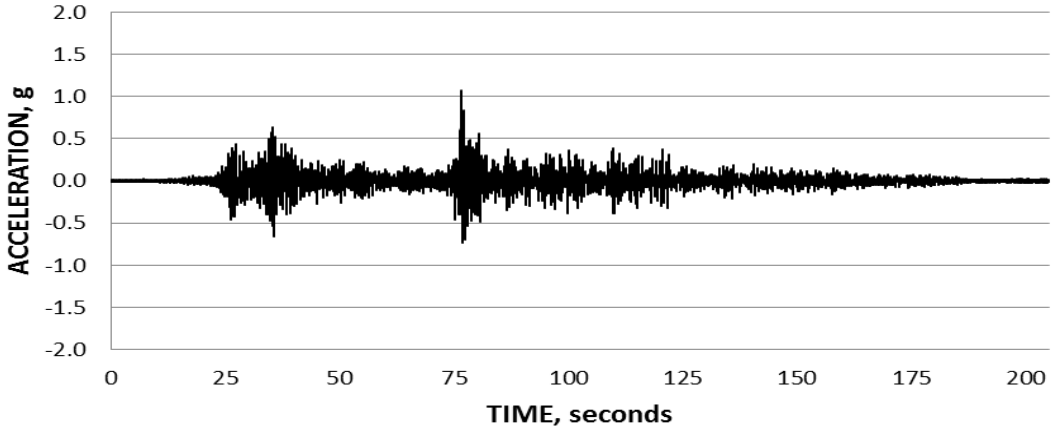

Figure B.8. 4th Floor Corner Acceleration Time History, Y direction

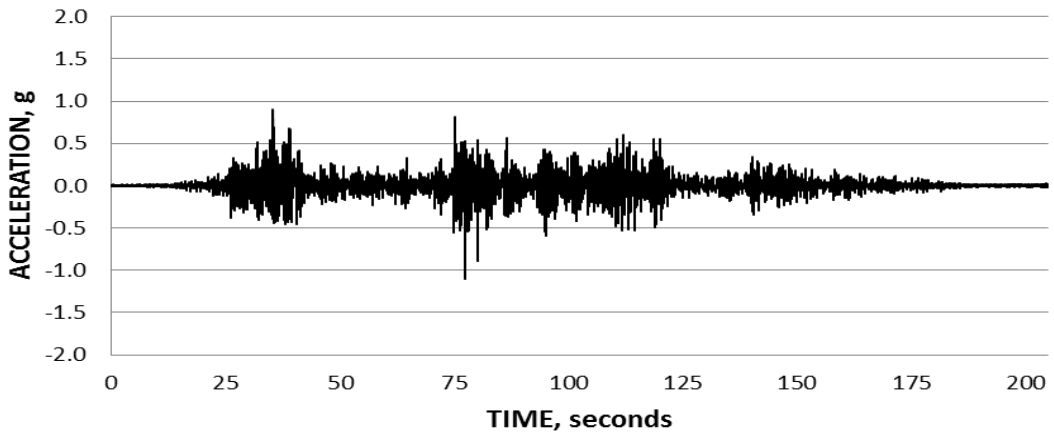

Figure B.9. 5th Floor Corner Acceleration Time History, X direction

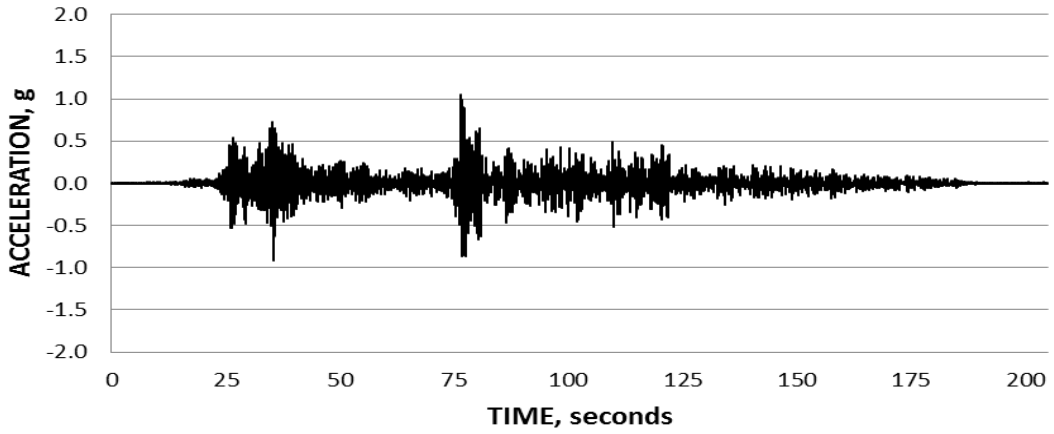

Figure B.10. 5th Floor Corner Acceleration Time History, Y direction

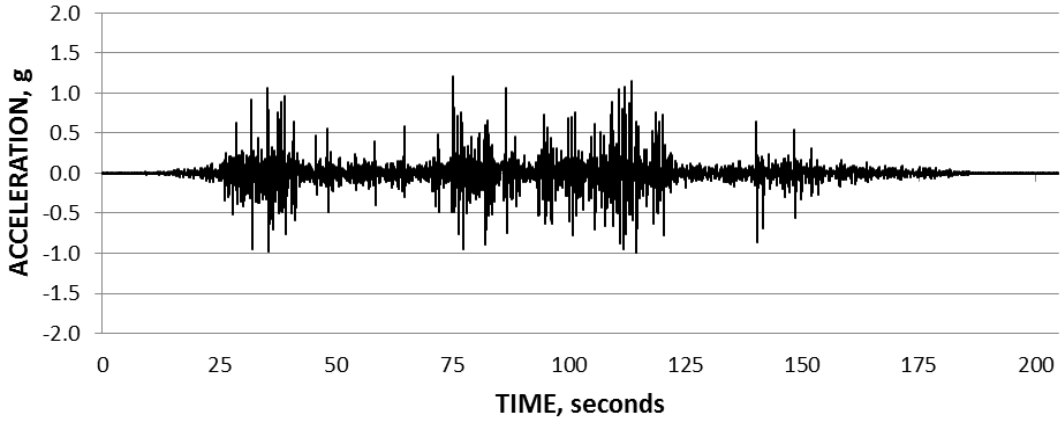

Figure B.11. PD-1 Acceleration Time History, U3, X direction

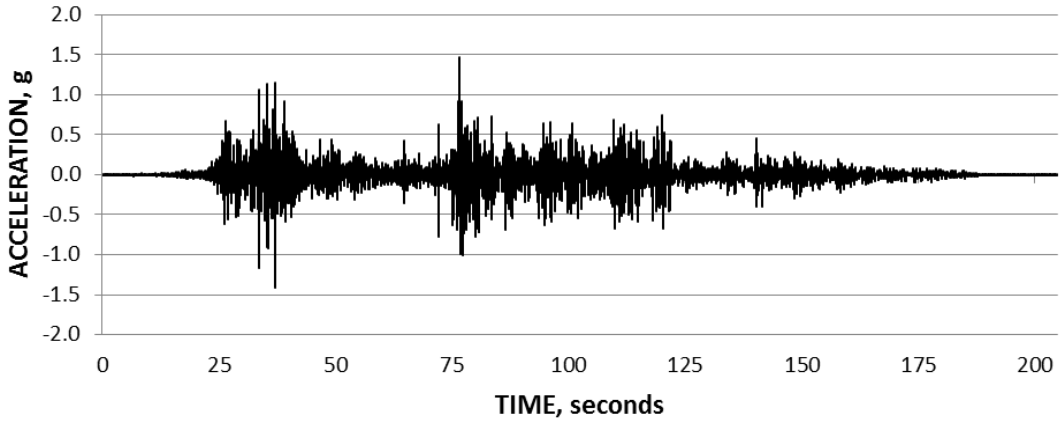

Figure B.12. PD-1 Acceleration Time History, U1, Y direction

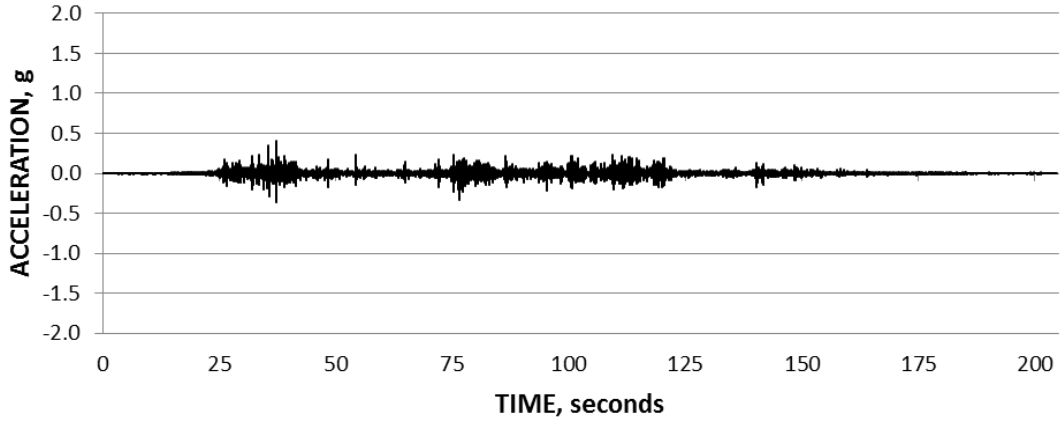

Figure B.13. PD-1 Acceleration Time History, U2, Z Direction

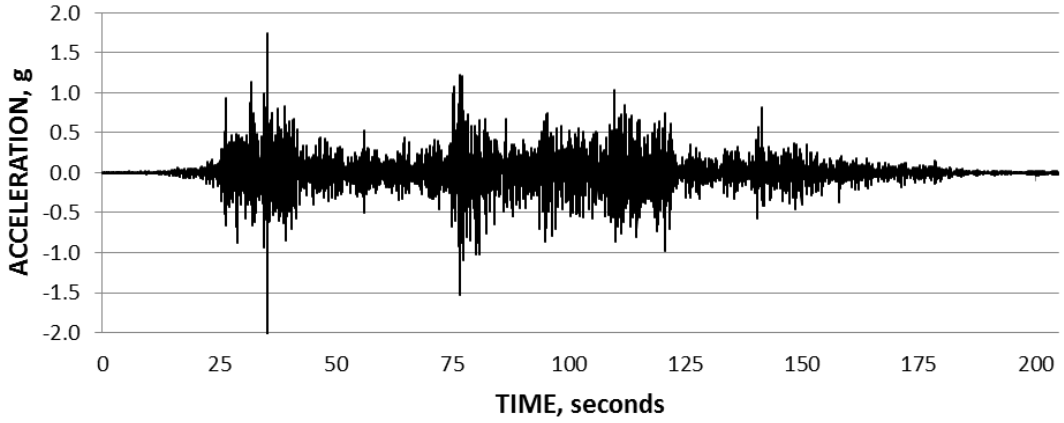

Figure B.14. PD-2 Acceleration Time History, U1, X direction

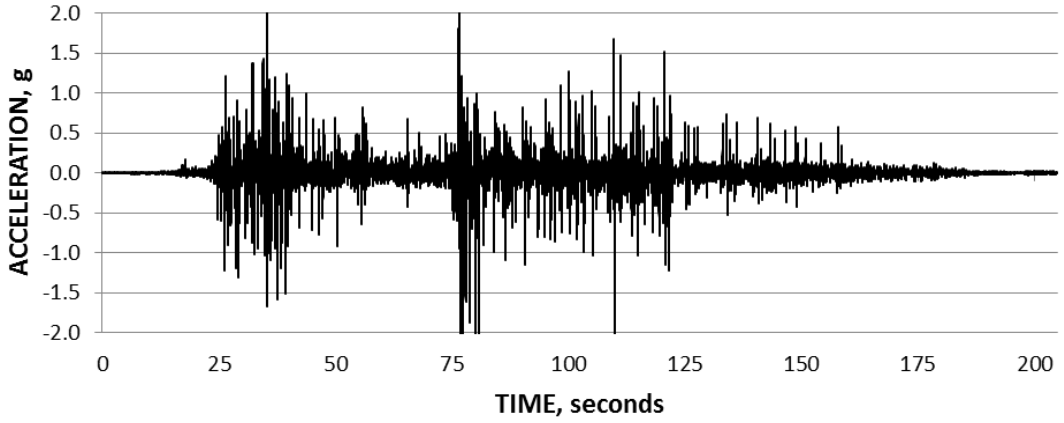

Figure B.15. PD-2 Acceleration Time History, U3, Y direction

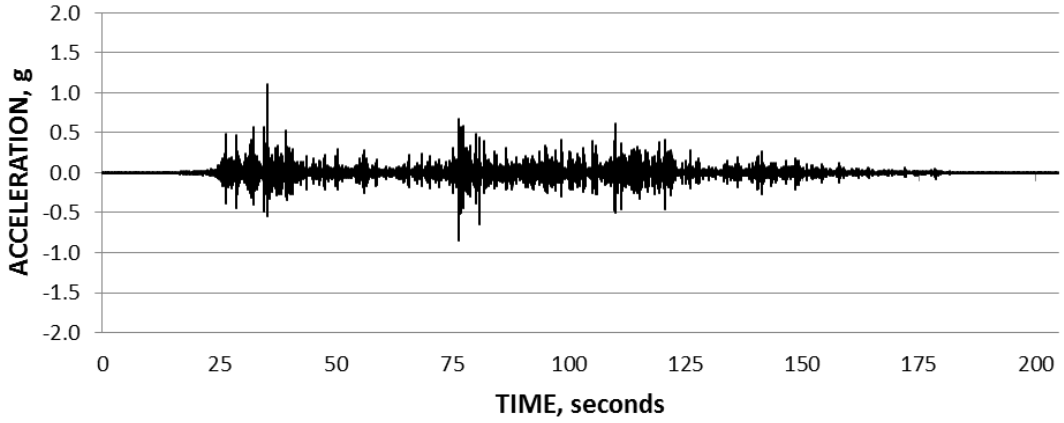

Figure B.16. PD-2 Acceleration Time History, U2, Z Direction

Appendix C: Glossary Definitions

Acceleration Amplification Ratio	This thesis defines acceleration amplification ratio as a measure of how the vibrational characteristics of an item compares to the vibration of the item's supporting structure. This term is used for the non-structural components of the experiments analyzed in this thesis, and is therefore an expansion of Chopra's traditional structural dynamics definition of acceleration amplification.
Critical Structure	Structures that are expected to perform at maximum level because they are deemed necessary to society, i.e. power plants, hospitals, etc.
Damping (of a structure)	Energy dissipated through friction, incrementally decreasing oscillations of a structure (Lindeburg & McMullin, 2011).
Drift Demand (of a building)	The relative lateral story and roof displacements of structures as a result of lateral loading. Demands may be due to seismic, wind, ice and/or blast loading.
Earthquake	Energy is released from the earth crust as a result of tectonic plate movement crust, traveling in waves.
Elastically Non-Yielding	System returns to its original position without any permanent strain upon loading and unloading.
Global drift	Roof deflection is the total horizontal displacement of the roof relative to its original position. Roof deflection is the displacement of the top story. Roof deflection is also known as global drift.
Global drift ratio	The global drift ratio is the peak global deflection divided by the height of the roof and measured in radians.
Inelastic Yielding	When loading causes permanent strain on a system with the possible occurrence of plastic hinging, or loss of rotational resistance.

Inter-story drift	Inter-story drift is the horizontal displacement of one story with respect to the story below (Lindeburg & McMullin, 2011).
Inter-story drift ratio	Inter-story drift ratio is the inter-story drift divided by the story height of that specific story and measured in radians.
Lateral Stiffness	The ability of a structure to withstand deflection upon loading (Hooke's Law).
Lateral System	For the purposes of this paper, a recognized seismic force-resisting system found in *ASCE 7-10* Table 12.2-1 (ASCE, 2010).
Mode	Modes represent the unique normalized shape orientation of the systems lumped masses. Each mode has a unique period and unique response in dynamic analysis.
Non-linear Dynamic Analysis	A system is accurately modeled, analyzed with a specific design earthquake, and both the responses and forces vary with time by which ultimately the maximum design force is selected.
Response (dynamic analysis)	When a time-varying load is applied to a structure for dynamic analysis, the resulting responses of system is its displacement, velocity, and acceleration. These quantities are used to determine member forces.
Regular/irregular Structure	A regular structure has no irregularities. Irregularities can be a result of irregular distributions in mass, stiffness, geometry, lateral strength, and/or any other physical properties that may cause excessive torsional behavior or non-conventional behavior of a system (Lindeburg & McMullin, 2011).
Time-History Analysis	Earthquake recorded ground motion with respect to time is converted into a time-varying force that is applied to a structure for dynamic response.